National Library of Canada
Bibliothèque nationale du Canada

Canadian Theses Service
Services des thèses canadiennes

Ottawa, Canada
K1A 0N4

CANADIAN THESES

THÈSES CANADIENNES

NOTICE

The quality of this microfiche is heavily dependent upon the quality of the original thesis submitted for microfilming. Every effort has been made to ensure the highest quality of reproduction possible.

If pages are missing, contact the university which granted the degree.

Some pages may have indistinct print especially if the original pages were typed with a poor typewriter ribbon or if the university sent us an inferior photocopy.

Previously copyrighted materials (journal articles, published tests, etc.) are not filmed.

Reproduction in full or in part of this film is governed by the Canadian Copyright Act, R.S.C. 1970, c. C-30. Please read the authorization forms which accompany this thesis.

AVIS

La qualité de cette microfiche dépend grandement de la qualité de la thèse soumise au microfilmage. Nous avons tout fait pour assurer une qualité supérieure de reproduction.

S'il manque des pages, veuillez communiquer avec l'université qui a conféré le grade.

La qualité d'impression de certaines pages peut laisser à désirer, surtout si les pages originales ont été dactylographiées à l'aide d'un ruban usé ou si l'université nous a fait parvenir une photocopie de qualité inférieure.

Les documents qui font déjà l'objet d'un droit d'auteur (articles de revue, examens publiés, etc.) ne sont pas microfilmés.

La reproduction, même partielle, de ce microfilm est soumise à la Loi canadienne sur le droit d'auteur, SRC 1970, c. C-30. Veuillez prendre connaissance des formules d'autorisation qui accompagnent cette thèse.

THIS DISSERTATION
HAS BEEN MICROFILMED
EXACTLY AS RECEIVED

LA THÈSE A ÉTÉ
MICROFILMÉE TELLE QUE
NOUS L'AVONS REÇUE

NL 339 (r. 88/01)

Canada

National Library of Canada / Bibliothèque nationale du Canada

Ottawa, Canada
K1A 0N4

TC –

ISBN 0-315-23395-8

CANADIAN THESES ON MICROFICHE SERVICE – SERVICE DES THÈSES CANADIENNES SUR MICROFICHE

PERMISION TO MICROFILM – AUTORISATION DE MICROFILMER

• Please print or type – Écrire en lettres moulées ou dactylographier

AUTHOR – AUTEUR

Full Name of Author – Nom complet de l'auteur

DAMARYS LOZADA-BRICEÑO

Date of Birth – Date de naissance
MARCH 28, 1953

Canadian Citizen – Citoyen canadien
☐ Yes / Oui ☒ No / Non

Country of Birth – Lieu de naissance
VENEZUELA

Permanent Address – Résidence fixe
536 Michener Park
Edmonton, Alberta T6H 4M5
CANADA

THESIS – THÈSE

Title of Thesis – Titre de la thèse

SIMULATION OF 'HIGH PRESSURE GAS DRIVE-
A COMPOSITIONAL APPROACH

Degree for which thesis was presented
Grade pour lequel cette thèse fut présentée
MSc in Petroleum Eng.

Year this degree conferred
Année d'obtention de ce grade
Fall 1985

University – Université
THE UNIVERSITY OF ALBERTA

Name of Supervisor – Nom du directeur de thèse
DR FAROUQ ALI

AUTHORIZATION – AUTORISATION

Permission is hereby granted to the NATIONAL LIBRARY OF CANADA to **microfilm** this thesis and to **lend** or **sell copies of the film.**

The author reserves other publication rights, and neither the thesis nor extensive extracts from it may be printed or otherwise reproduced without the author's written permission.

L'autorisation est, par la présente, accordée à la BIBLIOTHÈQUE NATIONALE DU CANADA de **microfilmer** cette thèse et de **prêter** ou de **vendre des exemplaires du film.**

L'auteur se réserve les autres droits de publication; ni la thèse ni de longs extraits de celle-ci ne doivent être imprimés ou autrement reproduits sans l'autorisation écrite de l'auteur.

ATTACH FORM TO THESIS – VEUILLEZ JOINDRE CE FORMULAIRE À LA THÈSE

Signature
D. Lozada

Date
July 28/85

NL-91 (r. 84-03)

Canada

THE UNIVERSITY OF ALBERTA

SIMULATION OF HIGH PRESSURE GAS DRIVE – A COMPOSITIONAL APPROACH

by

© DAMARYS LOZADA-BRICEÑO

A THESIS

SUBMITTED TO THE FACULTY OF GRADUATE STUDIES AND RESEARCH

IN PARTIAL FULFILMENT OF THE REQUIREMENTS FOR THE DEGREE

OF MASTER OF SCIENCE

IN

PETROLEUM ENGINEERING

DEPARTMENT OF MINERAL ENGINEERING

EDMONTON, ALBERTA

FALL, 1985

THE UNIVERSITY OF ALBERTA

RELEASE FORM

NAME OF AUTHOR Damarys Lozada-Briceño

TITLE OF THESIS Simulation of High Pressure Gas Drive – A Compositional Approach

DEGREE FOR WHICH THESIS WAS PRESENTED Master of Science

YEAR THIS DEGREE GRANTED 1985

Permission is hereby granted to THE UNIVERSITY OF ALBERTA LIBRARY to reproduce single copies of this thesis and to lend or sell such copies for private, scholarly or scientific research purposes only.

The author reserves other publication rights, and neither the thesis nor extensive extracts from it may be printed or otherwise reproduced without the author's written permission.

(Signed). . . . . D. Lozada-Briceño

PERMANENT ADDRESS:

Damarys Lozada
Intevep S.A.
APDO. 76343
Caracas 1070A
Venezuela

DATED . . May. 21. . . . 1985

THE UNIVERSITY OF ALBERTA

FACULTY OF GRADUATE STUDIES AND RESEARCH

The undersigned certify that they have read, and recommend to the Faculty of Graduate Studies and Research, for acceptance, a thesis entitled

SIMULATION OF HIGH PRESSURE GAS DRIVE –

A COMPOSITIONAL APPROACH

submitted by DAMARYS LOZADA-BRICEÑO

in partial fulfilment of the requirements for the degree of

Master of Science

in Petroleum Engineering

.....

Supervisor: S.M. Farouq Ali

.....

R.G. Bentsen

.....

K. Nandakumar

.....

.....

Date May 21, 85

ABSTRACT

A compositional, fully implicit numerical model, incorporating an equation of state, was developed, with the Jacobian being calculated numerically. The model implements one- and two-dimensional, three-phase flow with a variable number of components in a porous medium. Capillarity and gravitational forces were taken into account. Interfacial tension was included in the relative permeability curves. The production and injection terms were considered fully implicitly.

The model was used to study high pressure gas drives: condensing and vaporization gas drives, miscible (multiple contact) drive, and immiscible gas displacement, in order to simulate the mass transfer mechanisms.

In multicontact miscible displacement simulations, continuous convergence of hydrocarbon phase compositions and properties near the critical composition was achieved. Thus, stable convergence was possible with the model near and at the critical point. A change of saturation up to 50% is allowed at the critical point. The distinction between a miscible or immiscible displacement close to the critical point depends strongly upon the calibration of the equation of state with experimental data.

The simultaneous solution of the mass conservation equation and the phase equilibria relations presented convergence problems for the miscible displacement test. The problem was solved by extrapolation of the K-values of the grid blocks in question. Newton's method with numerical derivatives (as contrasted with analytical derivatives) can

be used to calculate the saturation pressure, i.e., the phase envelope of a fluid. This method can be used to solve nonlinear partial differential equations of compositional models in an efficient manner.

ACKNOWLEDGEMENTS

I wish to thank Dr. S.M. Farouq Ali for suggesting this study and for his guidance and constructive criticism.

Thanks are extended to Intevep S.A. for selecting the author for further educational training and for providing the financial support.

TABLE OF CONTENTS

CHAPTER		PAGE
I	INTRODUCTION	1
II	LITERATURE REVIEW	2
	II.1 Mathematical Formulation	4
	II.2 Treatment of Nonlinearities	17
	II.3 Method of Solution	24
III	STATEMENT OF THE PROBLEM	31
IV	MATHEMATICAL DESCRIPTION OF THE COMPOSITIONAL MODEL	33
	IV.1 Assumptions	33
	IV.2 Model Development	34
	IV.3 Initial and Boundary Conditions	36
	IV.4 Rock and Fluid Properties	37
	IV.5 Production-Injection Rates	42
	IV.6 Phase Equilibria	45
V	FINITE DIFFERENCE APPROXIMATIONS AND METHOD OF SOLUTION	48
	V.1 Finite Difference Approximation	48
	V.2 Expansion/Linearization of the Difference Equations and Solution Method	53
	V.3 Variable Substitution Method	62
	V.4 Hydrocarbon-Phase Appearance/Disappearance	64
	V.5 Expansion of Derivatives	65

CHAPTER PAGE

V.6 Saturation Pressure Calculation 68

V.7 Equations for Flash Calculations 69

V.8 Molar Balance 72

V.9 Surface Production Rates 73

VI COMPUTATIONAL PROCEDURE 75

VII RESULTS AND DISCUSSION 79

VII.1 Examples Studied 79

VII.2 Reservoir Data 80

VII.3 Simulation of Displacements in a One-Dimensional Reservoir 86

VII.4 Simulation of Displacements in a Two-Dimensional Reservoir 106

VII.5 Sensitivity Analysis 111

VII.6 Validation of Simulator Results 134

VII.7 Efficiency of the Model 143

VIII NUMERICAL AND MECHANISTIC PROBLEMS ENCOUNTERED IN THE DEVELOPMENT OF THE MODEL 146

IX CONCLUSIONS AND RECOMMENDATIONS 150

IX.1 Recommendations 151

BIBLIOGRAPHY 153

APPENDIX A DERIVATIVES OF ACCUMULATION AND PRODUCTION/INJECTION TERMS 159

VITA 167

LIST OF TABLES

Table		Page
II.1	Approximation of Nonlinear Terms-Density of Phases . . .	20
II.2	Approximation of Nonlinear Terms-Viscosity of Phases . .	21
II.3	Approximation of Nonlinear Terms-Composition of Phases .	22
II.4	Approximation of Nonlinear Terms-Relative Permeability of Phases	23
VII.1	Basic Reservoir Data Common to All Examples	81
VII.2	Reservoir Data Corresponding to Example Problems 1 and 2 for the 1-D Reservoir and to Example Problems 4 and 5 for the 2-D Reservoir	82
VII.3	Reservoir Data Corresponding to Example Problem 3 for the 1-D Reservoir and to Example Problem 6 for 2-D Reservoir	83
VII.4	Comparison of the Equilibrium K-Values Calculated by the Peng-Robinson Equation of State and Experimental Data	84
VII.5	Comparison of the Molar Volumes Calculated by the Peng-Robinson Equation of State and Experimental Data	85
VII.6	Basic Reservoir Data Used to Compare with Experimental Data	139
VII.7	Comparison of Computational Time (m sec) Using AMDAHL 5860 (FORTRAN G)	144

LIST OF FIGURES

Figure		Page
6.1	Flow diagram of the computational procedure	76
7.1	Example Problem 1: Composition path for condensing gas drive, multicontact miscible displacement at 0.56 and 0.20 PV and 20 grid blocks	87
7.2	Example Problem 1: Density profile for condensing gas drive, multicontact miscible displacement for grid block 1 and 2 vs pore volume fluid injected (PV)	88
7.3	Example Problem 1: Viscosity profile for condensing gas drive, multicontact miscible displacement for grid block 1 and 2 vs pore volume fluid injected (PV)	89
7.4	Example Problem 1: Gas saturation profile for condensing gas drive, multicontact miscible displacement at 0.26, 0.56 and 0.67 PV and 20 grid blocks	91
7.5	Example Problem 1: Overall composition profile for condensing gas drive, multicontact miscible displacement at 0.56 PV and 20 grid blocks	92
7.6	Example Problem 2: Composition path for condensing gas drive, immiscible displacement at 0.20 and 0.56 PV and 20 grid blocks	94
7.7	Example Problem 2: Viscosity profile for condensing gas drive, immiscible displacement for grid block 1 vs pore volume injected (PV)	95
7.8	Example Problem 2: Density profile for condensing gas drive, immiscible displacement for grid block 1 vs pore volume fluid injected (PV)	96
7.9	Example Problem 2: Gas saturation profile for condensing gas drive, immiscible displacement at 0.25, 0.36 and 0.67 PV and 20 grid blocks	97
7.10	Example Problem 2: Overall composition profile for condensing gas drive, immiscible displacement at 0.56 PV and 20 grid blocks	99
7.11	Example Problem 3: Composition path for high pressure gas drive, immiscible displacement at 0.22 and 0.56 PV and 20 grid blocks	100

Figure		Page
7.12	Example Problem 3: Composition profile for high pressure gas drive, immiscible displacement at 0.56 PV and 20 grid blocks	102
7.13	Example Problem 3: Density profile for high pressure gas drive, immiscible displacement for grid block 2	103
7.14	Example Problem 3: Viscosity profile for high pressure gas drive, immiscible displacement at 0.56 PV	104
7.15	Example Problem 3: Gas saturation profile for high pressure gas drive, immiscible displacement at 0.22 and 0.55 PV	105
7.16	Example Problem 4: Gas saturation contour for condensing gas drive, multicontact miscible displacement, in a 1/4 of a five-spot, at 0.61 PV. 5 × 5 grid	107
7.17	Example Problem 4: Gas saturation contour for condensing gas drive, multicontact miscible displacement, in a 1/4 of a five-spot, at 0.75 PV. 5 × 5 grid	108
7.18	Example Problem 4: Decane (mole fraction) contour for condensing gas drive, multicontact miscible displacement, in a 1/4 of a five-spot at 0.75 PV. 5 × 5 grid	109
7.19	Example Problem 4: n-butane (mole fraction) contour for condensing gas drive, multicontact miscible displacement, in a 1/4 of a five-spot at 0.75 PV. 5 × 5 grid	110
7.20	Example Problem 5: Gas saturation contour for condensing gas drive, immiscible displacement at 0.61 PV. 5 × 5 grid	112
7.21	Example Problem 5: Decane (mole fraction) contour for condensing gas drive, immiscible displacement, in a 1/4 of a five-spot at 0.61 PV. 5 × 5 grid	113
7.22	Example Problem 5: n-Butane (mole fraction) contour for condensing gas drive, immiscible displacement in a 1/4 of a five-spot at 0.61 PV. 5 × 5 grid	114
7.23	Example Problem 6: Gas saturation contour for high pressure gas drive, immiscible displacement in a 1/4 of a five-spot, at 0.55 PV. 5 × 5 grid	115
7.24	Example Problem 6: Methane (mole fraction) contour for high pressure gas drive, immiscible displacement in a 1/4 of a five-spot at 0.55 PV. 5 × 5 grid	116

Figure		Page
7.25	Example Problem 6: n-Butane (mole fraction) contour for high pressure gas drive, immiscible displacement in a 1/4 of a five-spot, at 0.55 PV. 5 × 5 grid	117
7.26	Effect of grid size on composition path at 0.24 PV for Example Problem 1: condensing gas drive, multicontact miscible displacement	119
7.27	Effect of grid size on composition path at 0.67 PV for Example Problem 1: condensing gas drive, multicontact miscible displacement	120
7.28	Effect of grid size on composition path at 0.20 PV for Example Problem 2: condensing gas drive, immiscible displacement	121
7.29	Effect of grid size on composition path at 0.67 PV for Example Problem 2: condensing gas drive, immiscible displacement	122
7.30	Effect of grid size on composition path at 0.56 PV for Example Problem 3: high pressure gas drive, immiscible displacement	123
7.31	Effect of grid size on gas saturation profile at 0.24 PV for Example Problem 1: condensing gas drive, multicontact miscible displacement	124
7.32	Effect of grid size on gas saturation profile at 0.67 PV for Example Problem 1: condensing gas drive, multicontact miscible displacement	125
7.33	Effect of grid size on gas saturation profile at 0.22 PV for Example Problem 2: condensing gas drive, immiscible displacement	126
7.34	Effect of grid size on gas saturation profile at 0.67 PV for Example Problem 2: condensing gas drive, immiscible displacement	127
7.35	Effect of grid size on gas saturation profile at 0.43 PV for Example Problem 3: high pressure gas drive, immiscible displacement	128
7.36	Effect of grid size on recovery of decane and comparison with two-dimensional reservoir for Example Problem 1	129
7.37	Effect of grid size on recovery of decane and comparison with two-dimensional reservoir for Example Problem 2	130

Figure		Page
7.38	Effect of grid size on recovery of decane for Example Problem 3	131
7.39	Comparison of decane recovery between one- and two-dimensional reservoirs for Example Problem 3	132
7.40	Overall composition comparison for Example Problem 1: condensing gas drive, multicontact miscible displacement at 0.56 PV with Ref (54)	135
7.41	Overall composition comparison for Example Problem 2: condensing gas drive, immiscible displacement, at 0.56 PV with Ref (54)	136
7.42	Velocity of miscible front for Example Problem 1	137
7.43	Relative permeability reported for Van Quy et al. (57)	140
7.44	Simulator results compared with experimental data. Overall composition of fluid produced vs. gas pore volume injected	141
7.45	Simulator results compared with experimental data. Cumulative mass produced per unit of area vs. pore volume injected	142

NOMENCLATURE

a = attraction parameter in equation of state

A' = cross-sectional area, ft^2 (m^2)

A = constant defined by Equation (IV-58)

b = Van der Waal's co-volume

B = constant defined by Equation (IV-59)

$\underline{B}$ = block matrix derivative of grid block ℓ with respect to $2n_c + 4$ unknowns of grid block $\ell + 1$

$\underline{B}_i$ = row i of $\underline{B}$ matrix, Equation (V-40)

$\underline{Bl}$ = reduced block matrix derivative $\underline{B}$ to $n_c + 1$ unknowns

$\underline{Bl}_i$ = row i of $\underline{Bl}$ matrix

c_f = formation (rock) compressibility, 1/psia (1/Pa)

c_{ij} = empirical interaction parameters

c_w = water compressibility, 1/psia (1/Pa)

C_i = accumulation term of component i, Equations (V-17), (V-18), lbm mol/D (kmol/s)

$\underline{C}$ = block matrix derivative of accumulation term C_i with respect to $2n_c + 4$ unknowns of grid block ℓ

$\underline{C}_i$ = row i of $\underline{C}$, Equation (V-40)

$\underline{Cl}$ = reduced block matrix derivative $\underline{C}$ to $n_c + 1$ unknowns

$\underline{Cl}_i$ = row i of $\underline{Cl}$ matrix

D = depth, measured vertically downward, ft (m)

$\underline{D}$ = block matrix derivative of grid block ℓ with respect to $2n_c + 4$ unknowns of grid block $\ell - 1$

$\underline{D}_i$ = row i of $\underline{D}$ matrix, Equation (V-40)

$\underline{D1}$ = reduced block matrix derivative $\underline{D}$ with respect to $n_c + 1$ unknowns

$\underline{D1}_i$ = row i of $\underline{D1}$ matrix

E_i = interblock flow term, Equations (V-15), (V-16), lbm mol/D (kmol/s)

$\underline{E'}$ = block matrix derivative of grid block ℓ with respect to $2n_c + 4$ unknowns of grid block ℓ

$\underline{E'}_i$ = row i of $\underline{E'}$ matrix, Equation (V-39)

$\underline{E1}$ = reduced block matrix derivative $\underline{E'}$ with respect to $n_c + 1$ unknowns

$\underline{E1}_i$ = row i of $\underline{E1}$ matrix

f_i = fugacity of a component i, psia (Pa)

f_i^L = liquid phase fugacity of component i, psia (Pa)

f_i^V = vapour phase fugacity of component i, psia (Pa)

F_i = residual molar balance equation for component i, lbm mol/D (kmol/s), Equation (V-14)

$\underline{F}$ = block matrix derivative of grid block ℓ with respect to $2n_c + 4$ unknowns of grid block $\ell + N_x$

$\underline{F}_i$ = row i of $\underline{F}$ matrix, Equation (V-40)

$\underline{F1}$ = reduced block matrix $\underline{F}$ to $n_c + 1$ unknowns

$\underline{F1}_i$ = row i of $\underline{F1}$ matrix

F_V = gas mole fraction

F_L = liquid mole fraction

g = acceleration due to gravity, 32.17 ft/s^2 (9.81 m/s^2)

g_c = conversion factor, 32.17 lbm ft/lb$_f$ s^2 (9.81 gm/g$_f$ s^2)

G_i = residual constraint equations for component i, Equations (V-21) to (V-24)

$\underline{H}$ = block matrix derivative of grid block ℓ with respect to $2n_c + 4$ unknowns of grid block $\ell - N_x$

$\underline{H}_i$ = row i of $\underline{H}$ matrix, Equation (V-40)

$\underline{Hl}$ = reduced block matrix derivative $\underline{H}$ with respect to $n_c + 1$ unknowns

$\underline{Hl}_i$ = row i of $\underline{Hl}$ matrix

JF_i = row i of Jacobian matrix of F_i

JG_i = row i of Jacobian matrix of G_i

k = absolute permeability, 6.328 darcy (m^2)

k_{rg} = gas relative permeability, fraction

k_{ro} = oil relative permeability, fraction

k_{rw} = water relative permeability, fraction

k_{row}, k_{rog} = oil relative permeability in oil-water system and gas-oil system respectively

k_{rgcw} = relative permeability to gas at connate water saturation, fraction

k_{rocw} = relative permeability to oil at connate water saturation, fraction

K_i = equilibrium ratio (K-value) of component i, $K_i = y_i/x_i$

L = distance, ft (m)

m = characteristic constant of each substance, Equation (IV-64)

M_i = molecular weight of component i, lbm/lbm mol(g/g mol)

MBI = incremental molar balance, fraction

MBC = cumulative molar balance, fraction

n_c = number of hydrocarbon components

n_t = total moles of component i in the reservoir, lb m mol (mol)

$\underline{\delta n}_t$ = total (net) moles produced during a time step, $\underline{\delta n}_t = n_t^n - n_t^{n+1}$ (kmol)

N = total number of unknowns: $2n_c + 4$

N_t = total number of grid blocks

N_x = number of grid blocks in x-direction

N_y = number of grid blocks in y-direction

p_g = gas pressure, psia (Pa)

p_o = oil pressure, psia (Pa)

p_{ref} = reference pressure, psia (Pa)

p_w = water pressure, psia (Pa)

p_{ci} = critical pressure of component i, psia (Pa)

P_{chi} = parachor of component i, $\text{dynes}^{\frac{1}{4}} \cdot \text{cm}^{1\frac{1}{4}}/\text{g mol}$

P_{cgo} = gas oil capillary pressure, psia (Pa)

P_{cow} = water oil capillary pressure, psia (Pa)

p_s = saturation pressure, psia (Pa)

p_{wf} = flowing bottomhole pressure, psia (Pa)

PI = productivity index, cu ft. cp/D · psi (m^3)

PV = pore volume of fluid injected

q = fluid production/injection rate, ft^3/D (m^3/s)

q_i = production/injection molar rate of component i, lbm mol/D (kmol/s)

q_i^* = specific molar rate, lbm mol/D · ft^3 (kmol/s · m^3)

q_{i_t} = total (net) production-injection mole rate of component i, lbm mol/D (kmol/s)

q_{ps} = production rate of phase p at surface conditions, ft^3/D (m^3/s)

R = universal gas constant 10.73 psia ft^3/lbm mol °R [83.137 E + 02 m^3Pa/kmol K]

S = fluid saturation, fraction

S_{gr} = residual gas saturation, fraction

S_{wi} = irreducible water saturation, fraction

S_{org} = residual oil saturation to gas, fraction

S_{orw} = residual oil saturation to water, fraction

t = time, days (s)

Δt = time step, days (s)

T = temperature, °R (K)

T_{ci} = critical temperature of component i, °R (K)

T' = constant part of transmissibility, kA'/L, md ft(m^3)

u = volumetric velocity, per area ft/D (m/s)

v = specific volume, cu ft/lbm mol (m^3/kmol)

v_{ci} = critical volume, specific, of component i, cu ft/lbm mol (m^3/kmol)

v'_c = critical volume, specific, of a mixture, cu ft/lbm mol (m^3/kmol)

V_b = grid bulk volume, ft^3 (m^3)

V_p = grid pore volume, ft^3 (m^3)

$w_{p_{\ell,k}}$ = upstream weight of phase p between grid block ℓ and k

x_i = mole fraction of component i in the oil phase

x_{ip} = mole fraction of component i in phase p

x_{iw} = mole fraction of component i in water phase

X = vector of unknowns, Equation (V-8)

X_a = vector of $n_c + 2$ unknowns, Equation (V-47)

X_b = vector of $n_c + 2$ unknowns, $(X_b = y_3, \ldots y_{n_c}, p, S_o, S_g, S_w)$

X1 = vector of primary unknowns, $(X1 = y_3, \ldots y_{n_c}, p, S_o, S_g)$

X_ℓ = vector of unknowns of grid block ℓ

X_k = vector of unknowns of grid block k

y_i = mole fraction of component i in the gas phase

Z = compressibility factor, Z = pv/RT

z_i = mole fraction of component i in the total hydrocarbon system

Greek

γ = specific weight, $\gamma = 1/144\ \rho g/g_c$, psia/ft or

$\gamma = 9.80665\ \rho g/g_c$, Pa/m

δ = iteration different operator,

$\delta X = X^{\nu+1} - X^{\nu}$

$\underline{\delta}$ = time difference operator, $\underline{\delta} t = t^{n+1} - t^n$

Δ = delta operator, $\Delta P = P_{i+1} - P_i$

$\nabla\cdot$ = divergence operator, $\nabla\cdot = \frac{\partial^2}{\partial x^2} + \frac{\partial^2}{\partial y^2} + \frac{\partial^2}{\partial z^2}$

∇ = gradient operator, $\nabla = \frac{\partial}{\partial x}\vec{i} + \frac{\partial}{\partial y}\vec{j} + \frac{\partial}{\partial z}\vec{k}$

λ = mobility, 1/cP (1/Pa·s)

λ_L = liquid mobility, $(\lambda_o + \lambda_w)$ 1/cP (1/Pa·s)

λ_T = total mobility of all fluids $(\lambda_o + \lambda_g + \lambda_w)$ 1/cP (1/Pa·s)

ϕ = porosity, fraction

μ = viscosity, cP (Pa·s)

μ_j^* = low pressure pure component viscosity, Equations (IV-25), (IV-26), cP (Pa·s)

μ^* = low pressure mixture viscosity, Equation (IV-29) cP (Pa·s)

ρ = mass density, lbm/ft^3 (kg/m^3)

$\bar{\rho}$ = molar density, lbm mol/ft^3 (kmol/m^3)

$\bar{\rho}_c$ = critical density of a mixture, lbm mol/ft^3 (kmol/m^3)

ρ_r = reduced density, $\bar{\rho}/\bar{\rho}_c$

$\rho(p)$ = mass density function of pressure, lbm/ft^3 (g/cm^3) (kg/m^3)

σ = interfactial tension, dynes/cm (N/m)

Φ = potential, psia (Pa)

Φ_h = Hubbert's potential, psia (Pa)

ψ_i = fugacity coefficient of component i,
$\psi_i^V = f_i^V/y_i\ p$ or $\psi_i^L = f_i^L/x_i\ p$

ω = acentric factor

Superscripts

$n+1$ = new time level

n = old time level

L = liquid

V = vapour

ν = iteration number

T = transpose

Subscripts

AV = average

c = critical property

g = gas

i,j = component number

i,j = grid block indices

ℓ,k = grid block indices

ℓ = phase, block index

L = liquid

o = oil

p = phase

r = reduced property

ref = reference property or variable

s = surface conditions

T = total

V = vapour

w = water

x, y, z = coordinate directions

Difference Operators

$$\Delta T''\Delta p = \Delta_x T''_x \Delta_x p + \Delta_y T''_y \Delta_y p + \Delta_z T''_z \Delta p$$

where for example,

$$\Delta_x T''_x \Delta_x p = T''_{x,i+\frac{1}{2}}(p_{i+1} - p_i) - T''_{x,i-\frac{1}{2}}(p_i - p_{i-1})$$

and $T''_{x,i+\frac{1}{2}}$ is the x-direction transmissibility between grid block i and $i+1$.

CHAPTER I

INTRODUCTION

High pressure gas drives – condensing and vaporizing gas drives, miscible slug processes, nitrogen drives – have received a great deal of attention over the past 35 years, and are among the first enhanced oil recovery techniques to be tested intensively in both the laboratory and the field. Following the Suez crisis in 1955, many high pressure gas drive projects were initiated, a few of which are still in operation. These include the gravity stabilized miscible drives in Alberta, the Hassi Massoud miscible drive in Algeria, and several gas drives in the U.S.A. High pressure gas drives have gained increased importance in recent years with the growing emphasis on nitrogen drives.

Numerical simulation of high pressure drives is still in a state of development, and its large scale implementation awaits the next generation of computers. Nevertheless, a number of "compositional" simulators have been reported for this purpose, but their use is limited to simulations of laboratory experiments or of elements of symmetry of well patterns. The present effort represents a step in this direction. It is intended to develop and test a state-of-the-art compositional simulator, capable of simulating multidimensional, three-phase, multicomponent flow in a porous medium. The simulator features a built-in equation of state, numerical derivatives (as opposed to analytical) in the Jacobian, and other refinements. A number of test problems are run to show the capability of the simulator, and also to point out the various areas of concern requiring future development.

CHAPTER II

LITERATURE REVIEW

Compositional effects in the flow of fluids in a porous medium and their mathematical representation have been the subject of many studies since 1950. Each study has contributed to the evolution of the present compositional simulators. The use of an equation of state to predict the phase behaviour of reservoir oils and the development of methods to predict the complete phase envelope of a system were the first steps taken toward the development of a new type of compositional simulator, which also included the phase equilibrium condition.

With the incorporation of an equation of state in the compositional simulators[16] several problems were resolved: lack of convergence close to the critical point due to the inconsistency of the existing correlations of density and viscosity for oil and gas, and the not smooth or continuous thermodynamic derivatives at this point. The solution of these problems led to the development and application of better methods of solution for the highly nonlinear partial differential equations of a compositional model.

Compositional models can be classified into two groups based on whether they include an equation of state (EOS) or fugacity relations for phase equilibrium conditions.

The following models belong to the first group which do not contain an EOS: Jacoby and Berry[24], Welge et al.[61], Attra[4], Kniazeff et al.[27], McFarlane et al.[30], Price-Donohue[41], Roebuck et al.[46,47], Nolen[36], Culham-Farouq Ali[13], Van Quy et al.[57,72],

Tsutsumi[56], and Kazemi[26]. The compositional simulators of Fussell and Fussell[16], Coats[10], Nghiem et al.[33], Young et al.[62], and Chien[9] form the second category with an equation of state incorporated.

Next, a brief description of the earlier simulators and a comparative study of the latest models is presented.

Jacoby and Berry[24] presented a tank-type model (compositional balance), which assumed uniform pressure and saturation in the reservoir and used vapour-liquid equilibrium to simulate a vaporization process. They demonstrated the need for using such methods for certain reservoir calculations.

Welge et al.[61] presented a one-dimensional linear model for the displacement of oil by an enriched gas. They assumed incompressible fluids, pressure constant or nearly constant, and a constant injection rate. Saturation profiles were divided into five moving regions and for each a flow equation was written. The method was based on an analogy between a three-component and a multicomponent system.

Attra[4] studied the gas cycling mechanism, and was first to report the effect of mass transfer on the gas displacement process. He simulated a one-dimensional flow system by a series of cells in which each of the fluids were equilibrated during a time step. In addition, the pressure throughout the system was predetermined and constant phase velocities were calculated according to the Buckley-Leverett incompressible fluid flow model.

Kniazeff and Naville[27] developed a one-dimensional radial model to simulate depletion of a gas condensate reservoir, thus

introducing pressure effects and saturation gradients into the model. Even though they considered two-phase flow composed of two components, the properties of the components were determined from pressure dependent functions.

McFarlane[30] developed a one-dimensional linear model, considering pressure effects, to study gas injection into a depleted oil reservoir. He did not consider hydrocarbon components on an individual basis; rather he considered the flow process as consisting of two distinct phases, oil and gas. The properties of the phases depended on pressure and composition. The model considered the coefficients of the pressure equation at time level n.

A comparative study is presented next, which considers the following points:

1. Mathematical formulation
2. Treatment of nonlinearity
3. Method of solution.

II.1 Mathematical Formulation

The general mathematical model is presented in Chapter IV. Equation (IV.1) presents the general molar balance equations, Equations (IV-3) and (IV-7) present the definition of potential and potential gradient for any phase. Equations (IV-8) to (IV-10) present Darcy's Law for the oil, gas and water phases. Equation (IV-11) presents the saturation constraint, and Equations (IV-12) through (IV-16) present the composition constraints and capillary pressure relation.

Phase equilibria are given by Equation (IV-17), or the fugacity equality condition if an equation of state is used; otherwise, the

following flash equilibrium equations are used:

$$F_L + F_V = 1, \tag{II-1}$$

$$z_i = F_L x_i + F_V y_i, \qquad i = 1, \ldots n_c \tag{II-2}$$

$$K_i = y_i / x_i, \qquad i = 1, \ldots n_c \tag{II-3}$$

$$x_i = \frac{z_i}{1 + F_V(K_i - 1)}, \qquad i = 1, \ldots n_c \tag{II-4}$$

$$\sum_{i=1}^{n_c} \frac{z_i(K_i - 1)}{1 + F_V(K_i - 1)} = 0, \tag{II-5}$$

$$F_L = \frac{\bar{\rho}_o S_o}{\bar{\rho}_o S_o + S_g \bar{\rho}_g}, \tag{II-6}$$

and

$$F_V = \frac{\bar{\rho}_g S_g}{\bar{\rho}_o S_o + \bar{\rho}_g S_g}. \tag{II-7}$$

The initial and boundary conditions required for the solution of the mathematical model are pressure, temperature and initial component concentration distributions over the entire reservoir. Boundary conditions are those derived from the condition that reservoir boundaries are impermeable to fluid flow.

The normally used assumptions are:

1. Isothermal, three-phase flow, consisting of n_c hydrocarbon components;

2. Water and hydrocarbon phases are mutually insoluble;

3. Phase equilibrium is attained within any element of the reservoir;

4. Diffusional effects are negligible.

Price-Donohue[41] Model

Consider two-phase, linear, horizontal and viscous flow. Assume capillarity and gravity are negligible. Applying these assumptions to the general equation (IV-1) and combining the flash equilibrium equations in order to obtain the partial differential equation in which the hydrocarbon component concentration, z_i, are the dependent variables, we have:

$$k \frac{\partial}{\partial x}\left[\frac{\rho_o k_{ro}}{\mu_o M_o} + \frac{\rho_g k_{rg}}{\mu_g M_g} K_i\right] \frac{z_i}{1 + F_V(K_i - 1)} \frac{\partial p}{\partial x} = \phi \frac{\partial}{\partial t}\left[\left(\frac{\rho_o S_o}{M_o} + \frac{\rho_g S_g}{M_g}\right) z_i\right],$$

$$i = 1,2,\ldots n_c \qquad \text{(II-8)}$$

$$\sum_i^{n_c} z_i = 1, \qquad \text{(II-9)}$$

$$S_o + S_g = 1, \qquad \text{(II-10)}$$

and

$$\sum_{i=1}^{n_c} \frac{z_i}{1 + F_V(K_i - 1)} = 1. \qquad \text{(II-11)}$$

The unknowns for this system of equations are $\frac{\partial p}{\partial x}$, z_i, and S_o. The boundary conditions are:

1. The molar flow rate and composition of the injected vapour is specified at the inlet. At the outlet, the fluid is produced at constant pressure.

Roebuck et al.[47] Model

Roebuck et al. presented a one-dimensional, linear-flow model, with the four assumptions listed previously. Water-oil capillary pressure was included but gravity was ignored. The fugacity conditions were not considered.

Applying these assumptions one can obtain

$$\frac{\partial}{\partial x}\left(k\,\frac{k_{ro}}{\mu_o}\rho_o Co_i\,\frac{\partial p_o}{\partial x} + k\,\frac{k_{rg}}{\mu_g}\rho_g Cg_i\,\frac{\partial p_g}{\partial x}\right) + q_o^*\rho_o Co_i + q_g^*\rho_g Cg_i$$

$$= \phi\,\frac{\partial}{\partial t}\,(S_o\rho_o Co_i + S_g\rho_g Cg_i), \quad i = 1,2,\ldots n_c \qquad \text{(II-12)}$$

where Co, Cg are mass fractions and q_o^* and q_g^* are volumetric flow rates per unit pore volume. The following relations complete the system of equations:

$$\sum_{i=1}^{n_c} Co_i = \sum_{i=1}^{n_c} Cg_i = 1, \qquad \text{(II-13)}$$

and

$$P_{cow} = p_o - p_w; \qquad \text{(II-14)}$$

Water mass balance:

$$\frac{\partial}{\partial x}\left(k\,\frac{k_{rw}}{\mu_w}\rho_w\,\frac{\partial p_w}{\partial x}\right) = \phi\,\frac{\partial}{\partial t}\,(S_w\rho_w) \qquad \text{II-15)}$$

These equations were differentiated first, and then discretized for numerical solution.

The unknowns are: Co_i, Cg_i, S_o, S_g, S_w, P_o and P_w. The boundary conditions are:

1. Specification of mass rate. If it is injection, the mass fraction or composition is given. If it is production the mass-fraction is consistent with the concentration of the components in the oil and gas phases present at the production point.
2. The pressure P_o is specified at the end of the region.

Culham-Farouq Ali[13] Model

Culham and Farouq Ali considered one- and two-dimensional two-phase flow (oil-gas) of a two-hydrocarbon mixture. Capillary forces, gravity and diffusional effects were neglected. Mass transfer between phases was implicitly accounted for in the formulation. Applying these assumptions to Equation (IV-1), one can obtain for n_c hydrocarbon components:

$$\nabla \cdot \left[k \left(\frac{k_{ro} \bar{\rho}_o}{\mu_o} + K_i \frac{k_{rg} \bar{\rho}_g}{\mu_g} \right) x_i \nabla p \right] + q_i^* = \phi \frac{\partial}{\partial t} [(S_o \bar{\rho}_o + S_g \bar{\rho}_g K_i) x_i], \quad i = 1,2,\ldots n_c \qquad \text{(II-16)}$$

The equation can be written in the following dimensionless form:

$$\nabla \cdot [A_i \nabla P] = [B_i - C_i] \frac{\partial S_o}{\partial \tau} + D_i \frac{\partial P}{\partial \tau} + \sum_{j=3}^{n_c} E_{i,j} \frac{\partial x_i}{\partial \tau}, \quad i = 1,2,\ldots n_c \qquad \text{(II-17)}$$

Given the assumption of only two hydrocarbon components, the last term of Equation (II-17) disappears. The coefficients A_i, D_i are

functions of pressure and saturation, and B_i, C_i are functions of pressure only, and are described in the original paper.

K-values were taken to be functions of pressure only. The boundary conditions for depletion were:

$$1.\quad \left.\frac{\partial P}{\partial x}\right|_{x=0} = 0.0, \quad \tau \geq 0 \tag{II-18}$$

$$2.\quad P(1,\tau) = f(\tau), \quad \tau \geq 0 \tag{II-19}$$

Van Quy et al.[57] Model

Van Quy et al. considered a one-dimensional, linear model, with multicomponent, two-phase flow (oil-gas). Diffusion was taken into account, while gravity and capillary pressure were neglected.

Applying the above assumptions, the equations become:

$$\frac{\partial}{\partial x}\left(k\ \frac{k_{ro}}{\mu_o}\frac{\rho_o}{M_o}M_i x_i \frac{\partial p}{\partial x} + \phi S_o D_{i,o}\frac{\partial}{\partial x}\left[\frac{\rho_o}{M_o}M_i x_i\right]\right)$$

$$+\frac{\partial}{\partial x}\left(k\ \frac{k_{rg}}{\mu_g}\frac{\rho_g}{M_g}M_i y_i \frac{\partial p}{\partial x} + \phi S_g D_{i,g}\frac{\partial}{\partial x}\left[\frac{\rho_g}{M_g}M_i y_i\right]\right)$$

$$= \phi\frac{\partial}{\partial t}\left(S_o\frac{\rho_o}{M_o}M_i x_i + S_g\frac{\rho_g}{M_g}M_i y_i\right), \quad i = 1,\ldots n_c \tag{II-20}$$

where D is the diffusion coefficient in a porous medium. For this case, D is not function of velocity. It was assumed that the components in each phase have the same diffusion coefficient, i.e., $D_{ij} = D_j$. Equations (II-3), (II-4) and the saturation constraints were substituted in (II-20) in order to obtain an equation with z_i as variable:

$$\frac{\partial}{\partial x}\left[\frac{k}{\phi}\alpha_i\frac{\partial p}{\partial x}z_i + S_g D_g \frac{\partial}{\partial x}(\beta_i z_i) + (1-S_g)D_o\frac{\partial}{\partial x}(\gamma_i z_i)\right]$$

$$= \frac{\partial}{\partial t}\left(\frac{\rho_g S_g}{M_g} + \frac{\rho_o S_o}{M_o}\right)z_i, \quad i = 1,\ldots n_c \qquad \text{(II-21)}$$

The coefficients α_i and β_i are given in the original paper. Other relations needed are:

$$\sum_{i=1}^{n_c} y_i - x_i = 0, \qquad \text{(II-22)}$$

$$\sum_{i=1}^{n_c} z_i = 0. \qquad \text{(II-23)}$$

This system of equations was solved for S_g, $\frac{\partial p}{\partial x}$ and z_i.

Boundary Conditions were:

1. rate of injection and z_i at inlet end given
2. constant pressure at the outlet.

Tsutsumi-Dixon[56] Model

Tsutsumi and Dixon considered two-dimensional, two-phase flow (oil-gas). Capillary pressure and gravity were taken into account. Diffusion effects were neglected. The K-values were considered to be a function of convergence pressure. With the above assumptions the equation of mass (mole) conservation becomes:

$$\nabla\cdot(T_g y_i \nabla\phi_g) + \nabla\cdot(T_o x_i \nabla\phi_o) + q_i^* = \phi\frac{\partial}{\partial t}[(\bar{\rho}_g S_g + \bar{\rho}_o S_o)z_i]$$

$$i = 1,\ldots n_c \qquad \text{(II-24)}$$

where

$$\nabla\phi_\ell = \nabla p_\ell - \gamma_\ell \nabla D, \quad \ell = o,g \qquad \text{(II-25)}$$

and

$$T_\ell = \bar{\rho}_\ell\, k\, \frac{k_{r\ell}}{\mu_\ell}, \quad \ell = o,g \qquad \text{(II-26)}$$

$$F_V(\tilde{\rho}_g S_g + \tilde{\rho}_o S_o) = \tilde{\rho}_g S_g, \qquad \text{(II-27)}$$

$$F_L(\tilde{\rho}_g S_g + \tilde{\rho}_o S_o) = \tilde{\rho}_o S_o \qquad \text{(II-28)}$$

$$\text{and} \quad \sum_{i=1}^{n_c} z_i = 1. \qquad \text{(II-29)}$$

Substituting Equation (II-27) into Equation (II-24) and using Equation (II-29) the gas pressure equation is formed:

$$F_V^{n+1} \left[\Delta T_o \, \Delta \phi_o + \Delta T_g \Delta \phi_g + Q \right]^{n+1}$$

$$= \frac{V_p}{\Delta t} \left[(\tilde{\rho}_g S_g)^{n+1} - F_V^{n+1} (\tilde{\rho}_g S_g + \tilde{\rho}_o S_o)^n \right] \qquad \text{(II-30)}$$

where $Q_i = \sum_{i=1}^{n_c} q_i^* \, \Delta x \, \Delta y \, \Delta z$.

The oil pressure equation is formed similarly. From Equation (II-24) z_i^{n+1} can be obtained. The implicit term $(\tilde{\rho}_g S_g + \tilde{\rho}_o S_o)^{n+1}$ is eliminated using Equation (II-30) and the equivalent oil pressure equation.

The unknowns are: p_o, p_g, S_o, S_g and z_i.

Kazemi et al.[26] Model

Kazemi et al. considered three dimensional, three-phase multi-component flow. Capillary forces and gravity were included. The K-values were considered to be functions of pressure and composition.

Taking into consideration the above assumptions, the hydrocarbon molar balance equation is given by Equation (II-24).

The authors considered a water volume balance, which may be written as follows:

$$\nabla \cdot [T_w(\nabla p_w - \gamma_w \nabla D)] + q_w^* = \frac{\partial}{\partial t}\left(\phi \frac{S_w}{B_w}\right), \qquad \text{(II-31)}$$

where

$$T_w = k \frac{k_{rw}}{\mu_w B_w}, \qquad \text{(II-32)}$$

and B_w is the formation volume factor of water. The hydrocarbon molar balance equation is summed over all components and multiplied by

$$\alpha(p_o) = \frac{1}{B_w}\left(\frac{S_g + S_o}{\delta_g S_g + \delta_o S_o}\right)^{n+1}, \qquad \text{(II-33)}$$

and added to the water equation, in order to obtain one equation in p_o, with the use of a capillary pressure relation.

Following the Tsutsumi-Dixon[56] procedure, the equation for z_i^{n+1} is formed.

The unknowns are: p_o, p_g, p_w, S_o, S_g, S_w and z_i.

Fussell and Fussell[16] Model

Fussell and Fussell were the first to introduce an equation of state into a compositional model. They considered three dimensions, and three-phase flow in a porous medium. Capillary and gravity forces

were included.

The mass (mole) conservation equation is presented below, after applying the above assumptions.

1. The hydrocarbon component molar balance is given by Equation (II-24)

2. The total hydrocarbon molar balance equation is

$$\nabla \cdot (T_g \nabla \phi_g) + \nabla \cdot (T_o \nabla \phi_o) + \sum_{i=1}^{n_c} q_i^* = \frac{\partial}{\partial t} [\phi(\bar{\rho}_g S_g + \bar{\rho}_o S_o)], \qquad \text{(II-34)}$$

3. The water molar balance equation is

$$\nabla \cdot (T_w \nabla \phi_w) + q_w^* = \frac{\partial}{\partial t} (\phi(\bar{\rho}_w S_w)) . \qquad \text{(II-35)}$$

4. The saturation constraint is transformed as:

$$\frac{RT}{p} (LZ_L + VZ_V + WZ_V) = 1, \qquad \text{II-36)}$$

The densities of all phases are calculated by $\bar{\rho} = \frac{p}{ZRT}$ where L,V,W are the moles per unit pore volume, i.e.,

$$L = \bar{\rho}_o S_o , \qquad \text{(II-37)}$$

$$V = \bar{\rho}_g S_g , \qquad \text{(II-38)}$$

$$W = \bar{\rho}_w S_w . \qquad \text{(II-39)}$$

5. The fugacity constraints are

$$fi^L = fi^V, \quad i = 1,2,\ldots n_c . \qquad \text{(II-40)}$$

The independent variables or unknowns are: L,V,W,p_o,p_g,p_w,x_i and y_i.

$i = 1,2,\ldots n_c$.

Young et al.[62] Model

Young et al. followed the Fussell and Fussell approach. They invoked the same assumptions from the molar balance equations and introduced the variables F and W, where

$$F = \bar{\rho}_o S_o + \bar{\rho}_g S_g , \qquad \text{(II-41)}$$

and

$$W = \bar{\rho}_w S_w . \qquad \text{(II-42)}$$

and the saturation constraint equation is transformed as follows:

$$F\left[\frac{(1-F_V)}{\bar{\rho}_o} + \frac{F_V}{\bar{\rho}_g}\right] - \frac{W}{\bar{\rho}_w} = 1, \qquad \text{(II-43)}$$

where F_V is the gas molar fraction: $F_V + F_L = 1$. The unknowns are: F, W, F_V, p_o, p_g, p_w and z_i .

Nghiem et al.[33] Model

The Nghiem et al. model employs the same assumptions as the Fussell et al. model and introduces interfacial tension in relative permeability curves.

The system of equations is:

1. The hydrocarbon molar balance equation, Equation (II-24)
2. The total hydrocarbon molar balance equation, Equation (II-34)
3. The water molar balance equation, Equation (II-35)

4. The saturation constraint equation, Equation (IV-11)
5. The fugacity constraint equations, Equation (II-40).

The water equation is multiplied by a factor:

$$\theta = \frac{\bar{\rho}_o S_o + \bar{\rho}_g S_g}{\bar{\rho}_o (S_o + S_g)} , \qquad \text{(II-44)}$$

which is evaluated at the initial time in a grid block and remains constant for the time step. The water equation is summed with the total hydrocarbon molar balance equation to obtain one equation for pressure (similar to the Kazemi et al. model).

The unknowns are: $p_o, p_g, p_w, S_o, S_g, S_w$ and z_i.

Coats[10] Model

Coats invoked the same assumptions as Young et al.[62] and Fussell et al.[16].

The system of equations is:

1. The hydrocarbon molar balance equation, Equation (II-24)
2. The water molar balance equation, Equation (II-35)
3. The capillary pressure relations, Equation (II-25)
4. The saturation and composition constraint equations, Equations (II-11), (II-12), (II-13)
5. The fugacity constraint equations, Equation (II-40).

The unknowns are: $S_o, S_g, S_w, x_i, y_i, p_o, p_g$ and p_w.

Chien et al.[9] Model

Chien considered three-dimensional, multiphase flow in a porous medium. Capillary and gravity forces were neglected. They assumed that a single water phase composed only of water coexisted with N_p hydrocarbon phases composed of n_c hydrocarbon components.

With the above assumptions, the mass conservation equations can be written as:

1. The water molar equation

$$\nabla \cdot [T_w \nabla p] + q_w^* = \frac{\partial}{\partial t} (\phi z_w') , \qquad \text{(II-45)}$$

2. The hydrocarbon molar balance equation

$$\nabla \cdot \left[\sum_{J=1}^{N_p} T_j x_{ij} \nabla p \right] + q_i^* = \frac{\partial}{\partial t} (\phi z_i'), \quad i = 1, \ldots n_c \qquad \text{(II-46)}$$

where z_i' and z_w' are hydrocarbon and water concentrations (moles/L^3), and x_{ij} is the mole fraction of component i in phase j.

The fugacity equalities are

$$f_{ij} = f_{il} , \quad j = 2, \ldots N_p \text{ and } i = 1, \ldots n_c . \qquad \text{(II-47)}$$

The constraint equations are

$$\sum_{i=1}^{n_c} x_{ij} = 1, \quad j = 1, \ldots N_p \qquad \text{(II-48)}$$

and

$$\sum_{J=1}^{N_p} S_j + S_w = 1. \qquad \text{(II-49)}$$

The saturation constraint can be expressed as

$$\sum_{J=1}^{N_p} (F_j/\bar{\rho}_j) + z_w/\rho_w = 1\,, \qquad \text{(II-50)}$$

where F_j is the phase concentration, and the overall amount of component i in a grid block, z_i, is expressed as

$$z_i = \sum_{j=1}^{N_p} F_j x_{ij}, \quad i = 1,\ldots n_c\,. \qquad \text{(II-51)}$$

The unknowns are: z_i, x_{ij}, F_j, z_w and p.

II.2 Treatment of Nonlinearities

The treatment of nonlinearities or nonlinear coefficients is very important in the solution of a system of partial differential equations. The method of solution for the system of equations depends strongly on it.

The nonlinearities appearing in the differential equations can be classified as weak nonlinearities, such as density, gravity, viscosity; or as strong nonlinearities, such as mole fraction, relative permeability, and capillary pressure.

Tables II.1 through II.5 present the different approximations in space and time that have been used in the various compositional models reported.

The following expressions are often used to approximate the various nonlinearities in space: U denotes any property such as gravity, density, viscosity, or mole fraction of a phase.

1. Average

$$U_{\ell_{i+\frac{1}{2}}} = 0.5(U_{\ell_i} + U_{\ell_{i+1}}), \quad \ell = o,g,w \qquad \text{(II-52)}$$

2. One-point Upstream

$$U_{\ell_{i+\frac{1}{2}}} = \begin{cases} U_{\ell_i} & \text{for flow from } i \text{ to } i+1 \\ U_{\ell_{i+1}} & \text{for flow from } i+1 \text{ to } i \end{cases} \qquad \text{(II-53)}$$

3. Two-point Upstream

This approximation applies to relative permeability or mobility of a phase ℓ[55].

$$\lambda_{\ell_{i+\frac{1}{2}}} = \begin{cases} (1+a_i)\lambda_{\ell_i} - a_i\lambda_{p_{i-1}} \\ \quad \text{for flow from } i \text{ to } i+1 \\ (2-a_{i+1})\lambda_{p_{i+1}} - (1-a_{i+1})\lambda_{\ell_{i+2}} \\ \quad \text{for flow from } i+1 \text{ to } i \end{cases} \qquad \text{(II-54)}$$

where a_i and a_{i+1} are geometric factors.

The implementation of two-point upstream relative permeability or mobilities in fully implicit simulators would drastically increase the bandwidth of the Jacobian matrix[55]. Thele et al.[54] made a comparison using Young[62] and Nghiem[33] formulations with one-point and two-point upstream for a multicontact miscible displacement,

showing a reduction in numerical dispersion in the composition profiles of methane and decane and composition paths.

Other schemes have been proposed by Au et al.[5] and Wheatley[60] but none of them has been implemented in compositional simulators. The time approximation of nonlinearities can be:

1. Explicit

$$U_\ell^{n+1} = U_\ell^n, \quad \ell = o,g,w \tag{II-55}$$

where U_ℓ can be density, gravity, viscosity, mole fraction, relative permeability or capillary pressure.

2. Implicit

The nonlinear terms or coefficients can be obtained using a simple iteration method, i.e.:

$$U_\ell^{n+1} = U_\ell^\nu, \quad \ell = o,g,w \tag{II-56}$$

where ν is the iteration number, and U_ℓ can be density, gravity, viscosity, or mole fractions. For the highly implicit formulation the nonlinear terms can be represented by expansion using a Taylor series:

$$U_\ell^{n+1} = U_\ell^n + \frac{\partial U_\ell}{\partial X} \underline{\delta X}, \quad \ell = o,g,w \tag{II-57}$$

where X can be a single variable or a vector of variables depending on U.

This time treatment has been reported[11] for relative permeability and capillary pressure. The oil relative permeability as a function of oil and gas saturation and the water and gas relative permeabilities

TABLE II.1

APPROXIMATION OF NONLINEAR TERMS

DENSITY OF PHASES

Author	Space Approximation		Time Approximation		
	Upstream	Average	n	n+½	n+1
Price-Donohue[41]	*[2]			*[1]	
Roebuck et al.[47]	*[2]				*
Culham-Farouq Ali[13]		*		*	
Van Quy et al.[57]	*[2]			*	
Tsutsumi-Dixon[56]	*		*		
Nolen[36]	*		*		
Kazemi et al.[26]		*	*		
Fussell-Fussell[16]		*	*		
Coats[10]	*				*
Nghiem et al.[33]	*		*		
Young et al.[62]	*		*		
Chien et al.[9]	*				*

*Not mentioned

[1]Average between n and n+1

[2]Determined at centre of block i

TABLE II.2

APPROXIMATION OF NONLINEAR TERMS

VISCOSITY OF PHASES

Author	Space Approximation		Time Approximation		
	Upstream	Average	n	n+½	n+1
Price-Donohue[41]	*[2]			*[1]	
Roebuck et al.[47]	*[2]				*
Culham-Farouq Ali[13]		*		*	
Van Quy et al.[57]	*[2]			*	
Tsutsumi-Dixon[56]	*		*		
Nolen[36]	*		*		
Kazemi et al.[26]		*	*		
Fussell-Fussell[16]		*	*		
Coats[10]	*				*
Nghiem et al.[33]	*		*		
Young et al.[62]	*		*		
Chien et al.[9]	*				*

*Not mentioned

[1]Average between n and n+1

[2]Determined at centre of block i

TABLE II.3

APPROXIMATION OF NONLINEAR TERMS

COMPOSITION OF PHASES

Author	Space Approximation		Time Approximation		
	Upstream	Average	n	$n+\frac{1}{2}$	n+1
Price-Donohue[41]	*[2]			*[1]	
Roebuck et al.[47]	*[2]				*
Culham–Farouq Ali[13]		*		*	
Van Quy et al.[57]	*[2]			*	
Tsutsumi–Dixon[56]	*				
Nolen[36]	*		*		
Kazemi et al.[26]	+		*		
Fussell–Fussell[16]	+		*		
Coats[10]	*				*
Nghiem et al.[33]	*		*		
Young et al.[62]	*		*		
Chien et al.[9]	*				*

+Not mentioned

[1]Average between n and n+1

[2]Determined at centre of block i

TABLE II.4

APPROXIMATION OF NONLINEAR TERMS

RELATIVE PERMEABILITY OF PHASES

Author	Space Approximation		Time Approximation		
	1-pt Upstream	2-pt Average	n	n+½	n+1
Price-Donohue[41]	*[2]			*[1]	
Roebuck et al.[47]	*[2]				*
Culham – Farouq Ali[13]	*			*	
Van Quy et al.[57]	*[2]			*	
Tsutsumi–Dixon[56]	*		*		
Nolen[36]	*		*		
Kazemi et al.[26]		+	*		
Fussell–Fussell[16]		+	*		
Coats[10]	*				*
Nghiem et al.[33]	*	*	*		
Young et al.[62]	*		*		
Chien et al.[9]	*				*

+Not mentioned

[1]Average between n and n+1

[2]Determined at centre of block i

are considered to be functions of water and gas saturation, respectively. The water-oil and gas-oil capillary pressures are considered to be functions of water and gas saturation, respectively.

II.3 Method of Solution

The methods that have been implemented to solve the system of difference equations of compositional models can be classified into:

1. Extended IMPES solution
2. Variation of the sequential solution method
3. Simultaneous solution method
4. Iterative method

1. Extended IMPES solution

This method uses the explicit form in the approximation of the nonlinear terms (transmissibility and capillary pressure at level n). This method suffers from instability problems. The hydrocarbon molar balance equation is summed over the n_c hydrocarbon components to form the total hydrocarbon equation in which x_i, y_i and z_i do not occur explicitly. This last equation is multiplied by a conversion factor and added to the water balance equation in order to form the pressure equation which is then linearized by Newton's method and solved over the entire grid for oil pressure by direct methods. The water saturation is computed explicitly from the water balance equation.

The overall composition z_i of each component is calculated explicitly. This equation is formed as originally proposed by Tsutsumi[56]: z_i is obtained from the hydrocarbon molar balance equation, and the implicit terms of $(S_o\bar{\rho}_o + S_g\bar{\rho}_g)^{n+1}$ are substituted

from the total hydrocarbon equation.

The iterative solution algorithm is as follows:

1. Solve for oil pressure over the entire grid by direct methods.
2. Solve for water saturation explicitly.
3. Solve for overall composition z_i explictly.
4. Flash the hydrocarbon mixture to obtain the compositions and saturations of oil-gas phases.
5. If convergence is not achieved the procedure is repeated again.

Kazemi et al.[26] and Nghiem et al.[33] presented this method for their formulation of compositional models. They differed in two aspects:

1. Kazemi used a water volume balance equation, while Nghiem used a water molar balance; therefore, the scaling factors used are different.
2. Both models neglect several terms in the linearization of the accumulation term of the pressure equation since an exact Jacobian is not necessary for convergence. Both authors differed in this linearization. Sometimes the approximate Jacobian may produce oscillations in the iterate values. Mansoori[29] proposed the use of numerical derivatives to avoid this problem, and Nghiem[34] suggested damping the pressure iterates.

Nghiem[32] proposed a new approach to the quasi-Newton methods for nonlinear equations called the quasi-Newton successive substitution method (QNSS) with application to compositional model. The use of QNSS does not require the computation nor the inversion of the Jacobian matrix at every iteration. This new method is applied to the solution

of the pressure equation associated with a compositional model. The author claimed improvement in convergence compared with the earlier described technique.

2. Variation of the sequential solution method

This method consists in reducing the unknowns $2n_c + 4$ to $n_c + 1$ by two procedures: applying the minimum variable Newton's Method (MVNR) or by the selection of the variables. Then, the system of difference equations is linearized as a function of the $n_c + 1$ variables by Newton's method, obtaining

$$J^{\nu}\delta X = -F^{\nu} \qquad \text{(II-57)}$$

where J is the Jacobian matrix of the linearized equations and F is the residual vector of those equations. The Jacobian and residual vector are evaluated at the last iteration ν; δX is the vector of the unknowns, the last unknown being the pressure.

The method of solution is as follows:

1. A pressure equation, for each grid block, is obtained from Equation (II-57) by Gaussian elimination of all unknowns other than (δp). The resulting system of N_t equations in N_t unknowns is solved by direct or iterative methods. Capillary pressure and transmissibities are explicit.

2. Other unknowns for each grid block are solved by back substitution, i.e., explicitly.

3. Convergence is attained where the residual is less than the tolerance, $|S_o^{\nu+1} - S^{\nu}| \leq \varepsilon$ and $|p^{\nu+1} - p^{\nu}| \leq \varepsilon$.

Fussell and Fussell[16] were the first to apply the MVNR method to compositional models. Applying this method, they reduced the number of unknowns from $2n_c + 4$ $(p, x_i, y_i, S_o, S_g, S_w)$ or (p, x_i, y_i, L, V, W) per grid block to $n_c + 1$ unknowns. These $n_c + 1$ unknowns depend on the type of fluid in each grid block: p, L, x_i for predominantly vapour, p, V, y_i for predominantly liquid and p for an undersaturated system.

Young et al.[62] used this sequential method. The procedure differs from that of Fussell et al. in the ordering of the equations and unknowns. Young[62] claimed that by this method a more strongly diagonally dominant Jacobian matrix is obtained.

They chose the unknowns of each grid block depending on:

1. If a grid block is two-phase, the unknowns are: p, W, F, V, z_i and y_i, $i = 1,2,\ldots n_c-1$. Due to the order of the equations, this system of equations is reduced to one equation with pressures as unknown from forward reduction.
2. If a grid block is single phase, the unknowns are: p, W, F and z_i, $i = 1,2,\ldots n_c-1$. The other variables are calculated by back substitution. Before starting a new iteration a flash calculation is made to obtain better estimates of V, L and densities.

3. Simultaneous solution method

This method of solution is used to solve highly or fully implicit models to obtain the most stable solution. This method of solution for difference equations is the most expensive one per time step, but the highly or fully implicit models can solve problems where other types of models may fail, or the machine time using such

simulators may be greater than that for a fully implicit model. The method of solution per time step is presented next.

In order to solve n_c+1 equations in n_c+1 unknowns Coats[10] proposed the following method:

The discretized $2n_c+4$ finite difference equations of a compositional model can be reduced by partial substitution to n_c+1 equations in n_c+1 unknowns, using the phase equilibria relations, since this system of equations does not have interblock terms. The solution method is as follows:

1. The $2n_c+4$ equations are linearized by Newton's method and are written as

$$J^{\nu}\delta X = -F^{\nu}, \qquad \text{(II-58)}$$

where J is the Jacobian matrix, δX is the vector of the unknowns and F the residual vector of the linearized equations and ν is the number of iterations.

2. The linearized composition constraint equations and fugacity equations are n_c+2 equations in $2n_c+1$ unknowns $\{x_i\}$, $\{y_i\}$ and p. Gaussian elimination is used to solve for n_c+2 unknowns in terms of the remaining n_c-1 unknowns.

$$\delta X_a = A^{\nu}\delta X_b + G^{\nu}. \qquad \text{(II-59)}$$

3. This equation and the saturation constraint equation are used to eliminate n_c+3 unknowns from the molar balance equations. The reduced equations can be written as:

$$J_1^{\nu}\delta X_c = -F_1^{\nu}, \qquad \text{(II-60)}$$

where $\delta X_c = (\delta y_3, \delta y_4 \ldots \delta y_{n_c}, \delta, P, \delta S_g, \delta S_o)$ is the vector of the primary unknowns. J_1 and F_1 are the reduced Jacobian matrix and the residual vector, respectively.

4. Solve Equation (II-60) by direct methods for δX_c and obtain the remaining unknowns δX_a by back substitution. The variables are updated by

$$X^{\nu+1} = X^{\nu} + \delta X . \qquad \text{(II-61)}$$

If convergence is not attained, all fluid and rock properties are recalculated and the procedure repeated again.

4. Iterative Methods

Culham—Farouq Ali[13] implemented the successive approximation method for the two-component, two-phase (oil-gas) model. They solved for pressure and saturation of each grid block simultaneously. The gas saturation and composition are calculated explicitly. The iteration process was terminated when the residual vector was less than a preset error.

Tsutsumi and Dixon[56] solved simultaneously two equations and the capillary pressure relations for the oil, and gas pressure and saturation. Then, they solved for the overall composition z_i explictly. The phase compositions and saturation were obtained from a flash calculation. If convergence was not attained the procedure was

repeated again. This method is very similar to the extended IMPES method. The methods differ in the form in which the pressures are calculated.

Price-Donohue[41] and Van Quy et al.[57] presented similar methods of solution. They solved for the pressure gradient such that $\Sigma z_i = 1$ for each grid block by a root search technique. Afterwards they solved for the overall composition explicitly. By flash equilibrium compositions of the phases and saturations were obtained. They repeated this procedure until convergence was obtained.

CHAPTER III

STATEMENT OF THE PROBLEM

Consider a one- or two-dimensional anisotropic porous medium sealed by an impermeable boundary. Initially, oil and gas and water exist in equilibrium in this system. It is assumed that hydrocarbons are not soluble in the water phase. Oil and gas phases are composed of n_c hydrocarbon components, where $n_c > 3$.

At time zero (initial condition), gas and/or water is injected, and oil/gas/water are produced against a specified back pressure or at a specified phase production rate. Effects of gravity and capillary pressure are taken into account.

Given the above conditions, the objectives of this study are:

1. To develop a fully implicit numerical simulator for compositional simulation, vaporization/condensation phenomena such as high pressure gas drive, and multicomponent gas drives, including high pressure nitrogen drive.
2. To carry out selected bench mark simulations to compare the results with the results previously reported for other simulators and for experimental laboratory displacements, consisting of the following:

   (i) Equilibrium two-phase displacement (slim tube displacement).

   (ii) Two-phase, condensing gas drive, immiscible displacement with mass transfer.

   (iii) Condensing gas multicontact miscible displacement.

3. To carry out selected test simulations to demonstrate the ability

of the model to perform certain types of simulations, consisting of the following:

(i) Condensing gas multicontact miscible displacement: one and two-dimensional runs.

(ii) Two-phase, condensing gas drive, immiscible displacement with mass transfer: one and two-dimensional runs.

(iii) Two-phase, vaporizing gas drive, immiscible displacement with mass transfer: one and two-dimensional runs.

CHAPTER IV

MATHEMATICAL DESCRIPTION OF THE COMPOSITIONAL MODEL

This section discusses the mathematical model developed to simulate multicomponent vaporizing or condensing miscible gas drives, or depletion performance of volatile oil or gas condensate reservoirs. The assumptions involved are presented. The phase equilibria model used (cubic equation of state) to account for compositional and pressure changes, is discussed.

IV.1 Assumptions

1. Isothermal three-phase flow of oil, gas, and water is simulated with oil and gas phases each consisting of three or more components. One or two-dimensional geometry is considered.
2. Water and the hydrocarbon phases are mutually insoluble.
3. Phase equilibrium is instantly attained within any element of the reservoir.
4. Mass transfer between the oil and gas phases for any hydrocarbon component is described by two-phase thermodynamic equilibrium (i.e. fugacity of component i in the liquid phase equals the fugacity of the same component in the gas phase, or the equality of the chemical potentials of the species over all the phases in which they occur).
5. Diffusional effects are negligible. Diffusional effects are neglected, because numerical dispersion is usually greater than physical dispersion.
6. Interfacial tension, gravity, capillary pressure, and rock compressibility are taken into account.

IV.2 Model Development

The general molar balance equation for each component i flowing in the oil, water and gas phases through a porous medium is given by

$$\nabla \cdot \left[k\left(x_i \bar{\rho}_o \frac{k_{ro}}{\mu_o}\right) \nabla \Phi_o + k\left(y_i \bar{\rho}_g \frac{k_{rg}}{\mu_g}\right) \nabla \Phi_g + k\left(x_{iw} \bar{\rho}_w \frac{k_{rw}}{\mu_w}\right) \nabla \Phi_w \right] + q_i^* = \frac{\partial}{\partial t} \left[\phi (x_i \bar{\rho}_o S_o + y_i \bar{\rho}_g S_g + x_{iw} \bar{\rho}_w S_w \right] . \quad \text{(IV-1)}$$

Potential Φ is based upon the definition of Hubbert's[22] potential Φ_h, and can be written as follows:

$$\Phi_h = \int_{p_i}^{p} \frac{dp}{\rho(p)} - gD, \quad \text{(IV-2)}$$

$$\Phi = \rho_{AV} \Phi_h = p - \gamma_{AV} D. \quad \text{(IV-3)}$$

where ρ_{AV} is the average density between the limits of the integral, and γ is the specific weight, defined as

$$\gamma = \rho \frac{g}{g_c} . \quad \text{(IV-4)}$$

Potential gradient for any phase is defined from Equation (IV-2) as

$$\nabla \Phi_h = \nabla p / \rho(p) - g \nabla D, \quad \text{(IV-5)}$$

$$\nabla \Phi = \rho(p) \nabla \Phi_h, \quad \text{(IV-6)}$$

$$\text{or} \quad \nabla \Phi = \nabla p - \gamma \nabla D. \quad \text{(IV-7)}$$

The generalized Darcy's law for each phase can be written as

$$u_o = - k \frac{k_{ro}}{\mu_o} \nabla \Phi_o, \qquad \text{(IV-8)}$$

$$u_w = - k \frac{k_{rw}}{\mu_w} \nabla \Phi_w, \qquad \text{(IV-9)}$$

$$\text{and} \quad u_g = - k \frac{k_{rg}}{\mu_g} \nabla \Phi_g . \qquad \text{(IV-10)}$$

The phase saturations are related by

$$S_o + S_g + S_w = 1, \qquad \text{(IV-11)}$$

and the composition constraints can be written as

$$\sum_i z_i = 1, \qquad \text{(IV-12)}$$

$$\sum_i x_i = 1, \qquad \text{(IV-13)}$$

and

$$\sum_i y_i = 1. \qquad \text{(IV-14)}$$

Capillary pressures are defined by

$$P_{cow} = p_o - p_w \qquad \text{(IV-15)}$$

and

$$P_{cgo} = p - p_o . \qquad \text{(IV-16)}$$

Phase equilibrium relations are given by the relation of the fugacities, i.e. the fugacity of component i in the liquid phase equals the fugacity of the same component in the gas phase

$$f_i^L = f_i^V, \quad i = 1,2, \ldots n_c. \tag{IV-17}$$

Taking account of the above assumptions, Equation (IV-1) takes the following form for the hydrocarbon components

$$\nabla \cdot k(x_i \bar{\rho}_o \lambda_o \nabla \Phi_o + y_i \bar{\rho}_g \lambda_g \nabla \Phi_g) + q_i^* = \frac{\partial}{\partial t} [\phi(x_i \bar{\rho}_o S_o + y_i \bar{\rho}_g S_g)],$$

$$i = 1,2, \ldots n_c \tag{IV-18}$$

where for a given phase, λ is defined by

$$\lambda = \frac{k_r}{\mu}. \tag{IV-19}$$

Equation (IV-1) for the water component becomes

$$\nabla \cdot (k \rho_w \lambda_w \nabla \Phi_w) + q_i^* = \frac{\partial}{\partial t} (\phi(\bar{\rho}_w S_w)),$$

$$i = n_c + 1. \tag{IV-20}$$

IV.3 Initial and Boundary Conditions

Initial conditions required for the solution of the mathematical model are pressure, temperature and initial component concentration distributions over the entire reservoir. Boundary conditions are that the normal derivatives of potential are zero on the boundaries, i.e. the reservoir boundaries are impermeable to fluid flow.

IV.4 Rock and Fluid Properties

IV.4.1 Rock Porosity

The rock porosity is taken to be a function of oil pressure,

$$\phi = \phi_{ref}(1 + c_f(p_o - p_{ref})) \qquad \text{(IV-21)}$$

where ϕ_{ref} is the rock porosity given at the reference pressure p_{ref}.

IV.4.2 Density

The oil and gas molar densities are considered to be functions of pressure, temperature and composition of the phase, and are calculated by the real gas law:

$$\bar{\rho}_\ell = \frac{p}{ZRT}, \qquad \ell = o,g \qquad \text{(IV-22)}$$

where Z, the compressibility factor, is calculated from the Peng-Robinson equation of state.

The molar density of the water phase is taken to be a function of pressure

$$\bar{\rho}_w = \bar{\rho}_{w_{ref}}(1 + c_w(p - p_{ref})). \qquad \text{(IV-23)}$$

As the oil, gas and water pahses are assumed to be in thermodynamic equilibrium, fluid properties are calculated at the gas pressure, which is one of the unknowns of the system.

IV.4.3 Viscosity

The water viscosity is assumed to be independent of pressure, and is calculated using the following equation

$$\frac{100}{\mu_w} = 2.4182[(T - 8.435) + \sqrt{8078.4 + (T - 8.435)^2} - 120], \quad \text{(IV-24)}$$

where T is temperature in °c.

Oil and Gas Viscosities

The method used for calculating oil and gas viscosities is a modification of the Lorenz-Bray-Clark[28] method, which uses the Stiel-Thodos correlation to account for the effect of composition, pressure and temperature on the viscosity of a hydrocarbon phase (liquid or gas).

The method consists of the following steps:

1. Calculation of the low pressure pure component viscosity by the Stiel-Thodos correlation[28].
2. Calculation of the low pressure mixture viscosity (μ^*) using the Herning and Zipperer equation[28].
3. Calculation of the density of the mixture (gas or liquid) at the temperature and pressure of interest using a cubic equation of state.
4. Calculation of the reduced density of the mixture using critical volume data for pure components.
5. Calculation of the viscosity of gas or liquid mixture at the pressure of the system by the Stiel-Thodos correlation[25].

1. Low pressure pure component viscosities (μ_j^*) are given by

$$\mu_j^* \, TMP_j = 34(10^5)T_{rj}^{0.94}, \quad T_{rj} \leq 1.5 \quad \text{(IV.25)}$$

$$\mu_j^* \, TMP_j = 17.78(10^5)(4.58T_{rj} - 1.67)^{5/8}, \quad T_{r_j} > 1.5 \quad \text{(IV-26)}$$

where $$T_{rj} = \frac{T}{T_{cj}} \quad \text{(Reduced temperature)} \,. \tag{IV-27}$$

and $$TMP_j = \frac{T_c^{1/6}}{(M_j^{1/2} p_{c_j}^{2/3})} \,. \tag{IV-28}$$

The result of the calculation is a table of values of μ_j^* for all pure components.

2. Low pressure mixture viscosity (μ^*)

Herning and Zipperer's equation is used to calculate the mixture viscosity for a liquid mixture:

$$\mu^* = \frac{\sum_{j=1} (x_j \mu_j \sqrt{M_j})}{\sum_{j=1} (x_j \sqrt{M_j})} \,. \tag{IV.29}$$

3. Density of the mixture (oil or gas phase) $\bar{\rho}$ at the pressure and temperature of interest is calculated using the Peng-Robinson equation of state.

4. Calculation of the reduced density of the mixture

1. Critical density of the mixture:

$$v_c' = \sum_j x_j v_{cj} \,, \tag{IV-30}$$

$$\bar{\rho}_c = \frac{1}{v_c'} \tag{IV.31}$$

2. Reduced density of the mixture:

$$\rho_r = \bar{\rho}/\bar{\rho}_c \,. \tag{IV-32}$$

5. Calculation of the viscosity of liquid/gas mixtures at the pressure and temperature of interest (μ):

$$[(\mu - \mu^*)MTP + 10^{-4}]^{1/4} = a_1 + b_1\rho_r + c_1\rho_r^2 + d_1\rho_r^3 + e_1\rho_r^4, \qquad \text{(IV-33)}$$

and

$$MTP = \frac{[\sum_{j=1} (x_j T_{cj})]^{1/6}}{[\sum_{j=1} (x_j M_j)]^{1/2} [\sum_{j=1} (x_j p_{cj})]^{2/3}}, \qquad \text{(IV-34)}$$

where a_1, b_1, c_1, d_1 and e_1 are coefficients, which can be calculated by adjusting experimental data or using the Stiel-Thodos coefficients. The Stiel-Thodos coefficients are:

$$a_1 = 0.1023$$
$$b_1 = 0.023364$$
$$c_1 = 0.058533$$
$$d_1 = 0.040758$$
$$e_1 = 0.0093324.$$

For a gas mixture, y_j replace x_j in Equations (IV-29), (IV-30) and (IV-34).

IV.4.4 Capillary Pressure and Relative Permeability

Capillary pressure and relative permeability data for an oil-water system and for a gas-oil system (with irreducible water) are read in tabular forms. Also, the model can accept data as polynomials.

Relative permeabilities can be calculated from the Naar-Henderson[6] correlations which follow:

$$k_{ro} = S_o^3(1 - S_g + S_w - 2S_{wi})/(1 - S_{wi})^4, \qquad \text{(IV-35)}$$

$$k_{rw} = (S_w - S_{wi})^4/(1 - S_{wi})^4, \qquad \text{(IV-36)}$$

and

$$k_{rg} = S_g^{\,3}(2 - S_g - 2S_{wi})/(1 - S_{wi})^4. \qquad \text{(IV-37)}$$

Three-phase relative permeabilities are calculated using Stone's[53] model, with the Dietrich and Bondor[6] modification:

$$k_{ro} = \frac{1}{k_{rocw}}(k_{row} + k_{rw})(k_{rog} + k_{rg}) - (k_{rw} + k_{rg}), \qquad \text{(IV-38)}$$

where k_{rocw} is the oil relative permeability at the irreducible water saturation.

IV.4.5 Relative Permeabilities with Interfacial Tension

When interfacial tension is considered, the relatives permeabilities are represented by the analytical expression given by Coats[10]. As he pointed out, the relations are not based on any theory or experimental evidence. They exhibit the behaviour of relative permeability with interfacial tension reduction: near the critical point, interfacial tension approaches zero, residual phase saturation decreases towards zero, and the relative permeability curves must approach straight lines.

$$k_{rg} = k_{rgcw}[f(\sigma)\bar{S}_g^{\,2} + (1 - f(\sigma))\bar{S}_g], \qquad \text{(IV-39)}$$

and

$$k_{ro} = f(\sigma)\bar{S}_o^{\,2} + (1 - f(\sigma))\bar{S}_o, \qquad \text{(IV-40)}$$

where

$$\bar{S}g = \frac{S_g - S^*_{gr}}{1 - S_{wi} - S^*_{gr}}, \qquad \text{(IV-41)}$$

$$\bar{S}_o = \frac{1 - S_g - S_{wi} - S^*_{org}}{1 - S_{wi} - S^*_{org}}, \qquad \text{(IV-42)}$$

$$f(\sigma) = (\sigma/\sigma_o)^{1/7}, \qquad \text{(IV-43)}$$

where σ is the interfacial tension, and σ_o is the initial tension. The parameters S^*_{gr} and S^*_{org} are the residual saturations for the gas and the oil, respectively. They are functions of interfacial tension:

$$S^*_{gr} = f(\sigma)\, S_{gr}, \qquad \text{(IV-44)}$$

and

$$S^*_{org} = f(\sigma)\, S_{org}. \qquad \text{(IV-45)}$$

IV.4.6 Interfacial Tension

The gas/oil interfacial tension is calculated from MacLeod-Sugden correlation[45].

$$\sigma^{1/4} = \sum_i P_{chi}(\bar{\rho}_o x_i - \bar{\rho}_g y_i), \qquad \text{(IV-46)}$$

where P_{chi} is the parachor of component i and densities are in units of gram-mol per cubic centimeter. In the case of under saturated oil mixtures, the saturation pressure is calculated and σ is calculated from Equation (IV-46) using equilibrium phase densities and composition at that pressure.

Interfacial tension is considered at the old time level in this formulation.

IV.5 Production-Injection Rates

IV.5.1 Production Rates

The molar mass production rate of component i in the system

is defined as

$$q_i = \begin{cases} x_i \bar{\rho}_o q_o + y_i \bar{\rho}_g q_g, & i = 1,2,\ldots n_c \quad \text{(IV-47)} \\ \bar{\rho}_w q_w, & i = n_c + 1 \quad \text{(IV-48)} \end{cases}$$

where q_o, q_g and q_w are the volumetric flow rates of oil, gas and water phases, respectively. They are defined by

$$q_\ell = -PI\lambda_\ell \Delta\Phi_\ell, \quad \ell = o,g,w \qquad \text{(IV-49)}$$

where PI is the productivity index, λ_ℓ is the mobility of the phase and $\Delta\Phi_\ell$ is the potential difference of the phase: $(\widetilde{\Delta p}_\ell - \gamma_\ell \Delta D)$ and $\Delta p_\ell = p_\ell - p_{wf}$, p_{wf} being the flowing bottomhole pressure specified and p_ℓ the block pressure.

Assuming that the potential differences in each phase are equal: $\Delta\Phi_o = \Delta\Phi_w = \Delta\Phi_g$, then the following production schemes were implemented:

Scheme 1: The production rate of oil at reservoir conditions is specified; then the other two flow rates can be calculated from mobility ratios:

$$q_\ell = \frac{\lambda_\ell}{\lambda_o} q_o, \quad \ell = g,w. \qquad \text{(IV-50)}$$

Scheme 2: The total production rate is specified at reservoir conditions, then

$$q_T = PI\lambda_T \Delta\Phi, \qquad \text{(IV-51)}$$

where $\lambda_T = \lambda_o + \lambda_g + \lambda_w$ is the total mobility. The production rate

of each phase can be calculated from

$$q_\ell = \frac{\lambda_\ell}{\lambda_T} q_T, \quad \ell = o,g,w \tag{IV-52}$$

Scheme 3: The total liquid production rate (oil + water) at reservoir conditions is specified

$$q_L = PI\lambda_L \Delta\Phi, \tag{IV-53}$$

where

$$\lambda_L = \lambda_o + \lambda_w. \tag{IV-54}$$

Then, the individual rates of each phase can be calculated from:

$$q_\ell = \frac{\lambda_\ell}{\lambda_L} q_L, \quad \ell = o,g,w. \tag{IV-55}$$

Scheme 4: The bottomhole pressure of the production well is specified and the volumetric flow rates can be calculated from Equation (IV-49). If the block pressure is lower than the specified bottomhole pressure, the well is shut off.

IV.5.2 Injection Rates

Injection of gas or dense fluids or water is considered. The following schemes are implemented:

Scheme 1: A specified rate is given at constant pressure and temperature, i.e. a constant molar rate is specified.

Scheme 2: The bottomhole pressure of the injection well is specified and the flow rate is calculated from Equation (IV-49). If the block

pressure is bigger than the bottomhole pressure given, the well is shut off.

IV.6 Phase Equilibria

The Peng-Robinson equation of state[39] is used to compute hydrocarbon liquid and gas phase densities and component fugacities. The equation is

$$p = \frac{RT}{v - b} - \frac{a(T)}{v(v + b) + b(v - b)} . \qquad \text{(IV-56)}$$

This equation can be written as

$$Z^3 - (1 - B)Z^2 + (A - 3B^2 - 2B)Z + (AB - B^2 - B^3) = 0, \qquad \text{(IV-57)}$$

where

$$A = \frac{ap}{R^2T^2} , \qquad \text{(IV-58)}$$

$$B = \frac{bp}{RT} \qquad \text{(IV-59)}$$

and

$$Z = \frac{pv}{RT} . \qquad \text{(IV-60)}$$

Equation (IV-57) yields one or three roots depending upon the number of phases in the system. In the two-phase region the largest root is the compressibility factor of vapour and the smallest root is the compressibility of the liquid.

For a temperature $T = T_c$ (critical temperature),

$$a(T_c) = 0.45724\ R^2T_c^2/p_c^2 \qquad \text{(IV-61)}$$

and

$$b(T_c) = 0.07780\ RT_c/p_c\ . \qquad \text{(IV-62)}$$

At temperatures other than T_c,

$$a(T) = a(T_c)\alpha(T_r,\omega),$$

and

$$b(T) = b(T_c)$$

where $\alpha(T_r,\omega)$ is a dimensionless function of reduced temperature and acentric factor:

$$\alpha^{1/2} = 1 + m(1 - T_r^{1/2}), \qquad \text{(IV-63)}$$

and

$$m = 0.37464 + 1.54226\omega - 0.26992\omega^2\ . \qquad \text{(IV-64)}$$

For a liquid mixture, the following relations are used:

$$a = \sum_i \sum_j x_i x_j a_{ij}, \qquad \text{(IV.65)}$$

and

$$b = \sum_i x_i b_i, \qquad \text{(IV.66)}$$

$$a_{ij} = (1 - c_{ij})a_i^{0.5}a_j^{0.5} \qquad \text{(IV.67)}$$

where c_{ij} are binary interaction coefficients.

For a gas mixture, y_i replaces x_i in Equations (IV.65) to (IV-66).

The fugacity coefficient of component j $\left(\psi_j = \dfrac{f_i}{px_j}\right)$ in a mixture is calculated from the following equation:

$$\ln \psi_j = \frac{b_j(Z-1)}{b} - \ln(Z-B) - \frac{A}{2\sqrt{2}B}\left(\frac{2\sum_i x_i a_{ij}}{a} - \frac{b_j}{b}\right)\ln\left(\frac{(Z-2.414B)}{(Z-0.414B)}\right) \quad \text{(IV-68)}$$

where $\psi_j = f_j^L/x_j p$ is the fugacity coefficient for a liquid mixture. For a gas mixture, y_i replaces x_i in Equation (IV.68) and $\psi_j = f_j^V/y_i p$.

CHAPTER V

FINITE DIFFERENCE APPROXIMATION AND METHOD OF SOLUTION

The mathematical equations of the compositional model, derived in Chapter IV, were solved numerically in view of the complexity of the system of equations involved.

V.1 Finite Difference Approximation

The compositional model consists of the following set of equations:

1. The molar balance difference equation for any hydrocarbon component i for a grid block:

$$\Delta[T'(\lambda_o x_i \bar{\rho}_o)^{n+1}(\Delta p_o^{n+1} - \gamma_o^n \Delta D)]$$

$$+ \Delta[T'(\lambda_g y_i \bar{\rho}_g)^{n+1}(\Delta p_g^{n+1} - \gamma_g^n \Delta D)] + q_i^{n+1} = \frac{V_b}{\Delta t}\delta[\phi(x_i \bar{\rho}_o S_o + y_i \bar{\rho}_g S_g)],$$

$$i = 1,2,\ldots n_c \qquad (V\text{-}1)$$

where the constant part of transmissibility T' is defined as

$$T' = kA'/L \qquad (V\text{-}2)$$

and $\gamma = \rho g/g_c$ is the specific weight of a phase. The gas and oil pressures are p_g and p_o respectively. All variables and fluid properties are computed at the new time level $n+1$, except γ, which is consider at the old time level n.

2. The water molar difference equation:

$$\Delta[T'(\bar{\rho}_w\lambda_w)^{n+1}(\Delta p^{n+1} - \Delta P_{cog}^{n+1} - \Delta P_{cow}^{n+1} - \gamma_w^n \Delta D)] + q_i^{n+1}$$

$$= \frac{V_b}{\Delta t}\underline{\delta}(\phi\bar{\rho}_w S_w), \quad i = n_c + 1. \tag{V-3}$$

3. The fugacity constraints,

$$f_i^L - f_i^V = 0, \quad i = 1,2,\ldots n_c \tag{V-4}$$

4. The mole fraction constraints,

$$\sum_i^{n_c} x_i = 1, \tag{V-5}$$

$$\sum_i^{n_c} y_i = 1. \tag{V-6}$$

5. The saturation constraint equation,

$$S_o + S_g + S_w = 1. \tag{V-7}$$

These $n_c + 1$ molar difference equations, n_c fugacity constraints, two mole fraction constraints and saturation constraint form a set of N equations for each grid block, where N is $2n_c + 4$.

The N unknowns corresponding to these equations are:

$$X = (x_1, x_2, \ldots x_{n_c}, y_1, y_2, \ldots y_{n_c}, p_g, S_o, S_g, S_w), \tag{V-8}$$

where $X_1 = x_1$, $X_2 = x_2, \ldots X_N = S_w$, in the order listed in Equation (V-8), and are referred to hereafter as X.

In order to express the set of N equations in residual form,

it is necessary to expand the difference operators as follows:

The $\underline{\delta}$ operator is defined as

$$\underline{\delta}g = g^{n+1} - g^{n}. \tag{V-9}$$

The Δ difference operator is defined as

$$\Delta[T'(\lambda_o x_i \bar{\rho}_o)^{n+1}(\Delta p_g^{n+1} - \Delta p_{cog}^{n+1} - \gamma_o^n \Delta D)] \equiv \Delta[T''_o \Delta\Phi_o]^{n+1} \tag{V-10}$$

where T''_o is the fluid-phase transmissibility, then

$$\Delta[T''_o \Delta\Phi_o]^{n+1} = \Delta_x(T''_{ox}\Delta_x\Phi_o)^{n+1} + \Delta_y(T''_{oy}\Delta_y\Phi_o)^{n+1} \tag{V-11}$$

and

$$\Delta_x(T''_{ox}\Delta_x\Phi_o)^{n+1} = T''^{n+1}_{ox,i+\frac{1}{2}}(\Phi^{n+1}_{o_{i+1}} - \Phi^{n+1}_{o_i}) + T''^{n+1}_{ox,i-\frac{1}{2}}(\Phi^{n+1}_{o_{i-1}} - \Phi^{n+1}_{o_i}) \tag{V-12}$$

where $T''_{ox,i+\frac{1}{2}}$ is the x-direction oil transmissibility evaluated between grid blocks i and $i+1$. The superscript $n+1$ indicates that all terms are evaluated at the new time level, the model is fully implicit.

In general, to evaluate the fluid flow transmissibility between grib block ℓ and k, the single point upstream approach is used. Then, the fluid flow transmissibility term $T''_{P_{\ell,k}}$ can be expanded as follows,

$$T''_{P_{\ell,k}} = w_{P_{\ell,k}} T''_{P_\ell} + (1 - w_{P_{\ell,k}}) T''_{P_k}, \tag{V-13}$$

where $w_{p_{\ell,k}}$ is equal to one if the potential of grid block ℓ is equal to or greater than the potential of grid block k for a phase p, and equal to zero otherwise. T''_{p_ℓ} and T''_{p_k} are the fluid flow transmissibilities of phase p for blocks ℓ and k respectively.

Let the system of N finite difference equations for any grid block ℓ be defined in residual form as follows:

1. The molar balance equations (Equation (V-1) and Equation (V-3)) can be written as follows:

$$F_i^{n+1} = -E_i^{n+1} + (C_i^{n+1} - C_i^n) - Q_i^{n+1} = 0,$$

$$i = 1,2,\ldots,n_c + 1 \qquad \text{(V-14)}$$

where

F_i is the residual molar balance equation for component i,

E_i is the interblock flow term for component i,

C_i is the accumulation term for component i, and

Q_i is the production/injection term for component i.

Next, each term is expanded as follows.

i) The term E_i for component i is written as follows for any hydrocarbon component:

$$E_i = \sum_{\substack{k=1 \\ k\neq\ell}}^{5} T'_{\ell,k}[w_{o_{\ell,k}}(\bar{\rho}_o\lambda_o x_i)_\ell(\Phi_{o_k} - \Phi_{o_\ell}) + (1 - w_{o_{\ell,k}})(\bar{\rho}_o\lambda_o x_i)_k(\Phi_{o_k} - \Phi_{o_\ell})$$

$$+ w_{g_{\ell,k}}(\bar{\rho}_g\lambda_g y_i)_\ell(\Phi_{g_k} - \Phi_{g_\ell})$$

$$+ (1 - w_{g_{\ell,k}})(\bar{\rho}_g\lambda_g y_i)_k(\Phi_{g_k} - \Phi_{g_\ell})], \quad i = 1,2,\ldots,n_c, \qquad \text{(V-15)}$$

where $T'_{\ell,k}$ is the transmissibility (Equation (V-2)) evaluated between grid blocks ℓ and k.

For water:

$$E_i = \sum_{\substack{k=1 \\ k\neq\ell}}^{5} T'_{\ell,k}[w_{w_{\ell,k}}(\bar{\rho}_w\lambda_w)_\ell(\Phi_{w_k} - \Phi_{w_\ell}) + (1 - w_{w_{\ell,k}})(\bar{\rho}_w\lambda_w)_k(\Phi_{w_k} - \Phi_{w_\ell})],$$

$$i = n_c + 1. \qquad \text{(V-16)}$$

ii) The accumulation term C_i is written as

$$C_i = \frac{V_b}{\Delta t}[\phi(\bar{\rho}_o S_o x_i + \bar{\rho}_g S_g y_i)], \quad i = 1,2,\ldots,n_c, \qquad \text{(V-17)}$$

and

$$C_i = \frac{V_b}{\Delta t}[\phi(\bar{\rho}_w S_w)], \quad i = n_c + 1. \qquad \text{(V-18)}$$

iii) The injection/production term Q_i as function of volumetric flow is written as

$$Q_i = x_i\bar{\rho}_o q_o + y_i\bar{\rho}_g q_g, \quad i = 1,2,\ldots,n_c, \qquad \text{(V-19)}$$

and

$$Q_i = \bar{\rho}_w q_w, \quad i = n_c + 1. \qquad \text{(V-20)}$$

2. Equations, in residual form, for fugacity, composition and saturation constraints are written as

$$G_i^{n+1} = (f_i^L - f_i^V)^{n+1} = 0, \quad i = 1,2,\ldots,n_c, \qquad \text{(V-21)}$$

$$G_i^{n+1} = 1 - \sum_{j=1}^{n_c} x_j^{n+1} = 0, \quad i = n_c + 1, \qquad \text{(V-22)}$$

$$G_i^{n+1} = 1 - \sum_{j=1}^{n_c} y_j^{n+1} = 0, \quad i = n_c + 2, \tag{V-23}$$

and

$$G_i^{n+1} = 1 - (S_o + S_g + S_w)^{n+1} = 0, \quad i = n_c + 2, \tag{V-24}$$

V.2 Expansion/Linearization of the Difference Equations and Solution Method

The solution method chosen to solve the compositional model was fully implicit, because of the highly nonlinear equations involved, and because of the time step instabilities produced by other methods. The following procedure is widely known, e.g. Coats[10] (1980). A Newtonian iterative method, utilizing numerical derivatives, was used to linearize the difference equations. The method consists in reducing the $2n_c + 4$ linear algebraic equations to $n_c + 1$ equations, and solving them simultaneously by a direct linear equation solving routine.

V.2.1 Space Discretization

The five-point difference scheme and natural ordering of blocks were used to relate the equation of grid block i with the neighboring grid blocks. A block centred scheme was used.

V.2.2 Time Discretization

Since a fully implicit method of solution was chosen, all terms and/or variables in the discretized difference equations were considered at time level $n+1$, except the specific weight γ which was considered at time level n.

V.2.3 Newtonian iteration

Consider F_1 to be a real function in several variables X such that

$$F_1(X) = 0. \tag{V-25}$$

This equation is approximated by its value at the latest iteration level plus a linear combination of the unknowns from partial differentiation of the function with respect to all unknowns:

$$\begin{aligned} F_1(X_1,X_2,\ldots,X_N)^{\nu+1} = {} & F_1(X_1,X_2,\ldots,X_N)^{\nu} \\ & + \frac{\partial F_1}{\partial X_1}(X_1,X_2,\ldots,X_N)^{\nu}(X_1^{\nu+1} - X_1^{\nu}) \\ & \vdots \\ & + \frac{\partial F_1}{\partial X_N}(X_1,X_2,\ldots,X_N)^{\nu}(X_N^{\nu+1} - X_N^{\nu}) \end{aligned} \tag{V-26}$$

or $$F_1(X)^{\nu+1} = F_1(X)^{\nu} + JF_1(X)^{\nu}(\delta X), \tag{V-27}$$

where ν is the iteration number, X is the unknown vector, JF_1 is the vector of the partial derivatives of the function with respect to each variable, evaluated at the old iteration ν, and δX is defined as

$$\delta X = X^{\nu+1} - X^{\nu}, \quad \nu = 1,2,\ldots \tag{V-28}$$

After solving for δX, $X^{\nu+1}$ can be calculated as:

$$X^{\nu+1} = \delta X + X^{\nu}. \tag{V-29}$$

Newton's method converges quadratically, but the first estimate (first iteration) must be carefully selected. Newton's method has the disadvantage that it requires the evaluation of the function $F_1(X)$ as well as its derivative for each iteration.

V.2.4 Modified Newton Method

The derivative of $F_1(X)$ can be approximated by

$$\frac{\partial F_1}{\partial X_i}(X)^{\nu} \simeq \frac{F_1(X_1, X_2 \ldots X_i + \epsilon \ldots X_N) - F_1(X_1, X_2 \ldots X_N)}{\epsilon} \qquad \text{(V-30)}$$

where ϵ is very small, 10^{-4}, or small enough to yield an accurate approximation of the derivative. These derivatives are called numerical derivatives.

V.2.5 Linearization of the Difference Equations

The finite difference equations, Equation (V-14) plus Equations (V-21) to (V-24) are real functions in several variables, and are linearized as follows:

1. The system of $n_c + 1$ molar balance equations (Equation (V-14)) for grid block ℓ and component i at νth iteration are written as

$$JF_i^{\nu}(\delta X) = -F_i(X^{\nu}), \qquad \text{(V-31)}$$

where

$$F_i(X^{\nu}) = -E_i^{\nu} + (C_i^{\nu} - C_i^{n}) - Q_i^{\nu}, \qquad \text{(V-32)}$$

and JF is the partial derivative matrix of F_i and JF_i^{ν} is row i of the matrix JF at νth iteration.

The δ operates on the vector of the unknowns as

$$\delta X = [\delta x_1, \delta x_2, \ldots \delta x_{n_c}, \delta y_1, \delta y_2 \ldots \delta y_{n_c}, \delta p_g, \delta S_o, \delta S_g, \delta S_w]^T \quad \text{(V-33)}$$

where $\delta x_1 = x_1^{\nu+1} - x_1^{\nu}$, $\delta x_2 = x_2^{\nu+1} - x_2^{\nu}, \ldots \delta S_w = S_w^{\nu+1} - S_w^{\nu}$. At the first iteration, X^0 is taken as its value at the old time level n X^n; then $X^{\nu+1} = \delta X + X^{\nu}$. At the solution, $F_i(X^{\nu+1})$ converges to $F_i(X^{n+1})$.

The molar balance equations are functions of the unknowns of grid block ℓ (X_ℓ) and of the unknowns of the neighboring grid blocks k (X_k), due to the interblock flow terms. The linearization of each term of Equation (V-14) is presented below:

Linearization of the term E_i

$$E_i^{\nu+1} = E_i^{\nu} + \left(\frac{\partial E_i}{\partial X_\ell}\right)^{\nu} \delta X_\ell + \sum_{\substack{k=1 \\ k \neq \ell}}^{5} \left(\frac{\partial E_i}{\partial X_k}\right)^{\nu} \delta X_k. \quad \text{(V-34)}$$

Linearization of the accumulation term C_i

$$C_i^{\nu+1} = C_i^{\nu} + \left(\frac{\partial C_i}{\partial X_\ell}\right)^{\nu} \delta X_\ell. \quad \text{(V-35)}$$

Linearization of the production/injection term Q_i

$$Q_i^{\nu+1} = Q_i^{\nu} + \left(\frac{\partial Q_i}{\partial X_\ell}\right)^{\nu} \delta X_\ell. \quad \text{(V-36)}$$

Then, Equation (V-31) can be written as follows

$$\left[-\left(\frac{\partial E_i}{\partial X_\ell}\right)^\nu + \left(\frac{\partial C_i}{\partial X_\ell}\right)^\nu - \left(\frac{\partial Q_i}{\partial X_\ell}\right)^\nu\right]\delta X_\ell - \sum_{\substack{k=1 \\ k\neq\ell}}^{5} \left(\frac{\partial E_i}{\partial X_k}\right)^\nu \delta X_k = -F_i(X^\nu),$$

$$i = 1,2,\ldots n_c + 1, \qquad \text{(V-37)}$$

Equation (V-37) for grid block ℓ at νth iteration is written as follows:

$$\underline{H}_i \delta X_{\ell-N_x} + \underline{D}_i \delta X_{\ell-1} + \underline{E}'_i \delta X_\ell + \underline{B}_i \delta X_{\ell+1} + \underline{F}_i \delta X_{\ell+N_x} = -F_i(X^\nu),$$

$$i = 1,2,\ldots n_c + 1 \qquad \text{(V-38)}$$

where $\underline{H}_i$, $\underline{D}_i$, $\underline{E}'_i$, $\underline{B}_i$, $\underline{F}_i$ form the Jacobian of the molar balance equation F_i, and are defined as

$$\underline{E}'_i = -\left(\frac{\partial E_i}{\partial X_\ell}\right)^\nu + \left(\frac{\partial C_i}{\partial X_\ell}\right)^\nu - \left(\frac{\partial Q_i}{\partial X_\ell}\right)^\nu, \qquad \text{(V-39)}$$

and

$$\underline{H}_i = -\left(\frac{\partial E_i}{\partial X_k}\right)^\nu \quad \text{if } k = \ell - N_x,$$

$$\underline{D}_i = -\left(\frac{\partial E_i}{\partial X_k}\right)^\nu \quad \text{if } k = \ell - 1,$$

$$\underline{B}_i = -\left(\frac{\partial E_i}{\partial X_k}\right)^\nu \quad \text{if } k = \ell + 1,$$

$$\underline{F}_i = -\left(\frac{\partial E_i}{\partial X_k}\right)^\nu \quad \text{if } k = \ell + N_x,$$

$$i = 1,2,\ldots n_c + 1 \qquad \text{(V-40)}$$

where N_x is the number of grid blocks in the x-direction. If only a one-dimensional grid is considered, the terms $\underline{H}_i$ and $\underline{F}_i$ are equal to zero.

2. Linearization of fugacity, composition and saturation constraint equations (Equations (V-21), (V-22), (V-23), (V-24)) for grid block ℓ, is presented next. These equations are functions of the unknowns of the grid block ℓ only, and can be written as

$$JG_i^{\nu}(\delta X_\ell) = -G_i(X^{\nu}), \quad i = 1,2,\ldots n_c + 3 \tag{V-41}$$

where JG is the partial derivative matrix of G_i and JG_i^{ν} is row i of the matrix JF at the νth iteration. The above equations can be expressed as follows:

Linearization of fugacity contraints

$$\left[\frac{\partial}{\partial X_\ell}(f_j^L - f_j^V)\right]^{\nu}\delta X_\ell = -(f_j^L - f_j^V)^{\nu}, \quad j = 1,2,\ldots n_c. \tag{V-42}$$

Linearization of composition constraints

$$\sum_{j=1}^{n_c} \delta x_j = 1 - \left(\sum_{j=1}^{n_c} x_j\right)^{\nu}, \tag{V-43}$$

$$\sum_{j=1}^{n_c} \delta y_j = 1 - \left(\sum_{j=1}^{n_c} \delta x_j\right)^{\nu}. \tag{V-44}$$

Linearization of saturation constraint

$$\delta S_o + \delta S_g + \delta S_w = 1 - (S_o + S_g + S_w)^{\nu}. \tag{V-45}$$

V.2.6 Method of Solution

The compositional model presented above consists of N equations in N unknowns for a given grid block, ℓ. The first $n_c + 1$ molar balance equations are functions of the unknowns for grid block ℓ and the neighboring grid block k. The remaining $n_c + 3$ constraint equations are functions of $2n_c + 4$ unknowns of grid block ℓ only. The last set of equations is used to eliminate $n_c + 3$ unknowns from the molar balance equations resulting in a system of $n_c + 1$ equations in $n_c + 1$ unknowns, which are solved simultaneously by a band algorithm. The first $n_c + 3$ unknowns are calculated by back substitution.

1. Reduction of the constraint equations

The linearized phase equilibria or fugacity and composition constraint equations (Equation (V-42) to Equation (V-44)) for grid block ℓ are $n_c + 2$ equations in $2n_c + 1$ unknowns $\{x_i\}$, $\{y_i\}$ and pressure. This set of equations is used to solve for $n_c + 2$ unknowns by Gaussian elimination. The reductions are presented below.

Recall Equation (V-41)

$$JG_i^{\nu}(\delta X) = -G_i(X^{\nu}), \quad i = 1,2,\ldots n_c + 2. \tag{V-46}$$

Define X_a as the vector of $n_c + 2$ unknowns:

$$X_a = [x_1, x_2, \ldots x_{n_c}, y_1, y_2] \tag{V-47}$$

Then, Equation (V-46) can be written as a function of the remaining unknowns $(y_3, y_4, \ldots y_{n_c}, p_g)$ as follows:

$$\begin{bmatrix} JG_{1,1} & JG_{1,2,} & \cdots & JG_{1,n_c+2} \\ \vdots & & & \\ & & & \\ JG_{n_c+2,1} & JG_{n_c+2,2} & \cdots & JG_{n_c+2,n_c+2} \end{bmatrix} \times \begin{bmatrix} \delta x_1 \\ \delta x_2 \\ \vdots \\ \delta x_{n_c} \\ \delta y_1 \\ \delta y_2 \end{bmatrix} = - \begin{bmatrix} G_1 \\ G_2 \\ \vdots \\ \\ \\ G_{n_c+2} \end{bmatrix} -$$

$$- \begin{bmatrix} JG_{1,n_c+3} & \cdots & JG_{1,2n_c+4} \\ & & \\ & & \\ JG_{n_c+2,n_c+3} & \cdots & JG_{n_c+2,2n_c+4} \end{bmatrix} \times \begin{bmatrix} \delta y_3 \\ \delta y_4 \\ \vdots \\ \delta y_{n_c} \\ \delta p_g \end{bmatrix} \qquad \text{(V-48)}$$

or

$$JG^{\nu}_{ia}(\delta X_a) = -G_i(X^{\nu}) - JG^{\nu}_{ib}(\delta X_b), \quad i = 1,2,\ldots n_c + 2 \qquad \text{(V-49)}$$

Equation (V-49) was solved for δX_a by Gaussian elimination using a subroutine from the IMSL Library. The results are expressed as follows:

$$\begin{bmatrix} \delta x_1 \\ \delta x_2 \\ \vdots \\ \delta x_{n_c} \\ \delta y_1 \\ \delta y_2 \end{bmatrix} = \begin{bmatrix} w_{1,1} & w_{1,2} & \cdots & w_{1,n_c-1} \\ w_{2,1} & w_{2,2} & \cdots & w_{2,n_c-1} \\ \vdots & & & \\ & & & \\ w_{n_c+2,1} & w_{n_c+2,2} & \cdots & w_{n_c+2,n_c-1} \end{bmatrix} \times \begin{bmatrix} \delta y_3 \\ \delta y_4 \\ \vdots \\ \delta y_{n_c} \\ \delta p_g \end{bmatrix} + \begin{bmatrix} bb_1 \\ bb_2 \\ \vdots \\ bb_{n_c+1} \\ bb_{n_c+2} \end{bmatrix} \qquad \text{(V-50)}$$

2. Consolidation of the system of $n_c + 1$ Equations

The linearized system of $n_c + 1$ molar balance equations Equation (V-38):

$$\underline{H}_i \delta X_{\ell-N_x} + \underline{D}_i \delta X_{\ell-1} + \underline{E}'_i \delta X_{\ell} + \underline{B}_i \delta X_{\ell} + \underline{F}_i \delta X_{\ell+N_x} = -F_i(X)^{\nu}, \quad \text{(V-51)}$$

can be written as function of variables $\delta X_a = [\delta x_1, \delta x_2, \ldots \delta x_{n_c}, \delta y_1, \delta y_2]$ and the remaining unknowns $\delta X_b = [\delta y_3, \delta y_4 \ldots \delta y_{n_c}, \delta p_g, \delta S_o, \delta S_g, \delta S_w]$ as follows:

$$\underline{H}_{ib}(\delta X_b)_{\ell-N_x} + \underline{D}_{ib}(\delta X_b)_{\ell-1} + \underline{E}'_{ib}(\delta X_b)_{\ell} + \underline{B}_{ib}(\delta X_b)_{\ell+1} + \underline{F}_{ib}(\delta X_b)_{\ell+N_x}$$
$$= [-F_i(X^{\nu}) + \underline{H}_{ia}(\delta X_a)_{\ell-N_x} + \underline{D}_{ia}(\delta X_a)_{\ell-1} + \underline{E}'_{ia}(\delta X_a)_{\ell} + \underline{B}_{ia}(\delta X_a)_{\ell+1}$$
$$+ \underline{F}_{ia}(\delta X_a)_{\ell+N_x}], \quad i = 1,2,\ldots n_c + 1. \quad \text{(V-52)}$$

Substituting δX_a for Equation (V-50) and eliminating δS_w using Equation (V-45), the above system of equations is reduced to $n_c + 1$ primary equations in $n_c + 1$ primary unknowns for a grid block ℓ. Finally, the consolidated system of equations can be written as follows:

$$\underline{H1}_i(\delta X1)_{\ell-N_x} + \underline{D1}_i(\delta X1)_{\ell-1} + \underline{E1}_i(\delta X1)_{\ell} + \underline{B1}_i(\delta X1)_{\ell+1} + \underline{F1}_i(\delta X1)_{\ell+N_x}$$
$$= -R1(X^{\nu}), \quad i = 1,2,\ldots n_c + 1 \quad \text{(V-53)}$$

where

$$\delta X1 = [\delta y_3, \delta y_4, \ldots \delta y_{n_c}, \delta p_g, \delta S_o, \delta S_g] \quad \text{(V-54)}$$

and $\underline{H1}_i$, $\underline{D1}_i$, $\underline{E1}_i$, $\underline{B1}_i$ and $\underline{F1}_i$ are the reduced Jacobian terms.

After solving Equation (V-53) for $\delta X1$ over the entire grid, by a band algorithm, the elminated unknowns $\delta X_a = [\delta x_1, \delta x_2, \ldots \delta x_{n_c}, \delta y_1, \delta y_2]$ and δS_w are calculated from Equation (V-50) and Equation (V-45), respectively, by back substitution. All $2n_c + 4$ unknowns over the entire reservoir are updated as

$$X^{\nu+1} = X^{\nu} + \delta X. \qquad \text{(V-55)}$$

The values $X^{\nu+1}$ are used to recalculate the terms $\underline{D}_i$, $\underline{E}'_i$, $\underline{B}_i$, $\underline{H}_i$, $\underline{F}_i$, and F_i in Equation (V-51) and these equations are reduced and solved again. These iterations continue until $\max(\delta X)$ and $\max(F_i)$ over entire grid are less than specified tolerances. The convergence criteria used were:

$$\max\left|\delta p_g / p_g^{\nu+1}\right| \leq 0.0001,$$

$$\max\left|\delta x_i / x_i^{\nu+1}\right| \leq 0.002, \quad i = 1,2,\ldots n_c$$

$$\max\left|\delta y_i / y_i^{\nu+1}\right| \leq 0.002, \quad i = 1,2,\ldots n_c$$

and

$$\max\left|F_i(x^{\nu+1})\right| \leq 0.01, \quad i = 1,2,\ldots n_c \qquad \text{(V-56)}$$

where this last criterion is called the residual criterion for convergence.

V.3 Variable Substitution Method

The model described in this chapter considers the general case when both oil and gas phases are present.

When only one hydrocarbon-phase is present, the phase equilibria or fugacity constraint equations do not apply. Therefore, the n_c fugacity equations and the mole fraction constraint of the absent phase are eliminated from the original system of equations (Equation (V-1), and Equations (V-3) through (V-7)). Then, the $2n_c + 4$ model equations become $n_c + 3$ equations in $n_c + 3$ unknowns. The unknowns are $\{x_i\}$, p_g, S_o and S_w for an oil-phase, or $\{y_i\}$, p_g, S_g and S_w for a gas-phase. The $n_c + 3$ model equations are: $n_c + 1$ molar balance equations

(Equation (V-1)), composition constraint of the existing phase, Equation (V-5) for an oil-phase or Equation (V-6) for a gas phase, and the saturation constraint, Equation (V-7).

The set of $n_c + 3$ equations is linearized by the Newtonian method, as linear combinations of the $n_c + 3$ unknowns, as described previously. The unknowns for a grid block containing an oleic phase only are:

$$\delta X = (\delta x_1, \delta x_2, \ldots \delta x_{n_c}, \delta p_g, \delta S_o, \delta S_w) \qquad \text{(V-57)}$$

and the unknowns for a grid block containing a vapour phase only are:

$$\delta X = (\delta y_1, \delta y_2, \ldots \delta y_{n_c}, \delta p_g, \delta S_g, \delta S_w) \qquad \text{(V-58)}$$

The model is reduced to $n_c + 1$ equations in $n_c + 1$ variables by eliminating δx_{n_c} for an oleic phase or δy_{n_c} for a vapour phase, using the remaining mole fraction constraint equation, Equation (V-43) or Equation (V-44), respectively, and eliminating δS_w, using Equation (V-45). The remaining $n_c + 1$ primary variables are:

$$\delta X = (\delta x_1, \delta x_2, \ldots \delta x_{n_c-1}, \delta p_g, \delta S_o) \qquad \text{(V-59)}$$

for a grid block containing an oleic phase, or

$$\delta X = (\delta y_1, \delta y_2, \ldots, \delta y_{n_c-1}, \delta p_g, \delta S_g) \qquad \text{(V-60)}$$

for a grid block containing a vapour phase.

In general, the solution method consists of solving $n_c + 1$ simultaneous equations in $n_c + 1$ unknowns for each grid block by

direct solution. Note that, in general, adjacent grid blocks may have different sets of primary variables, depending on the type and numbers of phases present.

V.4 Hydrocarbon-Phase Appearance/Disappearance

The model allows any grid block to change phases during a time step. The procedure is explained below.

1. Hydrocarbon-phase disappearance:

If two-hydrocarbon phases (gas/oil) are present in a grid block at the end of iteration ν, the solution X^{ν} includes S_o^{ν} and S_g^{ν}, i.e. the grid block remains in the two-phase state. But if one of these saturations is negative, it is set to zero before initiating the new iteration.

2. Hydrocarbon-phase appearance:

Detection of a second hydrocarbon-phase appearance in a single hydrocarbon grid block uses the following steps:

i. The saturation pressure is calculated if S_o^{ν} or S_g^{ν} is zero in a grid block. If the calculated p_s is less than the grid block p_g, the grid block remains in hydrocarbon single phase mode. If p_s is greater than p_g, then

ii. A flash calculation is made to separate the phases ($p_s > p_g$) and the composition of the phases and the corresponding saturations are used to start the new iteration.

V.5 Expansion of Derivatives

The interblock flow terms for any phase: $(\bar{\rho}_o x_i \lambda_o)$, $(\bar{\rho}_g y_i \lambda_g)$ or $\bar{\rho}_w \lambda_w$ are considered at time level $n + 1$, and are evaluated using the single point upstream approach. In the evaluation of potentials, the specific weight γ of a phase p is taken to be at level n.

As mentioned previously, the derivatives of E_i can be grouped into two different terms, the derivatives with respect to the unknowns of blocks ℓ (δX_ℓ) and the derivatives with respect to the unknowns of the neighboring block k (δX_k), and can be written as follows:

$$\partial E_i = \left(\frac{\partial E_i}{\partial X_\ell}\right) \delta X_\ell + \sum_{\substack{k=1 \\ k \neq \ell}}^{5} \frac{\partial E_i}{\partial X_k} \quad (\delta X_k),$$

$$i = 1,2,\ldots n_c + 1. \qquad \text{(V-61)}$$

Derivatives of E_i with respect to the unknowns of block ℓ are:

$$\frac{\partial E_i}{\partial X_\ell} = \sum_{p}^{o,g} \sum_{\substack{k=1 \\ k \neq \ell}}^{5} T'_{\ell,k} \Bigg[w_{p_{\ell,k}} \left(\frac{\partial}{\partial X_\ell} (\bar{\rho}_p \lambda_p x_{ip})_\ell \right) (\Phi_{p_k} - \Phi_{p_\ell})$$

$$- w_{p_{\ell,k}} (\bar{\rho}_p \lambda_p x_{ip})_\ell \left(\frac{\partial}{\partial X_\ell} (\Phi_{p_\ell}) \right)$$

$$- (1 - w_{p_{\ell,k}}) (\bar{\rho}_p \lambda_p x_{ip})_k \left(\frac{\partial}{\partial X_k} (\Phi_{p_\ell}) \right) \Bigg],$$

$$i = 1,2,\ldots n_c \qquad \text{(V-62)}$$

where x_{ip} is defined as x_i, the mole fraction of component i in the oleic phase, if $p = o$, or as y_i, the mole fraction of component

i in the vapour phase, if $p = g$ and $\partial(\bar{\rho}_\ell \lambda_\ell x_{ip})/\partial X_\ell$ is expanded by the chain rule.

Derivatives of E_i with respect to the unknowns of the neighboring blocks can be written as follows:

$$\frac{\partial E_i}{\partial X_k} = \sum_{p}^{o,g} T'_{\ell,k}\left[(1 - w_{p_{\ell,k}})\left(\frac{\partial}{\partial X_k}(\bar{\rho}_p \lambda_p x_{ip})_k\right)(\Phi_{p_k} - \Phi_{p_\ell}) + (1 - w_{p_{\ell,k}})(\bar{\rho}_p \lambda_p x_{ip})_k\left(\frac{\partial}{\partial X_k}(\Phi_{p_k})\right) + w_{p_{\ell,k}}(\bar{\rho}_p \lambda_p x_{ip})\left(\frac{\partial}{\partial X_k}(\Phi_{p_k})\right)\right], \quad k \neq \ell, \; i = 1,2,\ldots n_c. \tag{V-63}$$

Similarly, the water molar balance derivatives can be written as

$$\frac{\partial E_i}{\partial X_\ell} = \sum_{\substack{k=1 \\ k\neq\ell}}^{5} T'_{\ell,k}\left[w_{w_{\ell,k}}\left(\frac{\partial}{\partial X_\ell}(\bar{\rho}_w \lambda_w)_\ell\right)(\Phi_{w_k} - \Phi_{w_\ell}) - w_{w_{\ell,k}}(\bar{\rho}_w \lambda_w)_\ell\left(\frac{\partial}{\partial X_\ell}\Phi_{w_\ell}\right) - (1 - w_{w_{\ell,k}})(\bar{\rho}_w \lambda_w)_k\left(\frac{\partial}{\partial X_\ell}(\Phi_{w_\ell})\right)\right], \quad i = n_c + 1 \tag{V-64}$$

and

$$\frac{\partial E_i}{\partial X_k} = T'_{\ell,k}\left[(1 - w_{w_{\ell,k}})\left(\frac{\partial}{\partial X_k}(\bar{\rho}_w \lambda_w)_k\right)(\Phi_{w_k} - \Phi_{w_\ell}) + (1 - w_{w_{\ell,k}})(\bar{\rho}_w \lambda_w)_k\left(\frac{\partial}{\partial X_k}(\Phi_{w_k})\right) + w_{w_{\ell,k}}(\bar{\rho}_w \lambda_w)_\ell\left(\frac{\partial}{\partial X_k}(\Phi_{w_k})\right)\right], \quad i = n_c + 1. \tag{V-65}$$

Derivatives of Phase Equilibria

Recalling Equation (V-21) and Equation (V-41):

$$G_i^{n+1} = (f_i^L - f_i^V)^{n+1} = 0, \quad i = 1,2,\ldots n_c \tag{V-66}$$

and

$$JG_i^{\nu}\delta X = -G_i(X^{\nu}), \quad i = 1,2,\ldots n_c \tag{V-67}$$

where JG is the partial derivative matrix and JG_i is the row i corresponding to component i. The matrix JG can be expanded as

$$JG_{i,j} = \frac{\partial f_i^L}{\partial x_j}, \qquad \begin{matrix} i = 1,2,\ldots n_c, \\ j = 1,2,\ldots n_c, \end{matrix} \tag{V-68}$$

$$JG_{i,j} = \frac{\partial f_i^V}{\partial y_j}, \qquad \begin{matrix} i = 1,2,\ldots n_c, \\ j = 1,2,\ldots 2n_c, \end{matrix} \tag{V-69}$$

$$JG_{i,j} = \frac{\partial (f_i^L - f_i^V)}{\partial p_g}, \qquad \begin{matrix} i = 1,2,\ldots n_c, \\ j = 2n_c + 4, \end{matrix} \tag{V-70}$$

$$JG_{i,j} = 0, \qquad \begin{matrix} i = 1,2,\ldots n_c, \\ j = 2n_c+2,\ldots N, \end{matrix} \tag{V-71}$$

since the fugacity of component i in the liquid phase depends on composition $\{x_i\}$ and pressure, and the fugacity of component i in the vapour phase depends on the composition of the vapour phase $\{y_i\}$ and pressure.

Derivatives of the Composition Constraints

Recalling Equation (V-22) and Equation (V-23)

$$G_i^{n+1} = 1 - \sum_{j=1}^{n_c} x_j^{n+1}, \quad i = n_c + 1 \tag{V-72}$$

and

$$G_i^{n+1} = 1 - \sum_{j=1}^{n_c} y_j^{n+1}, \quad i = n_c + 2 \tag{V-73}$$

The derivatives are written as:

$$JG_{i,j} = 1, \quad \begin{matrix} i = n_c + 1, \\ j = 1,2,\ldots,n_c \end{matrix} \tag{V-74}$$

$$JG_{i,j} = 0, \quad \begin{matrix} i = n_c + 1, \\ j = n_c + 1,\ldots,2n_c + 1 \end{matrix} \tag{V-75}$$

$$JG_{i,j} = 0, \quad \begin{matrix} i = n_c + 2, \\ j = 1,2,\ldots n_c \text{ and} \\ j = 2n_c + 1 \end{matrix} \tag{V.76}$$

$$JG_{i,j} = 1, \quad \begin{matrix} i = n_c + 2 \\ j = 1,\ldots 2n_c \end{matrix} \tag{V-77}$$

Derivatives of accumulation terms and production terms are presented in Appendix A.

V.6 Saturation Pressure Calculation

The phase saturation pressure is calculated following Coat's[10] modification of the method of Fussel and Yanosik[17]. The method consists in solving $n_c + 1$ equations in $n_c + 1$ unknowns simultaneously.

For the liquid phase, the equations are the fugacity equations and the gas mole fraction constraint,

$$f_i^L - f_i^V = 0, \quad i = 1,2,\ldots n_c \tag{V-78}$$

and

$$\sum_{i=1}^{n_c} y_i = 1 \tag{V-79}$$

the unknowns being $y_1, y_2, \ldots y_{n_c}$, and p_s.

For the vapour phase, Equation (V-79) is substituted for $\sum_{i=1}^{n_c} x_i = 1$ and the unknowns are $(x_1, x_2, \ldots, x_{n_c}, p_s)$. This system of equations was solved by Newton's method, using numerical derivatives.

In the solution method for the compositional model described above the saturation pressure calculation is performed for each grid block in which $S_o^\nu = 0$ or $S_g^\nu = 0$. The calculated saturation pressure and the absent phase composition are used as the initial estimate for the next calculation of saturation pressure of the block under consideration. For blocks which have attained the critical point, Wilson's correlation is used in the computation of the saturation pressure; otherwise, the saturation pressure calculation converges to the trivial solution: equilibrium k-values are equal to one, (for the cases tested).

V.7 Equations for Flash Calculations

Single-stage flash separation can be described by the following equations: an overall material balance, component material balances, restrictive equations on the phase compositions, and thermodynamic phase equilibria equations. The overall material balance equation

can be written as

$$F_L + F_V = 1, \tag{V-80}$$

where F_L and F_V are the mole fractions of liquid and vapour in a mixture. The component material balance equation can be written as

$$z_i = F_L x_i + F_V y_i, \quad i = 1,2,\ldots n_c \tag{V-81}$$

The constraint composition equations are

$$\sum_i^{n_c} z_i = 1, \tag{V-82}$$

$$\sum_i^{n_c} x_i = 1, \tag{V-83}$$

and

$$\sum_i^{n_c} y_i = 1. \tag{V-84}$$

The thermodynamic phase equilibria equations can be expressed by

$$f_i^L = f_i^V, \quad i = 1,2,\ldots n_c. \tag{V-85}$$

Equilibrium ratios, K_i are defined as

$$K_i = \frac{y_i}{x_i}, \quad i = 1,2,\ldots n_c \tag{V-86}$$

and

$$K_i = \frac{\psi_i^L}{\psi_i^V} = \frac{f_i^L/x_i p}{f_i^V/y_i p} = R_i \frac{y_i}{x_i} \tag{V-87}$$

where $$R_i = \frac{f_i^L}{f_i^V} \qquad \text{(V-88)}$$

and ψ_i^L, ψ_i^V are the fugacity coefficients of the liquid and vapour phase, respectively.

Substituting Equations (V-80) and (V-86) in Equation (V-81) yields

$$x_i = \frac{z_i}{(1 + F_V(K_i - 1))}, \qquad i = 1,2,\ldots n_c \qquad \text{(V-89)}$$

and $\sum_{i=1}^{n_c} (y_i - x_i) = 0$ can be expressed as

$$g(F_V) = \sum_{i=1}^{n_c} \frac{z_i(K_i - 1)}{(1 - F_V(K_i - 1))} = 0 \qquad \text{(V-90)}$$

A flash calculation is performed every time a grid block changes from one hydrocarbon phase to two hydrocarbon phases, i.e. when the saturation pressure of the block is greater than the block pressure. Successive substitution iterations are performed during a time step for any two-hydrocarbon phase grid block when there is no convergence, i.e. $|f_i^L/f_i^V - 1| >$ tolerance. In such a case, initial estimates of equilibrium K-values are obtained/calculated from the last phase composition values.

The flash calculation by successive substitution consists in estimating K_i, solving Equation (V-90) for F_V, and calculating x_i directly from Equation (V-89), and y_i from Equation (V-86). The phase compositions (x_i, y_i) are used to calculate liquid and

vapour compressibility factors and the fugacity of the phases from the equation of state.

New estimates of K_i are calculated from:

$$K_i^{\nu+1} = K_i^{\nu} R_i^{\nu}, \qquad i = 1,2,\ldots n_c \tag{V-91}$$

where $R_i = f_i^L / f_i^V$ and ν is the iteration number.

The procedure is assumed to have converged when $\sqrt{\Sigma (f_i^L - f_i^V)^2}$ is less than a preset tolerance.

The saturations can be calculated from the definitions:

$$S_o = \frac{F_L / \bar{\rho}_o}{F_L / \bar{\rho}_o + F_V / \bar{\rho}_g} (1 - S_w) \tag{V-92}$$

and

$$S_g = 1 - (S_o + S_w) \tag{V-93}$$

V.8 Molar Balance

Cumulative and incremental molar balances are calculated for each component i in the reservoir at every time step. These are represented by

$$MBI_i = \frac{n_{t_i}^n - n_{t_i}^{n+1}}{q_{i_t} \Delta t}, \qquad i = 1,2,\ldots n_c + 1 \tag{V-94}$$

and

$$MBC_i = \frac{n_{t_i}^{o} - n_{t_i}^{n+1}}{\sum_{j=1}^{n+1} q_{i_t} \Delta t_j}, \quad i = 1,2,3,\ldots n_c + 1 \qquad \text{(V-95)}$$

where n_{t_i} is the total moles of component i in the reservoir at a given time, and q_{i_t} is the total producing/injecting molar rate in the reservoir at a given time.

The total moles of component i are given by the following equations for hydrocarbon components:

$$n_{t_i} = \sum_{j=1}^{N_t} [V_p(\bar{\rho}_o S_o x_i + y_i \bar{\rho}_g S_g)]_j, \quad i = 1,2,\ldots n_c \qquad \text{(V-96)}$$

where N_t is the total number of grid blocks; and for water component:

$$n_{t_i} = \sum_{j=1}^{N_t} [V_p(\bar{\rho}_w S_w)]_j, \quad i = n_c + 1 \qquad \text{(V-97)}$$

The total producing/injecting molar rate for the component i is given by

$$q_{i_t} = \sum_{j=1}^{N_t} (q_i)_j, \quad i = 1,2,\ldots n_c + 1 \qquad \text{(V-98)}$$

V.9 Surface Production Rates

The surface production rates (oil and gas) are obtained by a flash calculation at surface conditions of the produced fluids. Knowing the moles produced (n_{t_p}) and the total composition, the phase

production rates are as follows.

The oil production rate is given by

$$q_{o_s} = \frac{F_L \, n_{t_p}}{\bar{\rho}_{o_s}} \tag{V-99}$$

where F_L is the liquid mole fraction from a flash calculation at surface conditions and $\bar{\rho}_{o_s}$ is the density of the oil phase at standard conditions.

The total moles produced (n_{t_p}) is given by

$$n_{t_p} = \sum_{i=1}^{n_c} q_{i_t} \, \Delta t, \tag{V-100}$$

where q_{i_t} is the total producing molar rate of component i.

The gas production rate is given by

$$q_{g_s} = \frac{F_V \, n_{t_p}}{\bar{\rho}_{g_s}}, \tag{V-101}$$

and the water production rate is given by

$$q_{w_s} = \frac{q_w \, \bar{\rho}_{w_{resv}}}{\bar{\rho}_{w_s}}. \tag{V-102}$$

CHAPTER VI

COMPUTATIONAL PROCEDURE

A FORTRAN computer program was written to simulate numerically isothermal compositional displacement as formulated by the mathematical model described in Chapters IV and V.

This program has the following features:

1. It implements the fully implicit method. The Jacobian matrix is evaluated numerically.
2. It includes the Peng-Robinson Equation of State for equilibrium calculations.
3. It implements 1-D or 2-D areal modes.
4. It simulates a no flow boundary condition.
5. It implements the five-point scheme of discretization.
6. It accepts regular or irregular grid block sizes.
7. It simulates fluid phases composed of three or more components.
8. The injection and production rates are treated implicitly.
9. It allows for the presence of five wells, injection or production.
10. It implements the variable substitution method.
11. It implements automatic time step selection.

A brief description of the main units of the program is presented and the flow diagram of the computational procedure is shown in Figure 6.1.

Main Program

Basic data of the reservoir and fluids are read in Subroutine

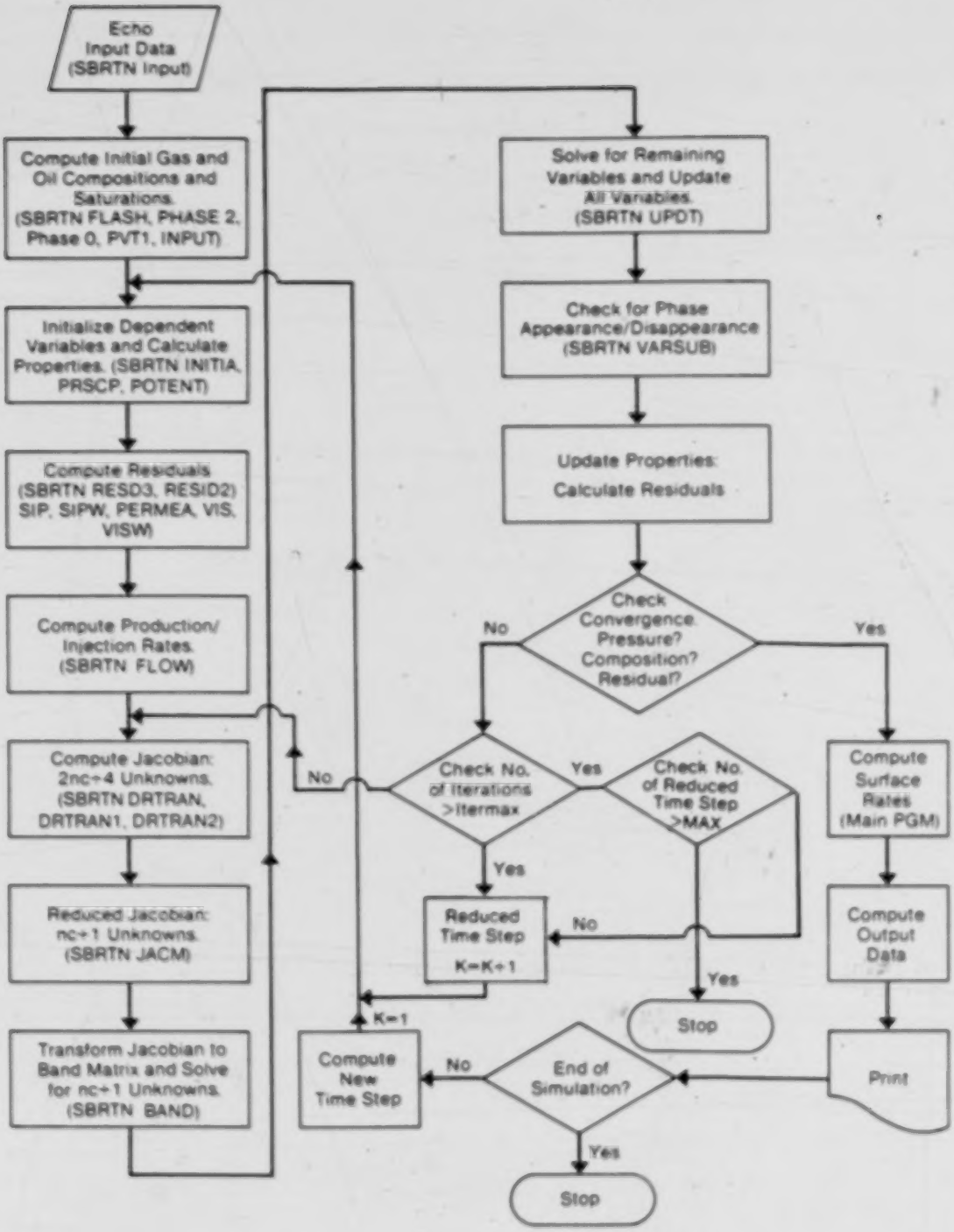
Echo Input Data (SBRTN Input)
Compute Initial Gas and Oil Compositions and Saturations. (SBRTN FLASH, PHASE 2, Phase 0, PVT1, INPUT)
Initialize Dependent Variables and Calculate Properties. (SBRTN INITIA, PRSCP, POTENT)
Compute Residuals (SBRTN RESD3, RESID2) SIP, SIPW, PERMEA, VIS, VISW)
Compute Production/ Injection Rates. (SBRTN FLOW)
Compute Jacobian: 2nc+4 Unknowns. (SBRTN DRTRAN, DRTRAN1, DRTRAN2)
Reduced Jacobian: nc+1 Unknowns. (SBRTN JACM)
Transform Jacobian to Band Matrix and Solve for nc+1 Unknowns. (SBRTN BAND)
Solve for Remaining Variables and Update All Variables. (SBRTN UPDT)
Check for Phase Appearance/Disappearance (SBRTN VARSUB)
Update Properties: Calculate Residuals
Check Convergence. Pressure? Composition? Residual?
No
Yes
Check No. of Iterations >Itermax
Yes
No
Check No. of Reduced Time Step >MAX
Yes
No
Reduced Time Step K=K+1
Yes
Stop
K=1
Compute New Time Step
No
End of Simulation?
Yes
Stop
Compute Surface Rates (Main PGM)
Compute Output Data
Print

Figure 6.1 Flow diagram of the computational procedure.

INPUT. These data consist of initial pressure, temperature, component and/or pseudocomponent identification, properties of pseudocomponents, interaction parameters and total composition distribution of the hydrocarbon mixture and water saturation. Reservoir properties: porosity, absolute permeability, reservoir thickness, grid sizes are read in tabular form or as constant properties. Relative permeability and capillary pressure data for the oil-water system and for liquid-gas system can be read in tabular form, or can be calculated from correlations, or entered as polynomials. Production and injection rates are read in.

Saturation pressure calculations (Subroutine PHASE1, PHASE0) are done initially if the total hydrocarbon mixture is indicated as a single phase, otherwise a flash calculation (Subroutine FLASH1) is undertaken in order to compute the oil and gas compositions and saturations at the initial reservoir conditions.

The constant part of the transmissibility terms and the block volumes are calculated in Subroutine TRANS. Dependent variables and properties are computed in Subroutines PRSCP and POTENT, respectively. Initial values for the first time step are computed in Subroutine INITIA.

Transmissibility coefficients are evaluated upstream and computation of residuals is done in Subroutines RESD3 and RESD2 Production/Injection molar rates are calculated in Subroutine FLOW, and are added algebraically to complete the residual. These calculations are carried out for every iteration. General derivatives are calculated in Subroutine DRTERM, and block matrix derivatives for the $2n_c + 4$ unknowns are computed in Subroutine DRTRAN 2. Reduction of

these block matrices to $(n_c+1) \times (n_c+1)$ order is done in Subroutine JACM.

In order to solve simultaneously the system of $n_c + 1$ primary equations for each grid block, the Jacobian matrix is transformed into a band matrix and solved, in Subroutine BAND, using a band solver routine from the IMSL Library. By back substitution of the primary variables, the remaining $n_c + 3$ variables are calculated and all variables are updated in Subroutine UPDT.

Detection of phase appearance or disappearance is undertaken in Subroutine VARSUB. Properties are updated and residuals are calculated, and therefore the convergence criteria are tested at this level.

If convergence is not reached, after a specified number of iterations is performed (i.e. if the change in saturation is greater than 0.2 per time step for the immiscible cases, or if any component disappears or becomes negative abruptly), the time step is reduced and the calculations are repeated for the current time step.

Molar balances are calculated after convergence. Total composition of the two-hydrocarbon phase grid blocks is computed from the values of oil and gas compositions and saturations. Then, flash calculations at surface conditions are made and surface production rates are calculated.

Finally, the results obtained at the new time level are printed out as output. Variables at the old time level are updated and the new time step is calculated and the solution is advanced.

CHAPTER VII

RESULTS AND DISCUSSION

The compositional model presented in Chapters V and VI was tested for a variety of flow problems to prove its capabilities. Three examples were selected such that two types of floods, multicontact miscible displacement and immiscible displacement with mass transfer were involved. Three tests were performed for a one-dimensional (1-D) reservoir, while three additional tests simulated a two-dimensional (2-D areal) reservoir.

VII.1 Examples Studied

Each example problem represents a simulator run with a particular set of physical properties. Six example problems were evaluated:

One dimensional reservoir:

1. Condensing gas drive, multicontact miscible displacement.
2. Condensing gas drive, immiscible displacement.
3. High pressure gas drive, immiscible displacement.

Two dimensional reservoirs:

4. Condensing gas drive, multicontact miscible displacement, in 1/4 of a five-spot.
5. Condensing gas drive, immiscible displacement, in 1/4 of a five-spot.
6. High pressure gas drive immiscible displacement in 1/4 of a five-spot.

VII.2 Reservoir Data

A methane, n-butane and n-decane system at 71.1°C (160°F) was chosen to test the model for two reasons: experimental phase equilibria data for this system is available from the literature, and a three-component system can be represented rigorously by means of a ternary diagram[23]. Also, this set of data has been used previously by other authors[10,54] to test and compare current compositional simulators. Therefore, this data is ideally suited for verifying the results of the present compositional model.

The basic reservoir data, common to all examples, is listed in Table VII.1. Data for the condensing gas drive, Example Problems 1 and 2, for one-dimensional reservoirs, and Examples 4 and 5, for two-dimensional reservoirs, is listed in Table VII.2. Data for the high pressure gas drive, Example Problem 3, for a one-dimensional reservoir, and Example Problem 6 for a two-dimensional reservoir, is listed in Table VII.3.

For all examples studied, the capillary pressure and gravity terms were set to zero ($P_{cog} = P_{cwo} = 0$, horizontal reservoir), with an irreducible water saturation set equal to 0.20. The relative permeability functions used in all examples are given by Equations (IV-39) to (IV-45). Initial interfacial tension for the condensing gas examples is 9.2 mN/m (dynes/cm), and for the high pressure gas examples is 0.07 mN/m. Comparison of experimental phase equilibria data and the molar volumes data for the methane, n-butane and decane system at 71.1°C (160°C) and the corresponding values calculated by the Peng-Robinson equation of state are displayed in Table VII.4 and Table VII.5, respectively. The interaction parameter for methane and

TABLE VII.1

BASIC RESERVOIR DATA COMMON TO ALL EXAMPLES

Permeability, m^2 (md)	$1.974\ 10^{-6}$ (2000)
Porosity, fraction	0.20
Rock Compressibility, 1/Pa (1/psi)	$5.8\ 10^{-10}$ ($4\ 10^{-6}$)
Water Compressibility, 1/Pa (1/psi)	$4.35\ 10^{-10}$ ($3\ 10^{-6}$)
Capillary Pressure, Pa (psi)	0
Temperature, °C (°F)	71.1 (160)
Initial Water Saturation, fraction	0.2
Initial Oil Saturation, fraction	0.8
Initial Gas Saturation, fraction	0.0
Productivity Index, m^3 Pa.s/Pa.s (ft^3 - cP/D . psi)	$4.84\ 10^{-9}$ ($1.012\ 10^{5}$)

TABLE VII.2

RESERVOIR DATA CORRESPONDING TO EXAMPLE PROBLEMS 1 AND 2 FOR THE 1-D RESERVOIR AND TO EXAMPLE PROBLEMS 4 AND 5 FOR THE 2-D RESERVOIR

Dimensions for linear (1-D) reservoir, m (ft)		
Length		72.2 (250)
Width		30.48 (100)
Thickness		15.24 (50)
1/4 of a five-spot, area m^2 (acres)		142.24 × 142.24 (5)
Thickness, for 2-D m (ft)		1.750 (5.74)
Initial Oil Composition, mole fraction		
Methane		0.2
n-Butane		0.2
Decane		0.6
Initial and Production Pressure, Pa (psi)		$139{,}90\ 10^5$ (2000)
Number of Grid Blocks		20
Time Step, s (D)		$6.48\ 10^5$ (7.5)
Injection Rates at Reservoirs Conditions m^3/s (ft^3/d)	Examples 1 and 4	Examples 2 and 5
	$1.74\ 10^{-4}$ (530)	$1.74\ 10^{-4}$ (530)
Injection Composition, mole fraction	Examples 1 and 4	Examples 2 and 5
Methane	0.684	0.8
n-Butane	0.316	0.2

TABLE VII.3

RESERVOIR DATA CORRESPONDING TO EXAMPLE PROBLEM 3 FOR THE 1-D RESERVOIR AND TO EXAMPLE PROBLEM 6 FOR 2-D RESERVOIR

Dimensions for linear (1-D) reservoir, m (ft)	
Length	24.38 (80)
Width	30.48 (100)
Thickness	15.24 (50)
1/4 of a five-spot, area m^2 (acres)	110.2 × 110.2 (3)
Thickness, for 2-D m(ft)	1.866 (6.122)
Initial Oil Composition, mole fraction	
Methane	0.62
n-Butane	0.30
Decane	0.08
Initial and Production Pressure, Pa (psi)	$189.88\ 10^5$ (2754)
Number of Grid Blocks	20
Time Step, s (D)	$6.48\ 10^5$ (7.5)
Injection Rates, at Reservoir Conditions	Examples 3 and 6
m^3/s (ft^3/D)	$1.74\ 10^{-4}$ (530)
Injection Composition, mole fraction	
Methane	0.99
n-Butane	0.01

TABLE VII.4

COMPARISON OF THE EQUILIBRIUM K-VALUES CALCULATED BY THE PENG-ROBINSON EQUATION OF STATE AND EXPERIMENTAL DATA[43,51]

Experimental Temperature = 71.1°C (160°F)

Composition (mole fraction)	Pressure-Calculated Pa (psia)	K_{exp} (Ref.43,51)	K_{cal}	Error %
Methane = 0.422	134,84 10^5 (1955.62)	2.290	2.287	0.131
n-Butane = 0.116		0.251	0.261	3.828
Decane = 0.462		0.0094	0.0101	7.861
Methane = 0.428	134,24 10^5 (1947.05)	2.180	2.1714	0.394
n-Butane = 0.229		0.2725	0.2875	5.504
Decane = 0.343		0.0145	0.0139	4.138
Methane = 0.444	134.47 10^5 (1950.33)	2.000	1.9916	0.450
n-Butane = 0.333		0.3200	0.3297	3.030
Decane = 0.222		0.0263	0.2218	15.665
Methane = 0.485	135.49 10^5 (1965.05)	1.705	1.6976	0.434
n-Butane = 0.412		0.4055	0.4163	2.663
Decane = 0.103		0.0615	0.0496	19.333
Methane = 0.564	200,88 10^5 (2913.59)	1.700	1.7015	0.06
n-Butane = 0.087		0.3290	0.3378	2.67
Decane = 0.347		0.0318	0.0314	1.26
Methane = 0.583	202,77 10^5 (2940.98)	1.575	1.578	0.24
n-Butane = 0.167		0.4030	0.3975	1.36
Decane = 0.250		0.0624	0.0526	15.75
Methane = 0.621	206,25 10^5 (2991.46)	1.375	1.3921	1.244
n-Butane = 0.227		0.5435	0.5133	5.556
Decane = 0.151		0.1642	0.1190	27.523

TABLE VII.5

COMPARISON OF THE MOLAR VOLUMES CALCULATED BY THE PENG-ROBINSON EQUATION OF STATE AND EXPERIMENTAL DATA

Composition (mole fraction)	Temperature: 71.1°C (160°F) Pressure Pa (psia)		Molar Volume l/g-mol		Error %
			Experimental [Ref (44,50)]	Calculated	
Methane = 0.2746 n-Butane = 0.3359 Decane = 0.3895	$B.P._{exp}$	$81.70\ 10^5$ (1185.)	0.1324		
	$B.P._{calc}$	$78.58\ 10^5$ (1139.69)		0.1324	3.59
		$41.37\ 10^5$ (600)	0.2333	0.2334	0.01
		$68.95\ 10^5$ (1000)	0.1503	0.1509	0.41
Methane = 42.65 n-Butane = 0.2656 Decane = 0.3079	$B.P._{exp}$	$137.21\ 10^5$ (1990)	0.1176		
	$B.P._{calc}$	$132.17\ 10^5$ (1917)		0.1213	3.11
		$68.95\ 10^5$ (1000)	0.2037	0.2030	0.34
		$86.18\ 10^5$ (1250)	0.1672	0.1670	0.11
		$120.66\ 10^5$ (1750)	0.1286	0.1289	0.23
Methane = 0.5989 n-Butane = 0.1857 Decane = 0.2154	$B.P._{exp}$	$212.01\ 10^5$ (3075)	0.1030		
	$B.P._{calc}$	$206.85\ 10^5$ (3000.07)		0.1037	0.65
		$68.95\ 10^5$ (1000)	0.2647	0.2614	1.23
		$137.90\ 10^5$ (2000)	0.1395	0.1381	1.05
		$189.61\ 10^5$ (2750)	0.1104	0.1094	0.86

$B.P._{exp}$ indicates experimental bubble point, $B.P._{calc}$ indicates calculated bubble point.

decane were set to 0.038, while the remaining ones were set to zero.

VII.3 Simulation of Displacements in a One-Dimensional Reservoir

VII.3.1 Example Problem 1: Condensing Gas, Multicontact Miscible Displacement

The overall composition of each grid block, after 0.20 and 0.56 pore volume injected (PV) is shown in Figure 7.1. These points form the composition path through the reservoir. The ternary diagram shown in this figure indicates the mechanism by which the displacement process occurs.

As shown in Figure 7.1, the original oil composition, point o, is poor in the intermediate component and it is to the left of the limiting tie line. The injection gas, point G, is at or on the other side of the critical tie line and is rich in the intermediate component. These conditions are used to define a multicontact condensing gas process[23]. At first, gas G and oil o are not miscible because most of the mixtures fall within the two-phase region. But as the gas G contacts the oil, the oil is enriched with intermediate components and its composition follows the bubble point curve (point I), until it reaches the critical point C. At the critical point, the injected gas is miscible with the oil and can be effectively displaced by this process. Thus, a piston-like displacement could be accomplished in the absence of gravity override and viscous fingering.

During the two-phase period, gas and oil continuously converge towards the critical point. As is shown in Figure 7.2 and Figure 7.3,

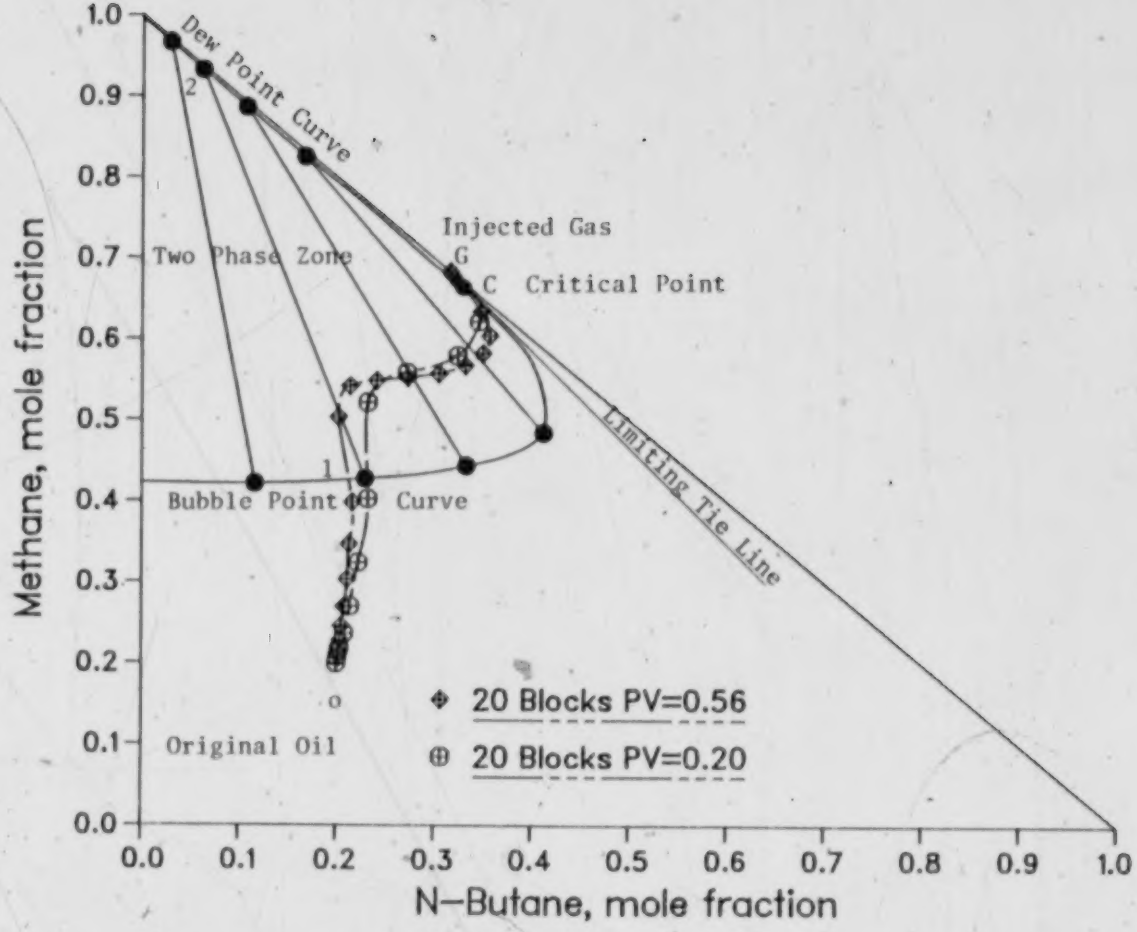

Figure 7.1 Example Problem 1: Composition path for condensing gas drive, multicontact miscible displacement at 0.56 and 0.20 PV and 20 grid blocks.

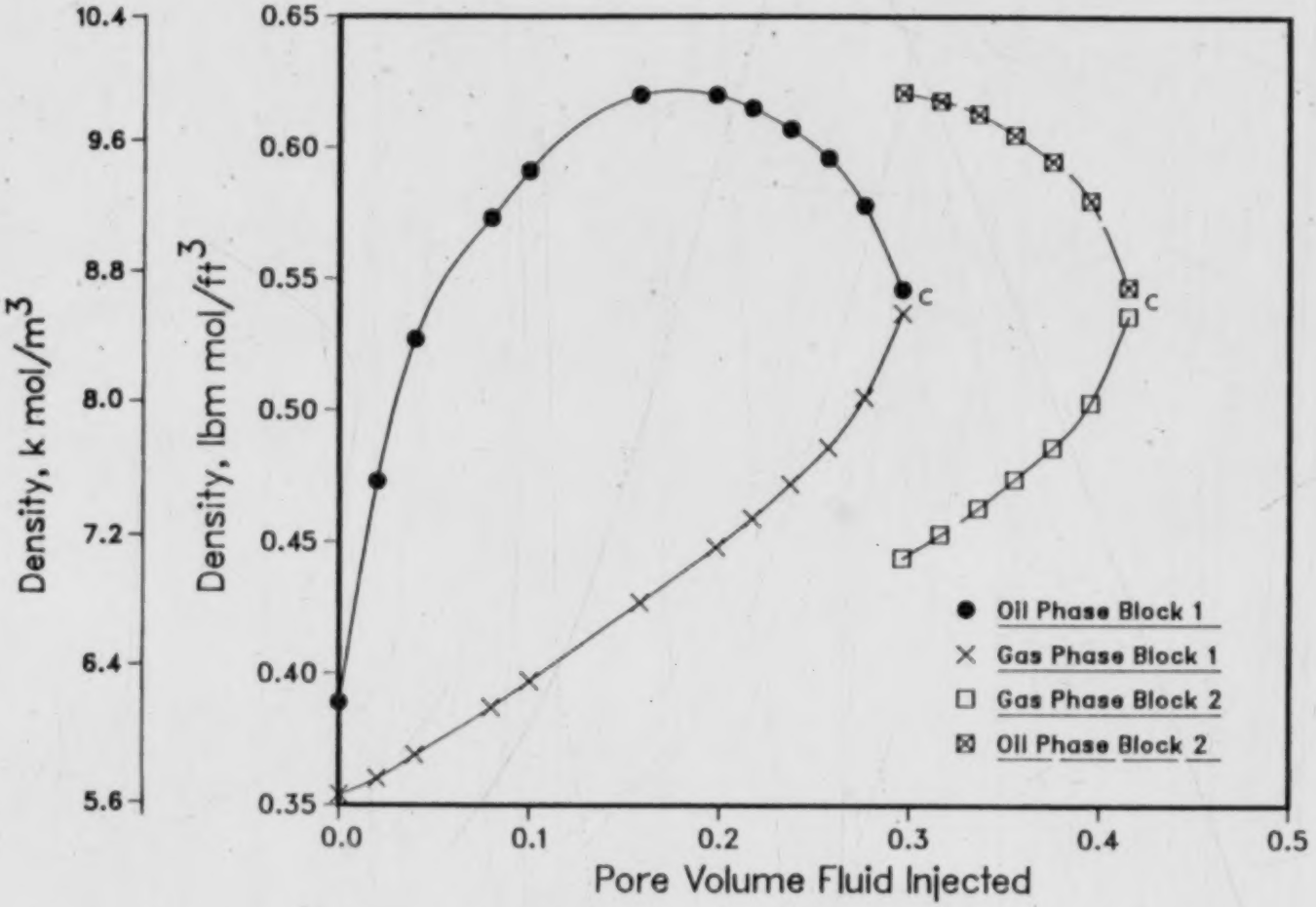

Figure 7.2 Example Problem 1: Density profile for condensing gas drive, multicontact miscible displacement for grid block 1 and 2 vs pore volume fluid injected (PV).

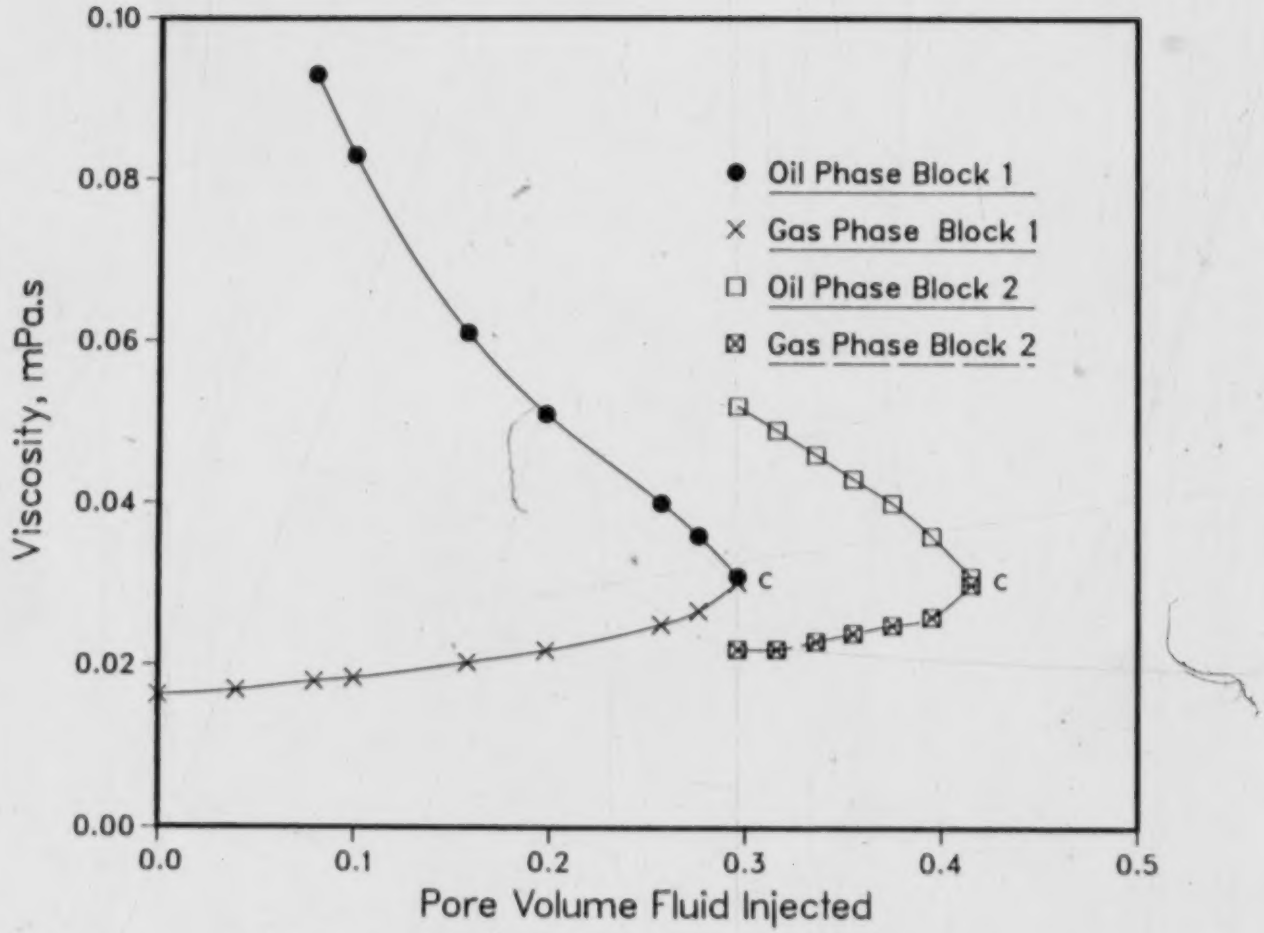

Figure 7.3 Example Problem 1: Viscosity profile for condensing gas drive, multicontact miscible displacement for grid block 1 and 2 vs pore volume fluid injected (PV)

the densities and viscosities of the oil and gas phases also converge to the critical point C.

Figure 7.4 shows the gas saturation profile with a smearing front at different pore volumes injected. The three zones mentioned earlier can be seen starting at the injection point. The first zone is a monophasic zone, or diffusion zone between the injected gas and the miscible front. The second zone is a two-phase region in thermodynamic equilibrium: the gas composition changes following the dew point curve, from the critical point to point 2 (Figure 7.1), and the oil composition changes following the bubble point curve from the critical point to point 1 (Figure 7.1). The third zone, the monophasic oil zone, includes a region where the oil composition changes from point 1 to the original composition o (Figure 7.1).

A simplified analytical solution shows[61,14] that the composition path should enter and exit the two-phase zone along tie line extensions and should jump from the initial oil composition to the two-phase region. Neither of these phenomena is exhibited by Figure 7.1 due to numerical dispersion. The transition region from the original oil composition to the two-phase region is much larger than that expected on the basis of physical dispersion[12]. As shown by Figures 7.4 and 7.5 this transition region extends from grid block 13 to 20 for 0.56PV. Also, the n-butance profile in Figure 7.5 shows an overshoot after the miscible front, point C. These problems are due to numerical dispersion, and have been noted in the literature[10,54].

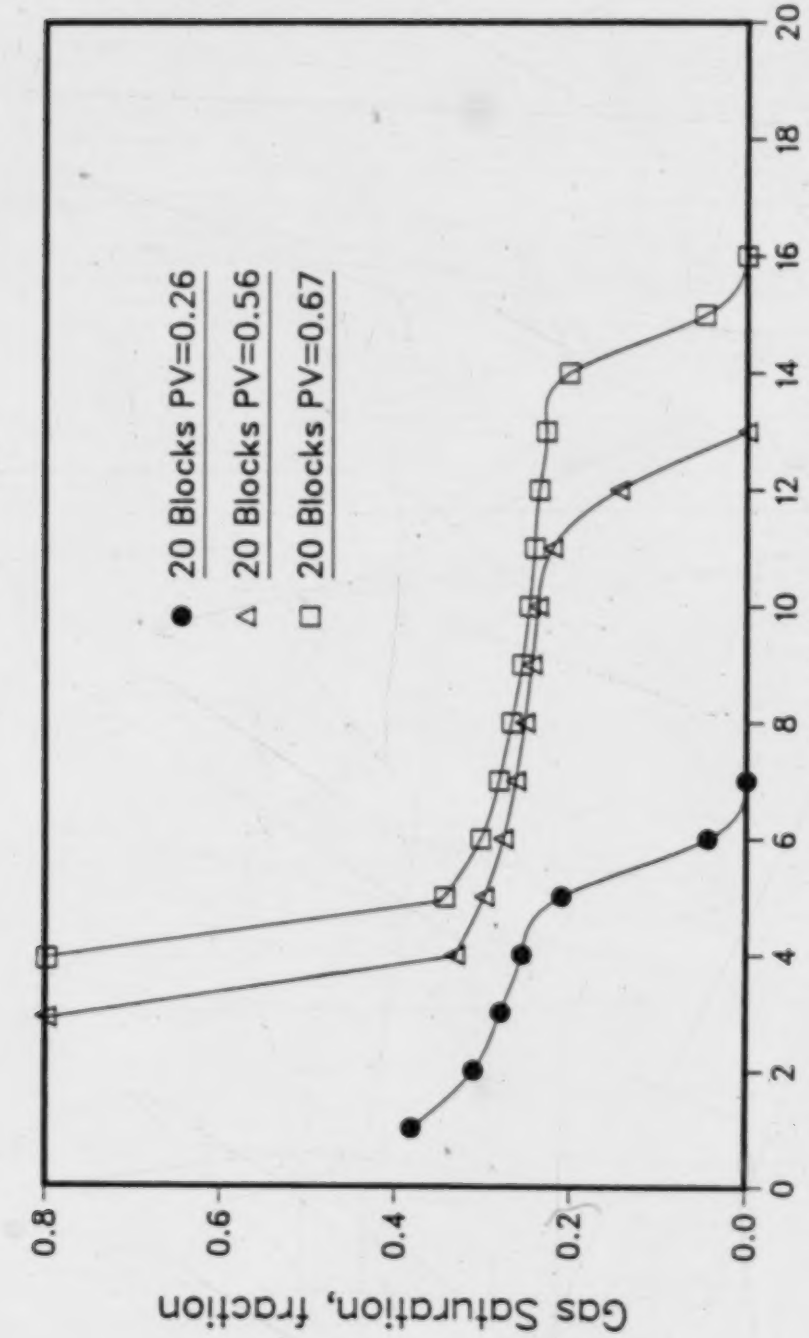

Figure 7.4 Example Problem 1: Gas saturation profile for condensing gas drive, multicontact miscible displacement at 0.26, 0.56 and 0.67 PV and 20 grid blocks

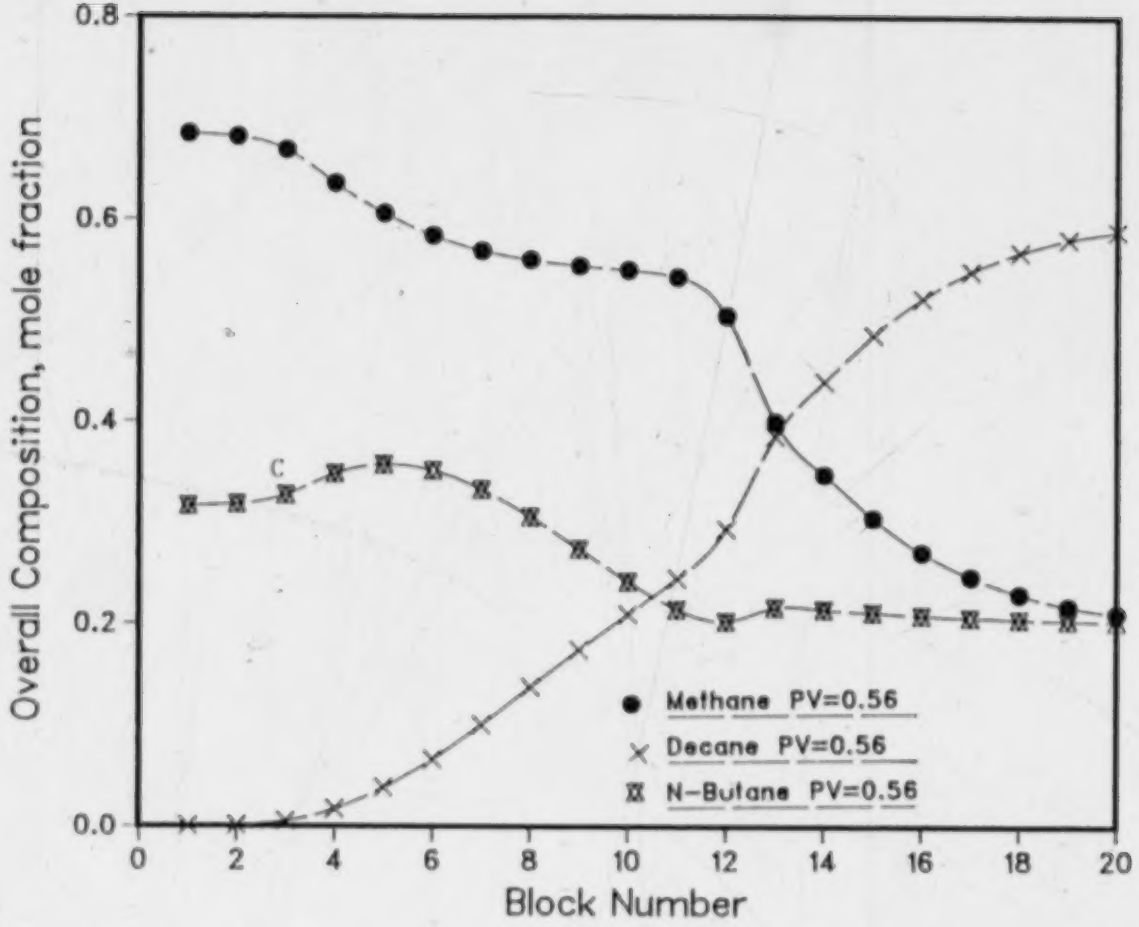

Figure 7.5 Example Problem 1: Overall composition profile for condensing gas drive, multicontact miscible displacement at 0.56 PV and 20 grid blocks

VII.3.2 Example 2: Condensing Gas, Immiscible Displacement

Figure 7.6 shows the overall composition of each grid block or compositional path upon the injection of 0.20 PV and 0.56 PV, respectively. The process represented by this ternary diagram is similar to that in Example Problem 1, except that in Example Problem 2, the injected gas is not as rich. The injected gas G and the initial reservoir oil o are on the same side of the limiting tie line. This condition defines the process as an immiscible displacement with mass transfer.

As can be observed in Figure 7.6, the oil cannot be enriched to the critical point C. The maximum enrichment is limited by the tie line that passes through the injected gas composition. This condition creates a two-phase transition zone, where the oil phase is enriched and follows the bubble point curve from point 1 to point 3, while the gas phase follows the dew point curve up to point 2, as the two phases are in thermodynamic equilibrium.

In Figure 7.6, the path at 0.20 PV shows more numerical dispersion than the path at 0.56 PV. This is so, because both paths should match, and furthermore, the path for 0.56 PV enters and leaves the two-phase zone along tie line extensions through the original oil and the injected gas compositions, while the path at 0.20 PV does not.

In Figures 7.7 and 7.8 the viscosity and density curves converge to a value determined by the point of maximum enrichment, where all fluid properties are invariant due to thermodynamic equilibrium. Figure 7.9 presents the gas saturation profile at

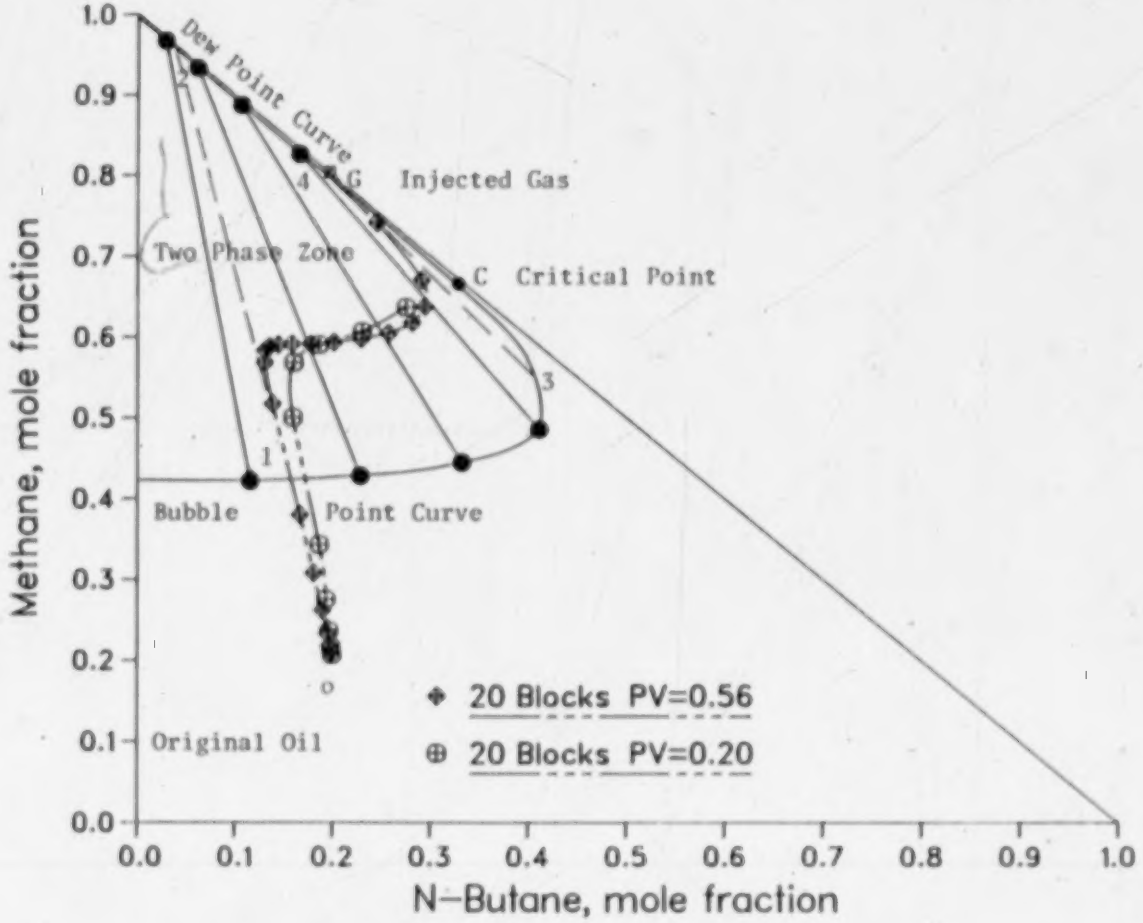

Figure 7.6 Example Problem 2: Composition path for condensing gas drive, immiscible displacement at 0.20 and 0.56 PV and 20 grid blocks

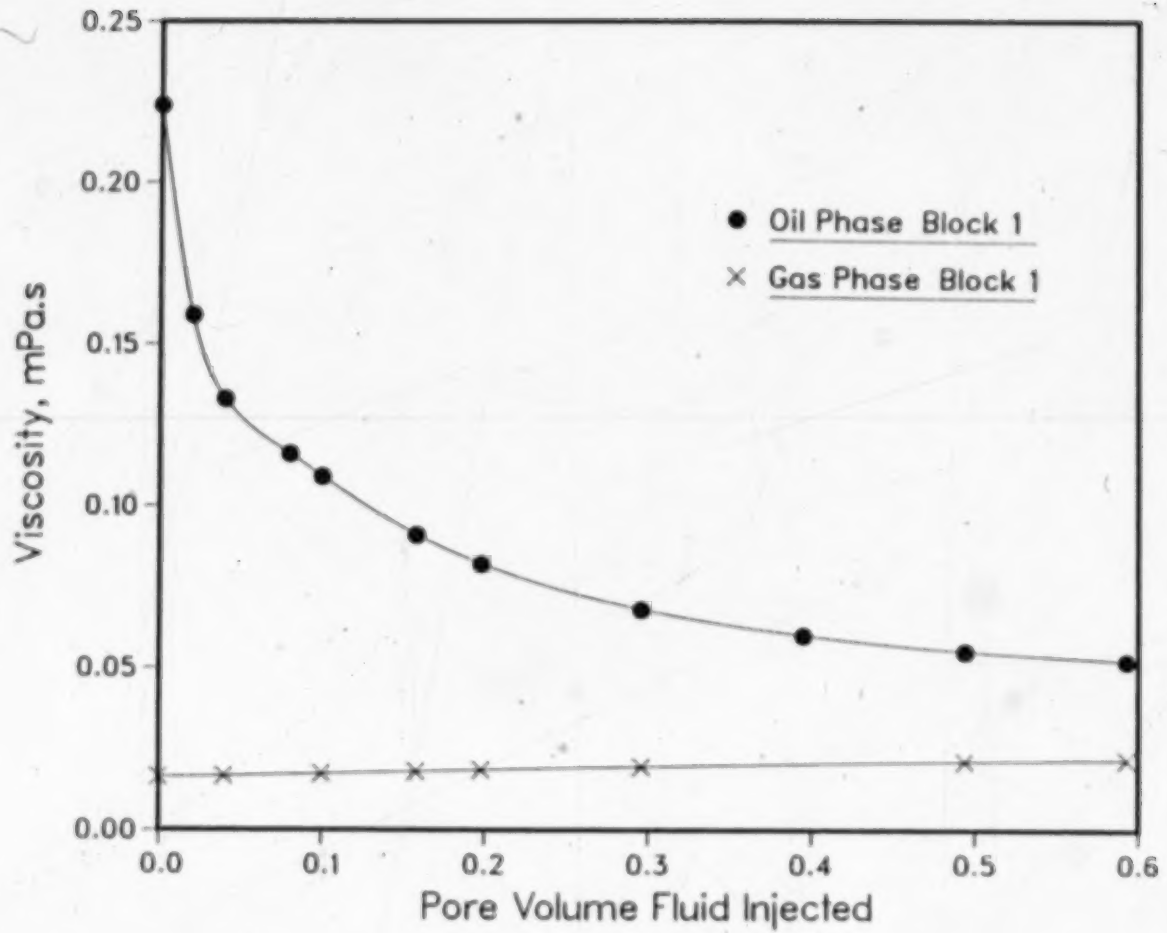

Figure 7.7 Example Problem 2: Viscosity profile for condensing gas drive, immiscible displacement for grid block 1 vs pore volume injected (PV)

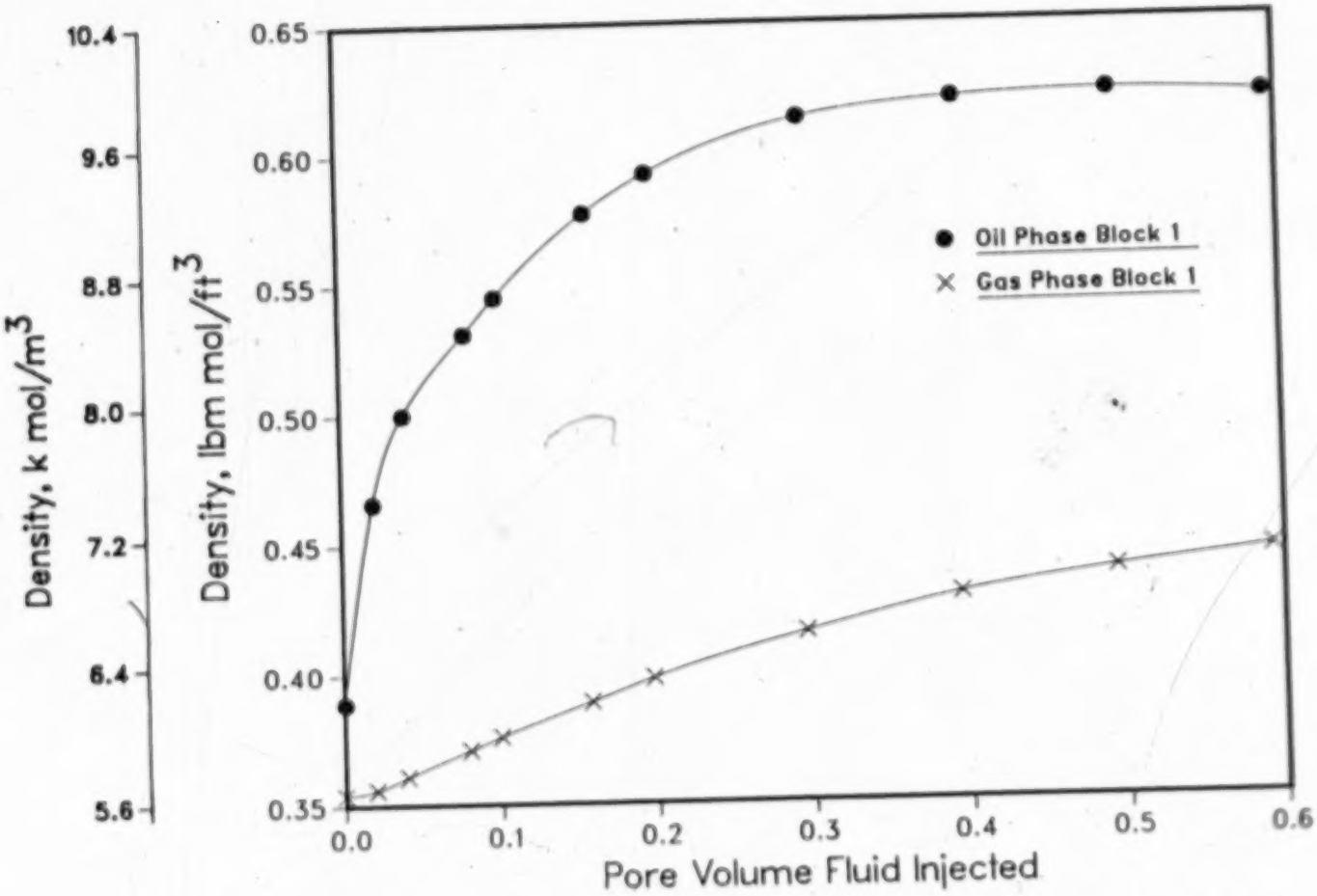

Figure 7.8 Example Problem 2: Density profile for condensing gas drive, immiscible displacement for grid block 1 vs pore volume fluid injected (PV)

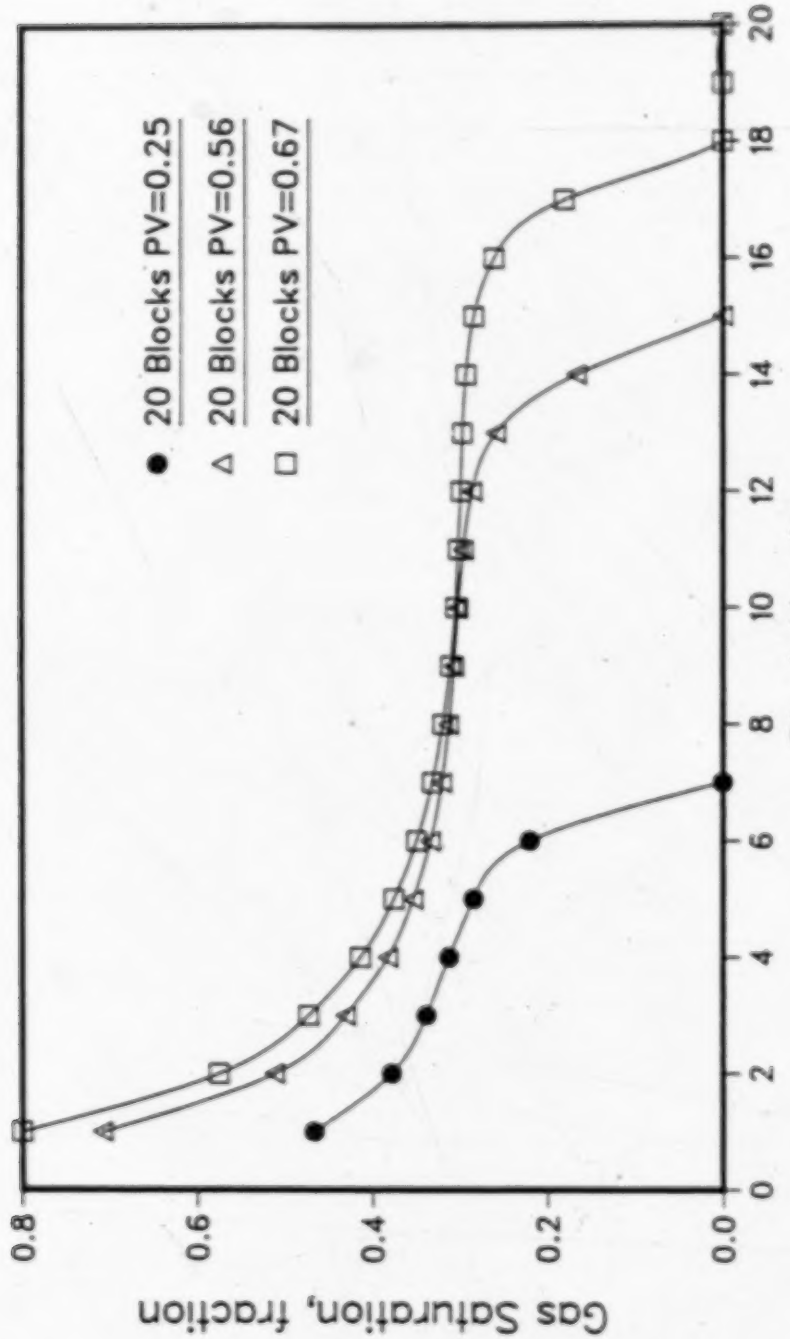

Figure 7.9 Example Problem 2: Gas saturation profile for condensing gas drive, immiscible displacement at 0.25, 0.36 and 0.67 PV and 20 grid blocks

different pore volumes injected. It shows three zones. The first zone is a monophasic gas zone located next to the injection well. This zone is only created if the heaviest component in the enriched liquid phase is appreciably volatile; if so, the oil phase will be completely evaporated near the injection point. The second zone is the two-phase transition zone, which is in complete thermodynamic equilibrium. The third zone is a monophasic oleic region, which includes a transition zone from point 1 to the original oil composition (Figure 7.6) and can be seen in Figure 7.10 from grid block 15 to 20 for 0.56PV.

All these results are affected by numerical dispersion as in Example Problem 1, but to a lesser extent.

VII.3.3 Example Problem 3: High Pressure Gas, Immiscible Displacement

Figure 7.11 presents the composition path at 0.56 PV for a high pressure gas displacement. This figure illustrates the process when a lean gas G is injected into a reservoir with enriched oil o. As the lean gas comes into contact with the oil, it becomes enriched with the intermediate component and displaces the original oil, leaving a residual oil saturation. This process is therefore called a vaporization or high pressure gas drive.

During this process, the gas at the front can be enriched by multiple contacts to a point which is determined by the oil composition: point o in Figure 7.11. If a tie line (with the exception of the critical tie line) can pass through the original oil composition, it determines the maximum enrichment of the gas, and the process is called immiscible displacement with mass transfer. If the critical tie line passes through the point representing the original oil composition,

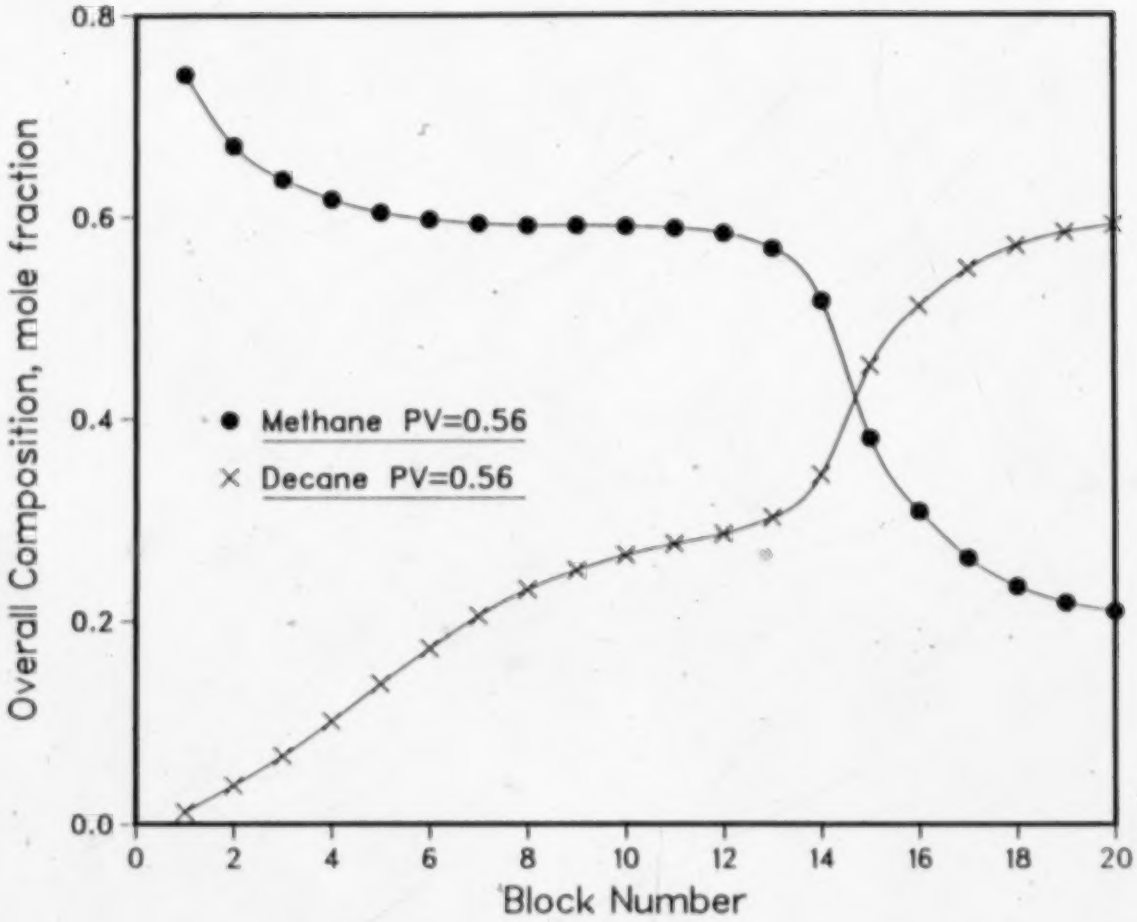

Figure 7.10 Example Problem 2: Overall composition profile for condensing gas drive, immiscible displacement at 0.56 PV and 20 grid blocks

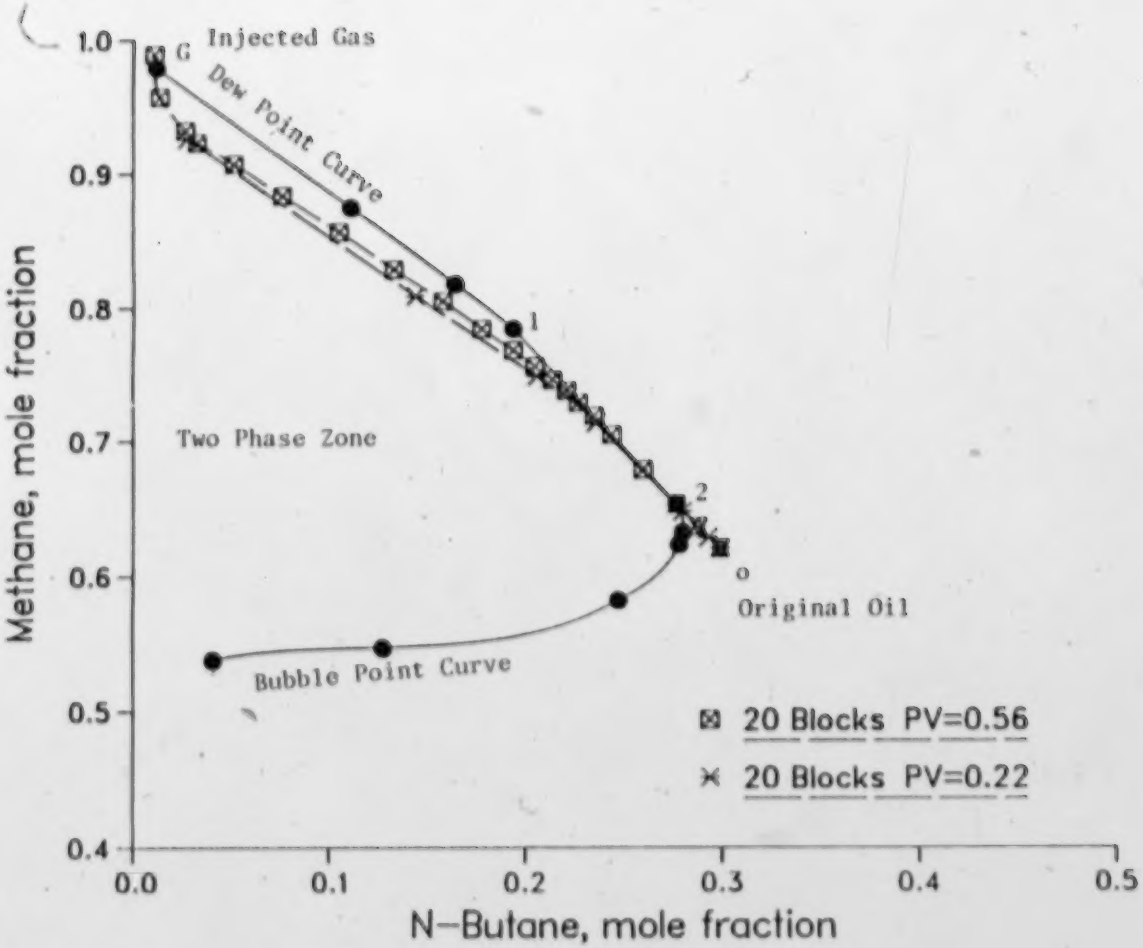

Figure 7.11 Example Problem 3: Composition path for high pressure gas drive, immiscible displacement at 0.22 and 0.56 PV and 20 grid blocks

the injected gas can achieve miscibility at the front with the original oil and the process is called multicontact miscible displacement by vaporization. The example presented in Figure 7.11 shows this type of immiscible displacement.

Figure 7.12 shows the composition profiles for the oil phase, the gas phase and the mixture. It is seen that the oil and gas phases in the first few blocks have been denuded of n-butane, upon the injection of 0.56 PV. These grid blocks form a two-phase zone of residual oil saturation and the following blocks form a two-phase transition zone.

Figure 7.13 shows the density of the oil and gas phases of grid block 2 with respect to pore volumes injected. Reduction of oil and gas phase densities is observed as the grid block composition converges to the point of maximum enrichment and it is denuded of the intermediate component. The maximum observed in the gas phase density curve is due to numerical dispersion (size of the grid blocks).

Figure 7.14 shows the viscosity profile of the oil and gas phases. The oil viscosity of the grid blocks close to the injection well has increased due to the vaporization of the intermediate component. The oil viscosity in block 18 is smaller than that in block 20 as oil phase changes (Figure 7.11) from undersaturated (point o) to saturated (point 2) by vaporization of n-butane.

Figure 7.15 shows the gas saturation profile at two different pore volumes injected. In this figure three zones can be distinguished starting at the injection point; first, a monophasic gas zone, due to volatilization of the heaviest components or residual oil; second, two-phase zone, which includes a region with residual oil saturation, and third a monophasic zone with the original fluid composition.

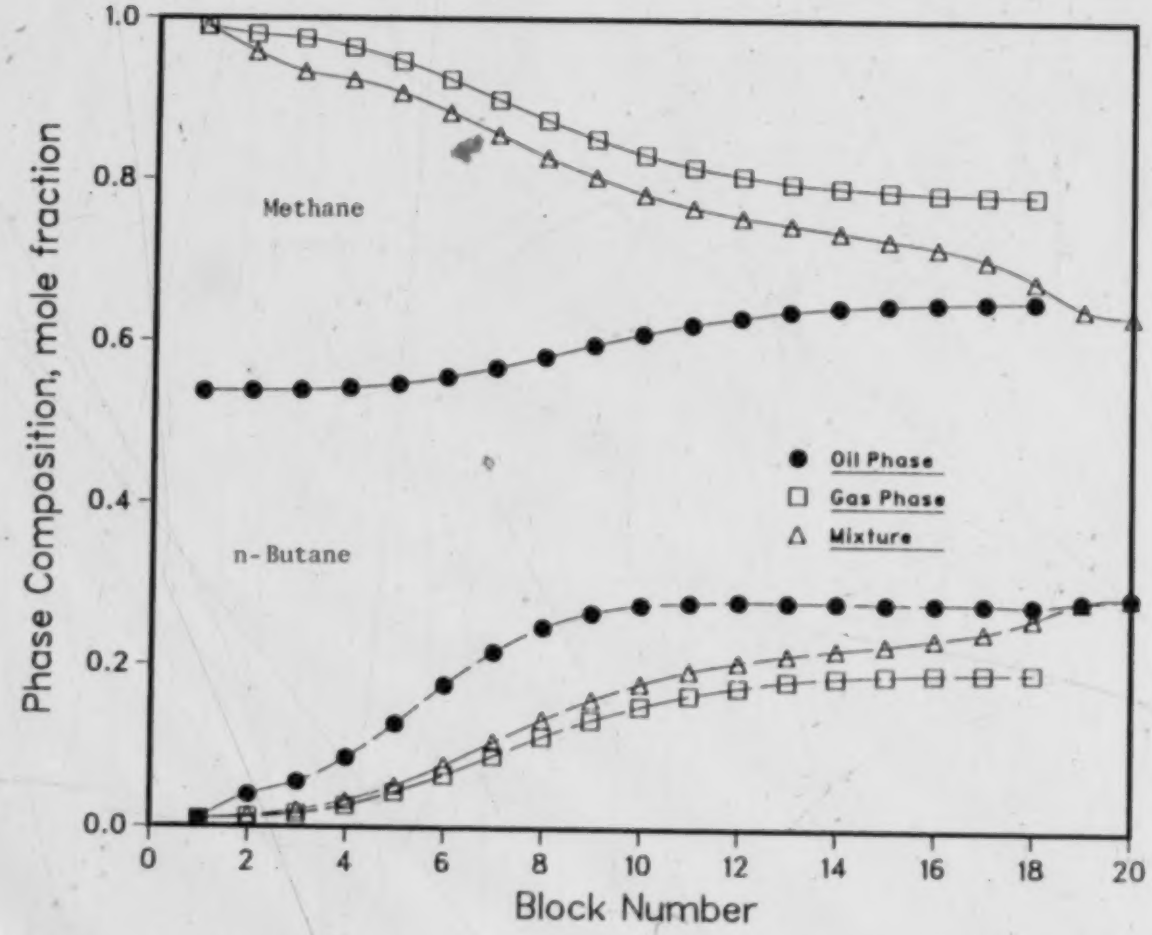

Figure 7.12 Example Problem 3: Composition profile for high pressure gas drive, immiscible displacement at 0.56 PV and 20 grid blocks

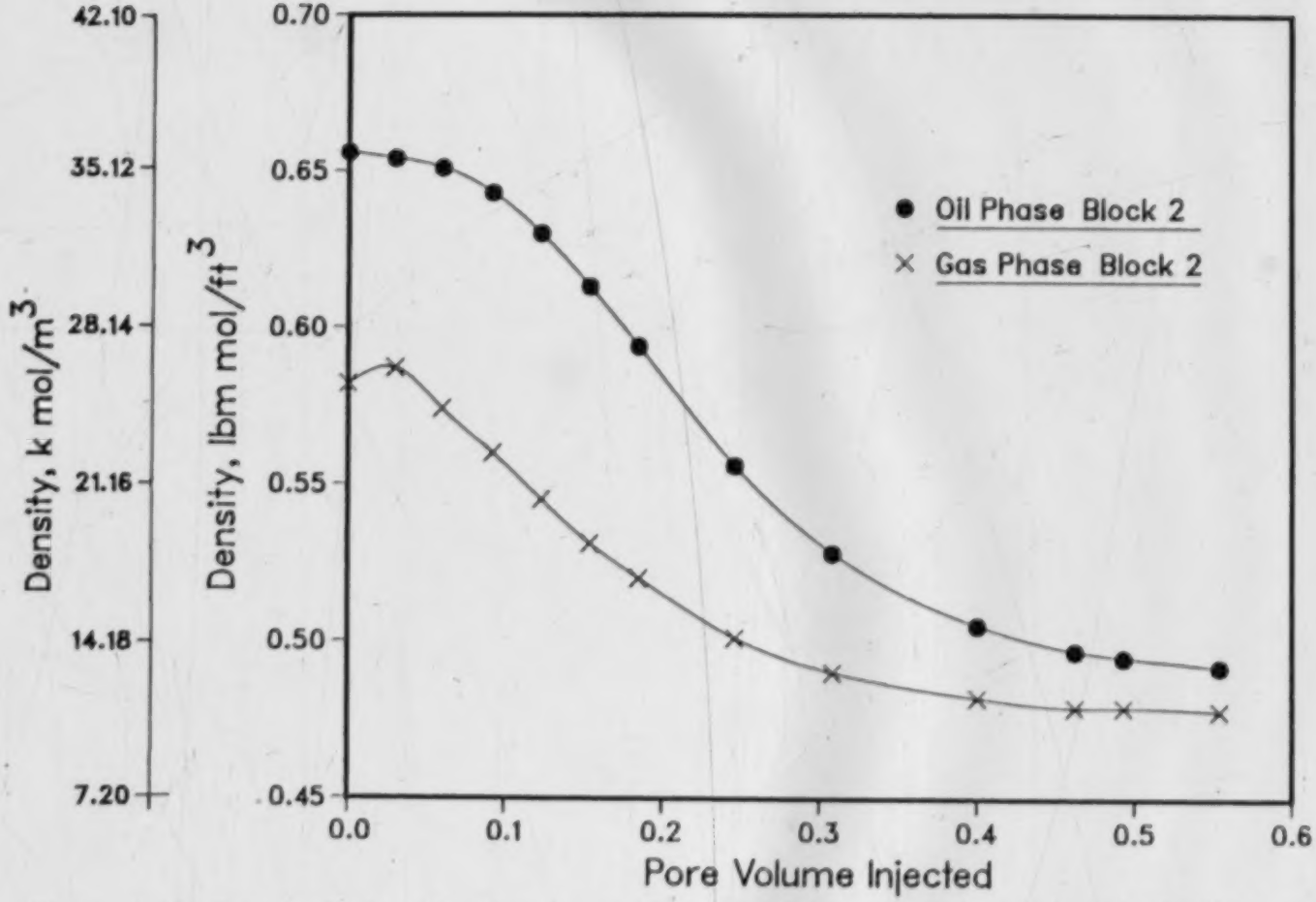

Figure 7.13 Example Problem 3: Density profile for high pressure gas drive, immiscible displacement for grid block 2

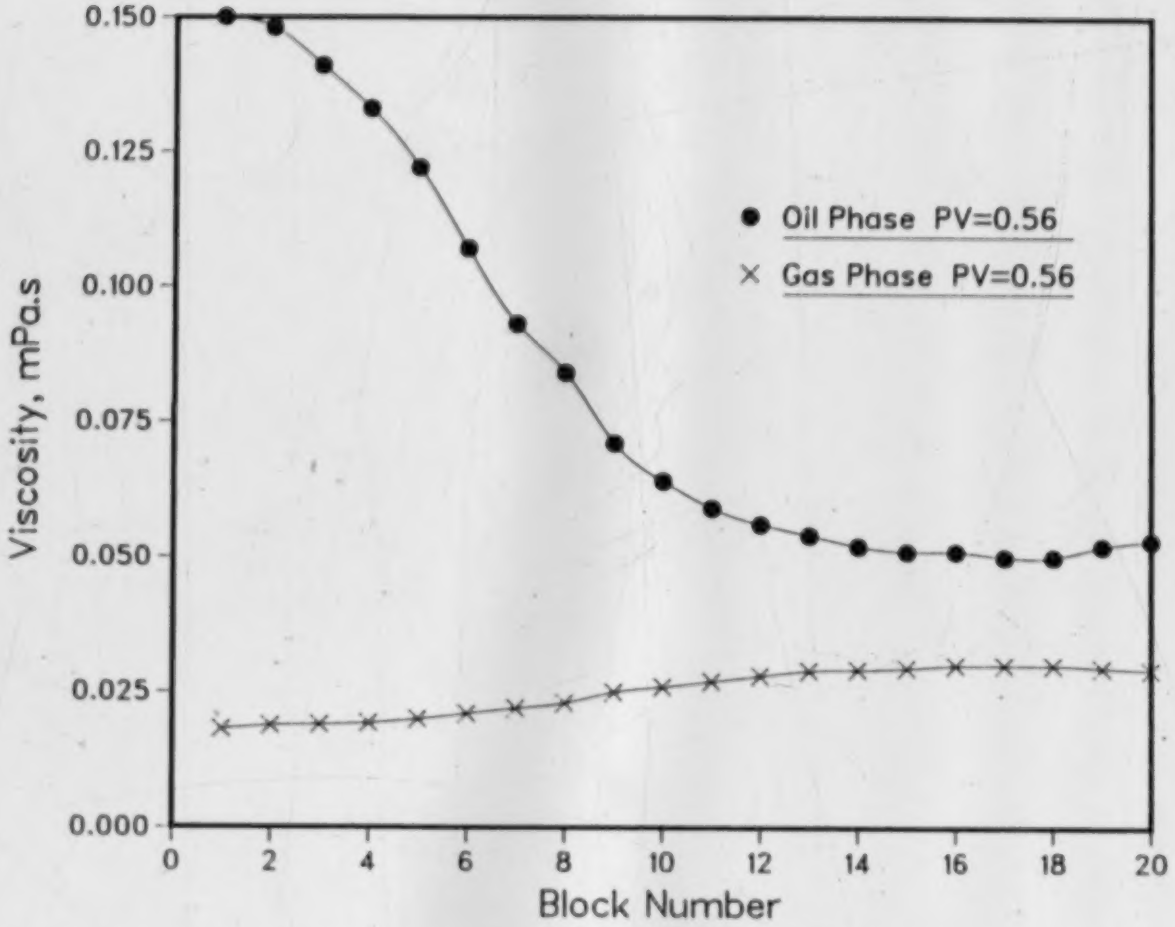

Figure 7.14 Example Problem 3: Viscosity profile for high pressure gas drive, immiscible displacement at 0.56 PV

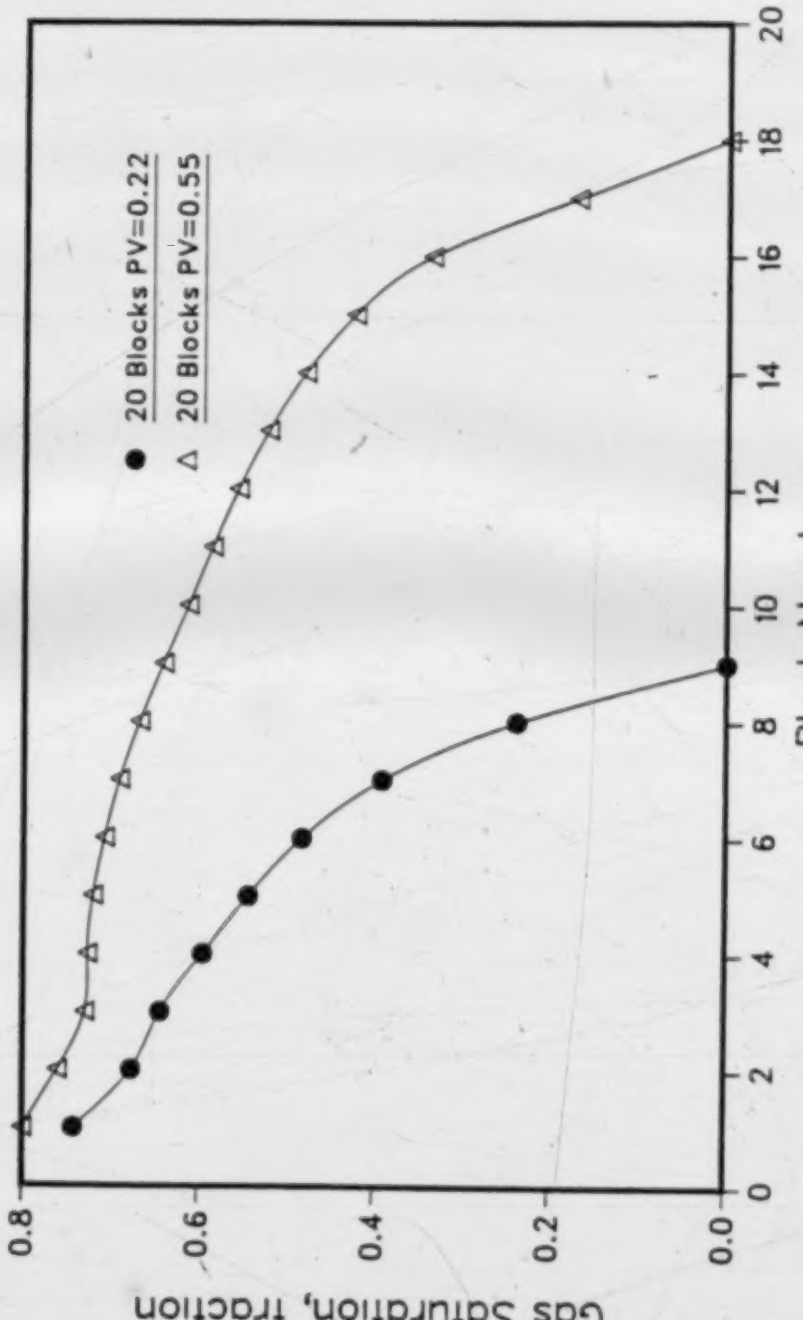

Figure 7.15 Example Problem 3: Gas saturation profile for high pressure gas drive, immiscible displacement at 0.22 and 0.55 PV

As can be observed from Figure 7.11, the composition path enters and exits the two-phase zone along tie line extensions, denoting reduced numerical dispersion, as compared to the other two examples. This is to be expected because although the total length of the system is smaller, the same number of grid blocks was used.

VII.4 Simulation of Displacements in a Two-Dimensional Reservoir

Two-dimensional runs were made to test the capability of the present model and to compare the results with one-dimensional reservoir runs.

Example Problems 4 and 5, condensing gas drives in two dimensions correspond to Examples 1 and 2 in one dimension. The total volume of the reservoir was maintained constant; thus the area of 1/4 of a five-spot flood pattern was set to 142.24×142.24 m^2 (5 acres).

Figures 7.16 and 7.17 present the gas saturation contour map for Example Problem 4: condensing gas, multicontact miscible displacement after the injection of 0.61 and 0.75 pore volume. It can be observed that the miscible front ($S_g = 0.8$) is distorted due to grid orientation effect which, for earlier times, causes faster movement along the sides rather than the diagonal, as can be observed in the gas saturation contours of 0.70 through 0.30. Also the gas saturation front is smeared out covering a large area of the flood pattern. Comparing these figures, it can be concluded that the saturation contour of 0.1 moves faster than the contours of the higher saturations, as was expected[61].

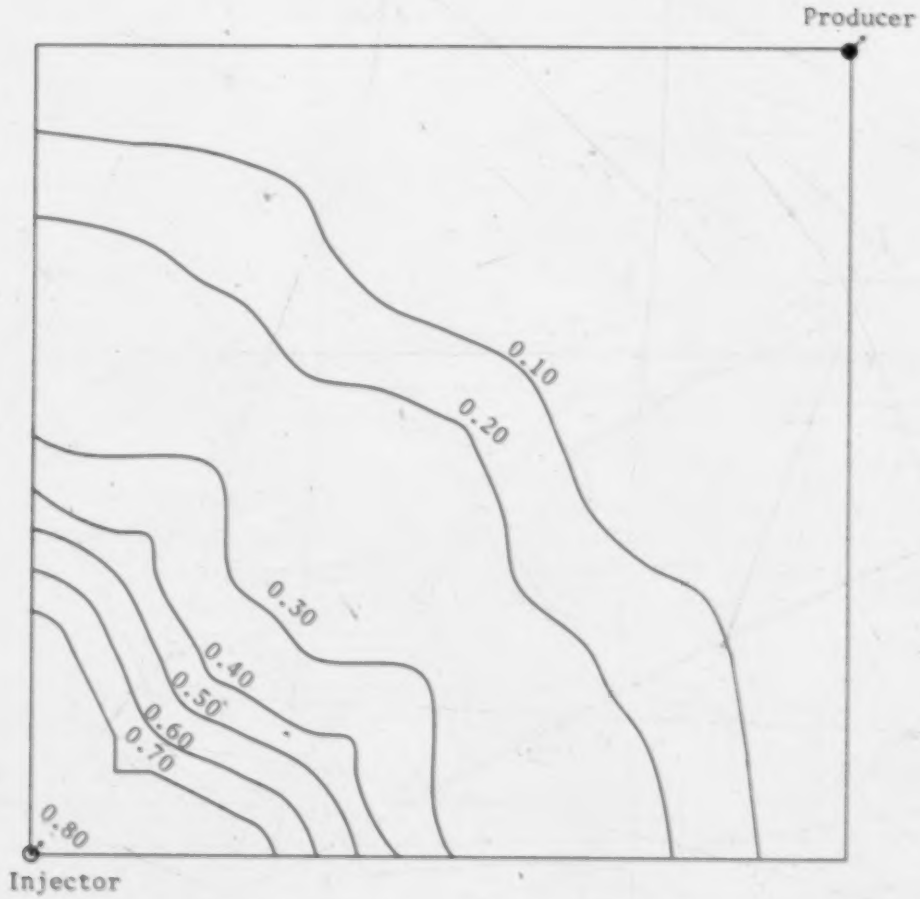

Figure 7.16 Example Problem 4: Gas saturation contour for condensing gas drive, multicontact miscible displacement, in a 1/4 of a five-spot, at 0.61 PV. 5 × 5 grid

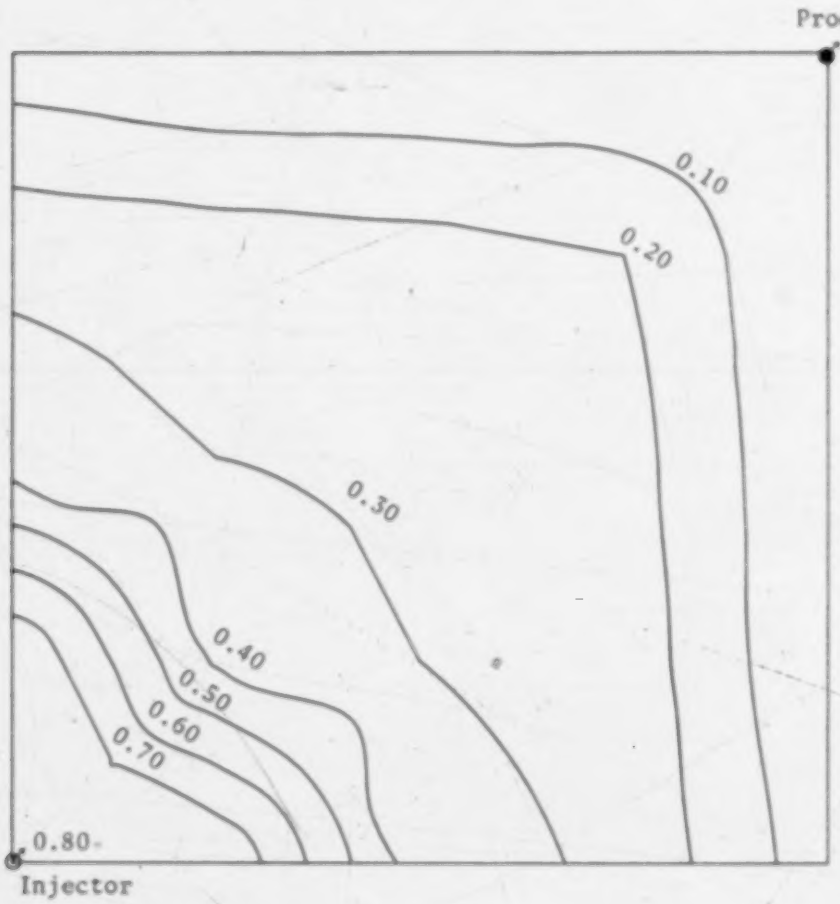

Figure 7.17 Example Problem 4: Gas saturation contour for condensing gas drive, multicontact miscible displacement, in a 1/4 of a five-spot, at 0.75 PV. 5 × 5 grid

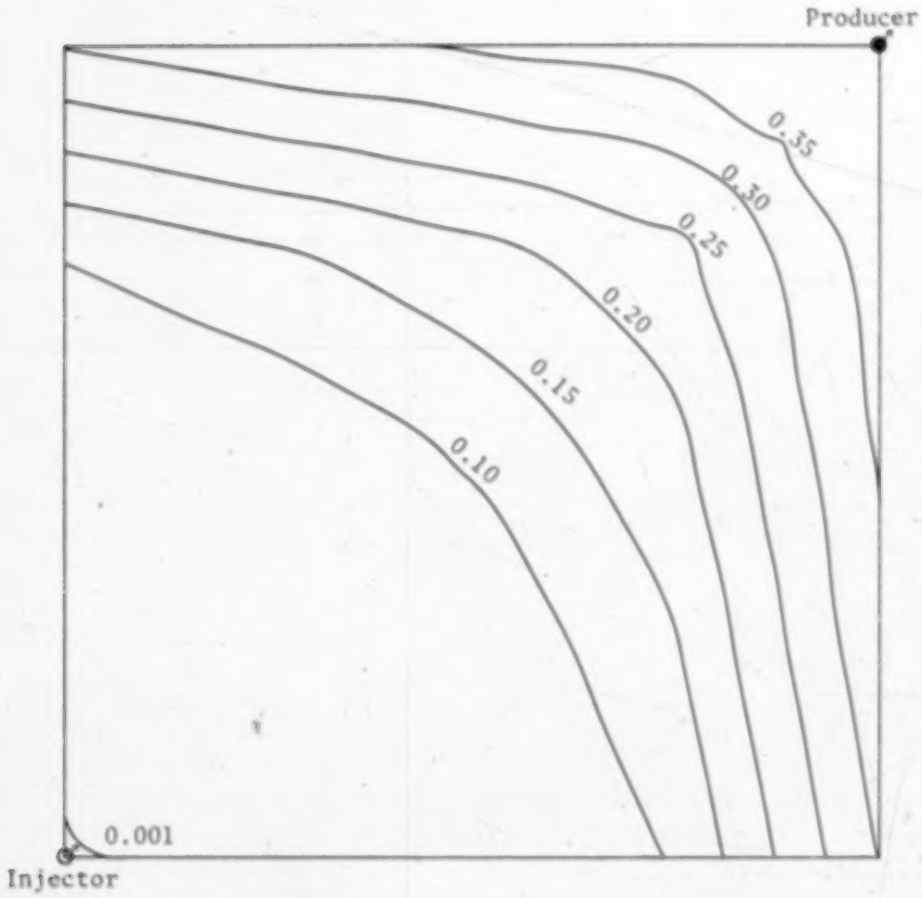

Figure 7.18 Example Problem 4: Decane (mole fraction) contour for condensing gas drive, multicontact miscible displacement, in a 1/4 of a five-spot at 0.75 PV. 5 × 5 grid

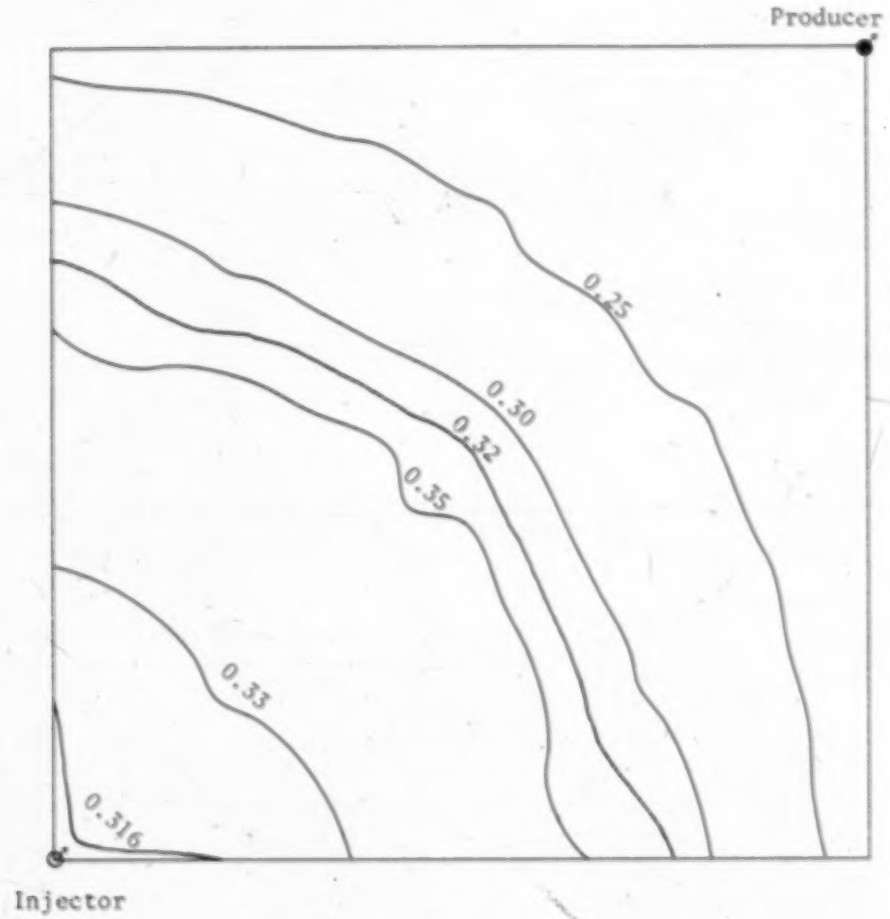

Figure 7.19 Example Problem 4: n-butane (mole fraction) contour for condensing gas drive, multicontact miscible displacement, in a 1/4 of a five-spot at 0.75 PV. 5 × 5 grid

Figure 7.18 shows the contours of the mole fraction of decane at 0.75 PV. Note that close to the injection well decane has been totally displaced.

The contour map for n-butane at 0.75 PV (Figure 7.19) shows the same type of overshoot in front of the miscible front (0.316 mole fraction) as in the linear case (Figure 7.1), demonstrating that this is a major numerical dispersion effect[14,61]. These figures show that the advance of the miscible front is highly affected by the grid orientation effect.

The contour maps for the condensing gas immiscible displacement: Example Problem 5, at 0.61 PV (Figures 7.20 through 7.22) show the same process as described for Example Problem 2. Almost the entire reservoir is in the two-phase region, and the oil has been displaced and volatilized close to the injection well. Figure 7.22 giving the n-butane mole fraction contours shows that there is an overshoot close to the injection well and a depression close to the production well, as in the linear case (Figure 7.6). Based on a simplified analytical solution[61] these effects should not exist.

Figures 7.23 through 7.25 show the contour maps of gas saturation, decane and n-butane mole fractions for Example Problem 6: the high pressure gas drive, immiscible process. The area of a 1/4 of a five-spot of a flood pattern was chosen as $110.2 \times 110.2\ m^2$ (3 acres).

The process is the same as described for Example Problem 3. Figure 7.23 shows that the oil phase has been displaced by the injected gas, and disappeared at the injection well by volatilization of the heaviest component (Figure 7.24). Also, n-butane has been

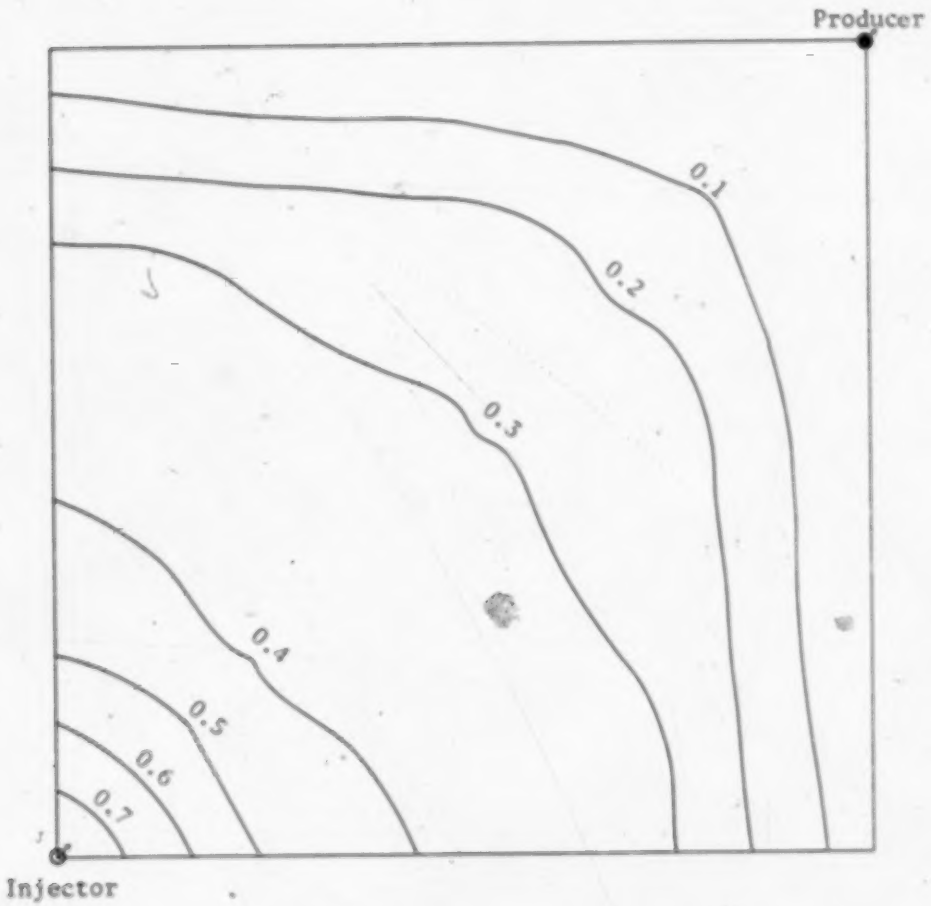

Figure 7.20 Example Problem 5: Gas saturation contour for condensing gas drive, immiscible displacement at 0.61 PV. 5 × 5 grid

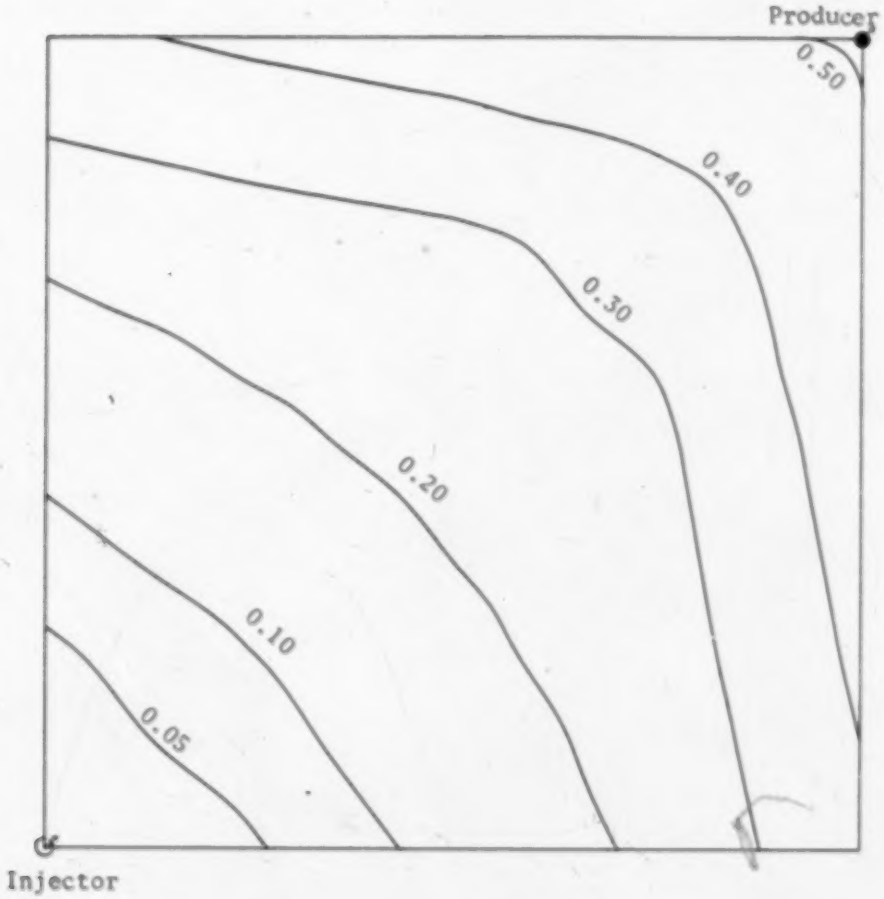

Figure 7.21 Example Problem 5: Decane (mole fraction) contour for condensing gas drive, immiscible displacement, in a 1/4 of a five-spot at 0.61 PV. 5 × 5 grid

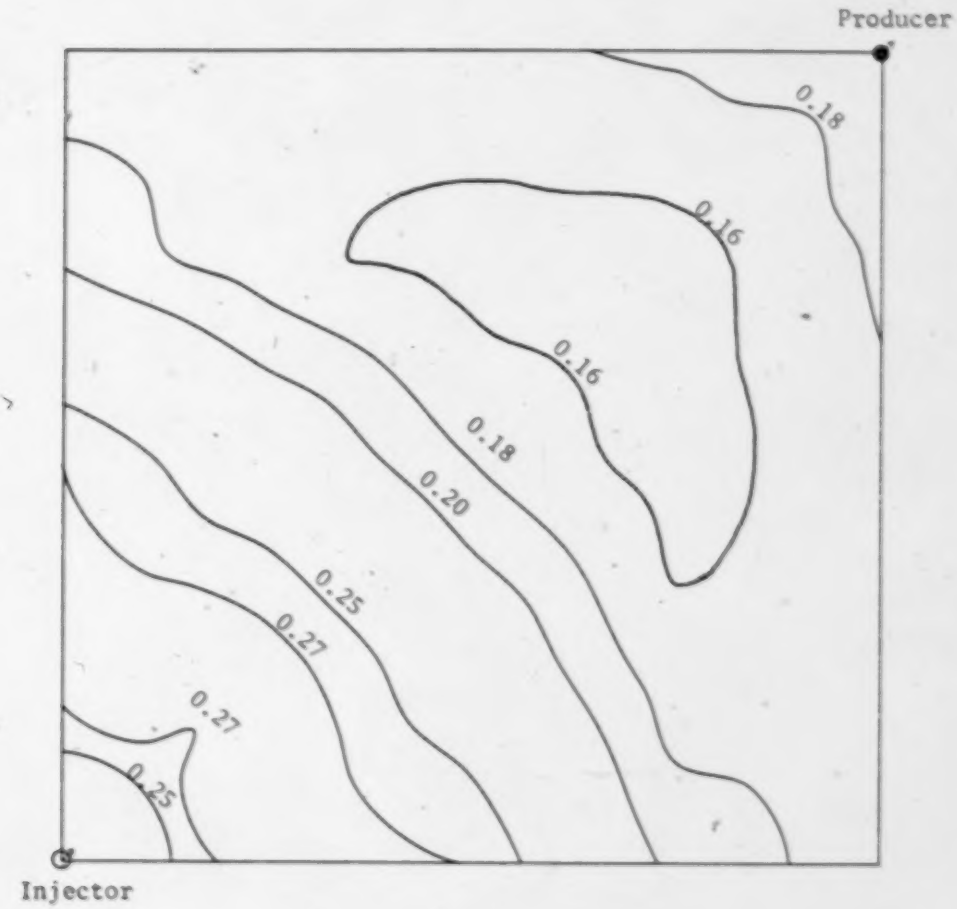

Figure 7.22 Example Problem 5: n-Butane (mole fraction) contour for condensing gas drive, immiscible displacement, in a 1/4 of a five-spot at 0.61 PV. 5 × 5 grid

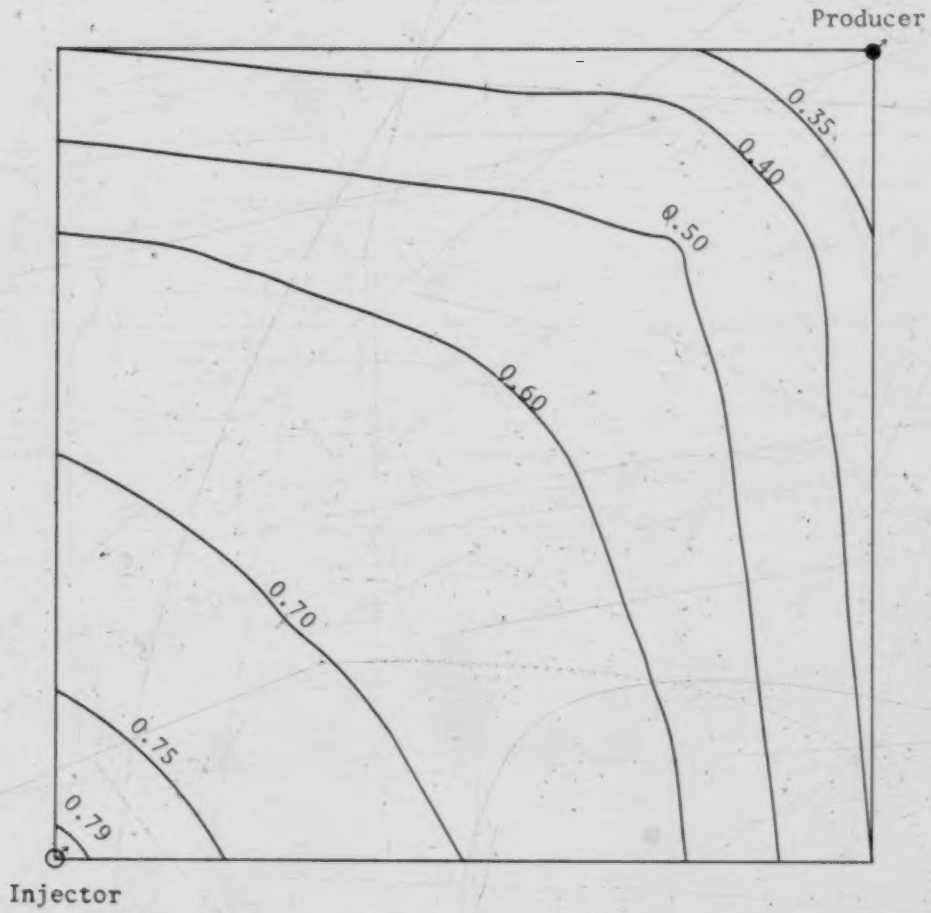

Figure 7.23 Example Problem 6: Gas saturation contour for high pressure gas drive, immiscible displacement in a 1/4 of a five-spot, at 0.55 PV. 5 × 5 grid

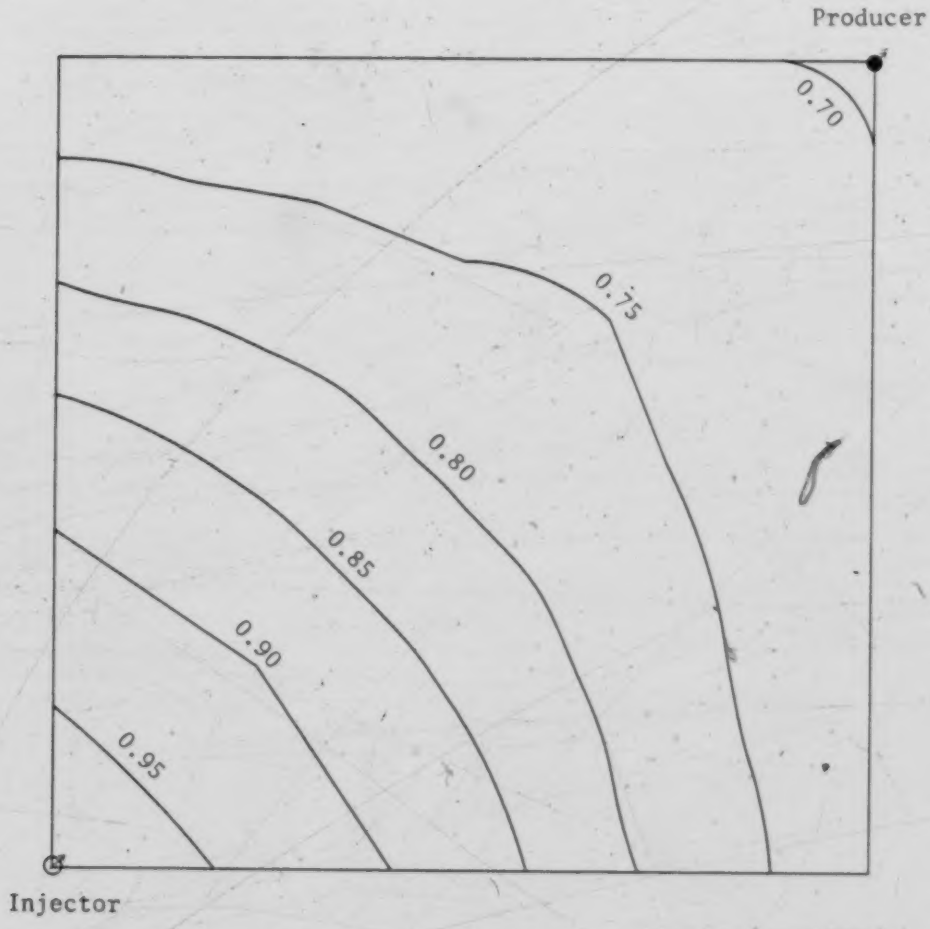

Figure 7.24 Example Problem 6: Methane (mole fraction) contour for high pressure gas drive, immiscible displacement in a 1/4 of a five-spot at 0.55 PV. 5 × 5 grid

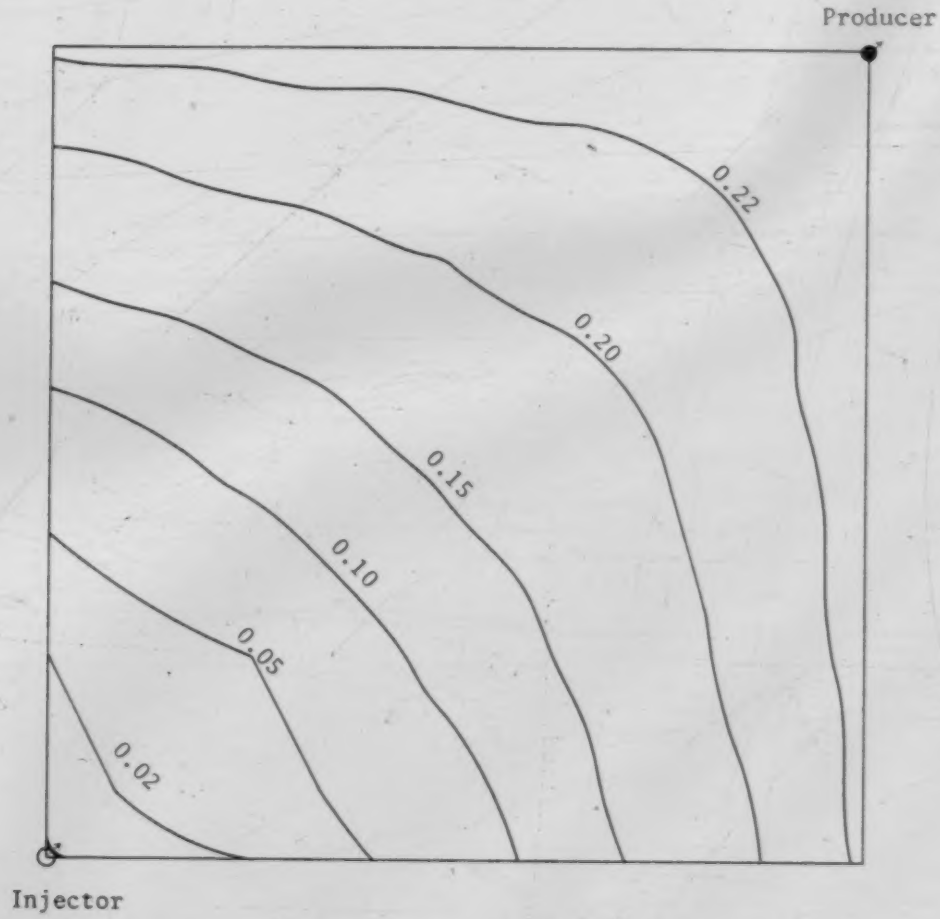

Figure 7.25 Example Problem 6: n-Butane (mole fraction) contour for high pressure gas drive, immiscible displacement in a 1/4 of a five-spot, at 0.55 PV. 5 × 5 grid

vaporized and produced. (Figure 7.25; the 0.02 and 0.05 contours are distorted due to grid orientation).

VII.5 Sensitivity Analysis

VII.5.1 Grid Size Sensitivity

One-Dimensional Reservoir

In order to study grid size sensitivity, various runs were conducted with the objective of analyzing each example problem studied before. The time step used was 7.5 days for each run, except for the 40 grid block runs, where it was reduced to 3.75 days.

Figures 7.26 to 7.39 demonstrate the effect of grid size on the composition path, gas saturation and recovery of decane.

As the grid size is refined, the solutions tend to converge to a limiting case. This limiting case was not found for the examples studied. Even though the composition paths for the high pressure gas drive are very close (Figure 7.30), the decane recovery curves for different grid size differ significantly (Figure 7.38). Figures 7.28 to 7.30 show that for the immiscible example problems, condensing or high pressure gas drive, the composition path can enter and exit the two-phase zone along tie line extensions, by increasing the number of grid blocks and at high pore volumes injected. But for the multi-contact miscible displacement example, Figures 7.26 and 7.27, while increasing the number of blocks reduces the numerical dispersion, its effects are still pronounced. The overshoot of n-butane past the miscible front is reduced with 40 grid blocks, but not eliminated.

Figures 7.30 to 7.35 show that the gas saturation fronts tend to smear out more as the number of grid blocks is reduced. The

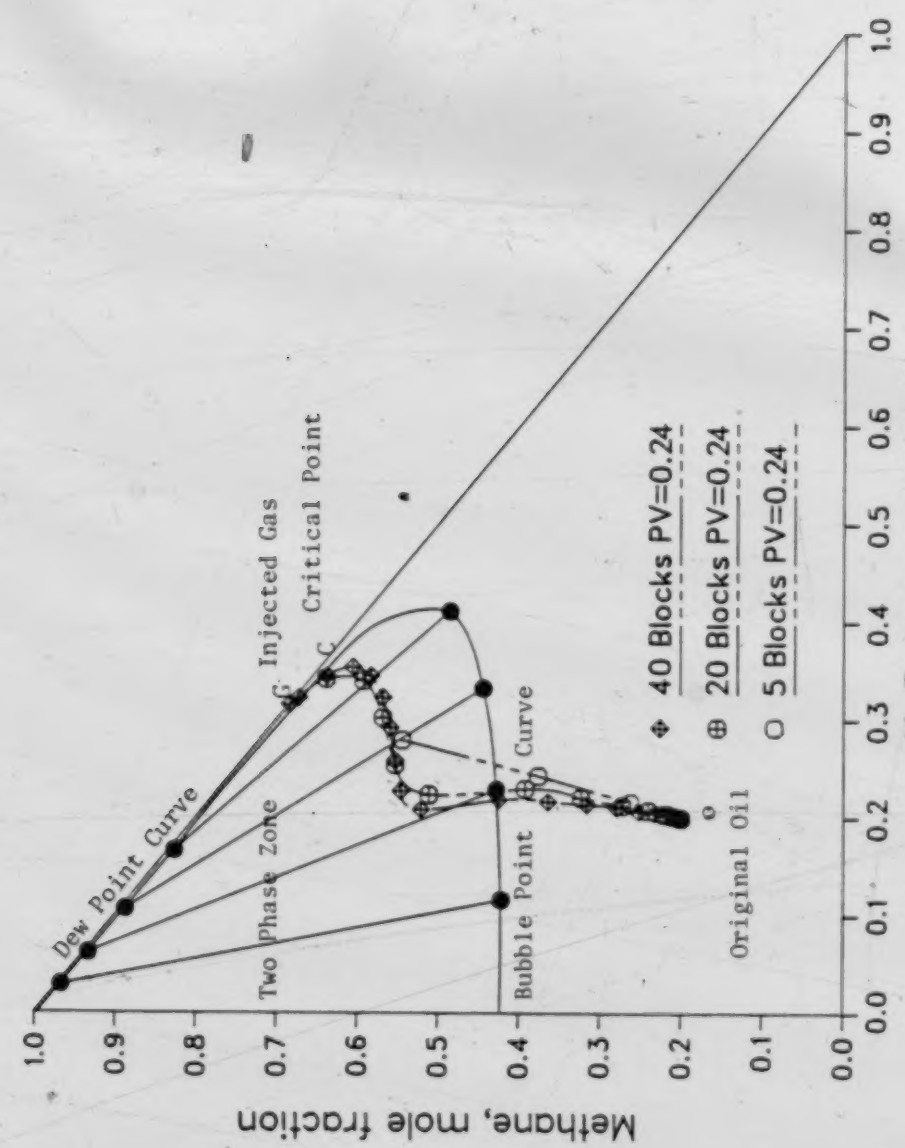

Figure 7.26 Effect of grid size on composition path at 0.24 PV for Example Problem 1: condensing gas drive, multicontact miscible displacement

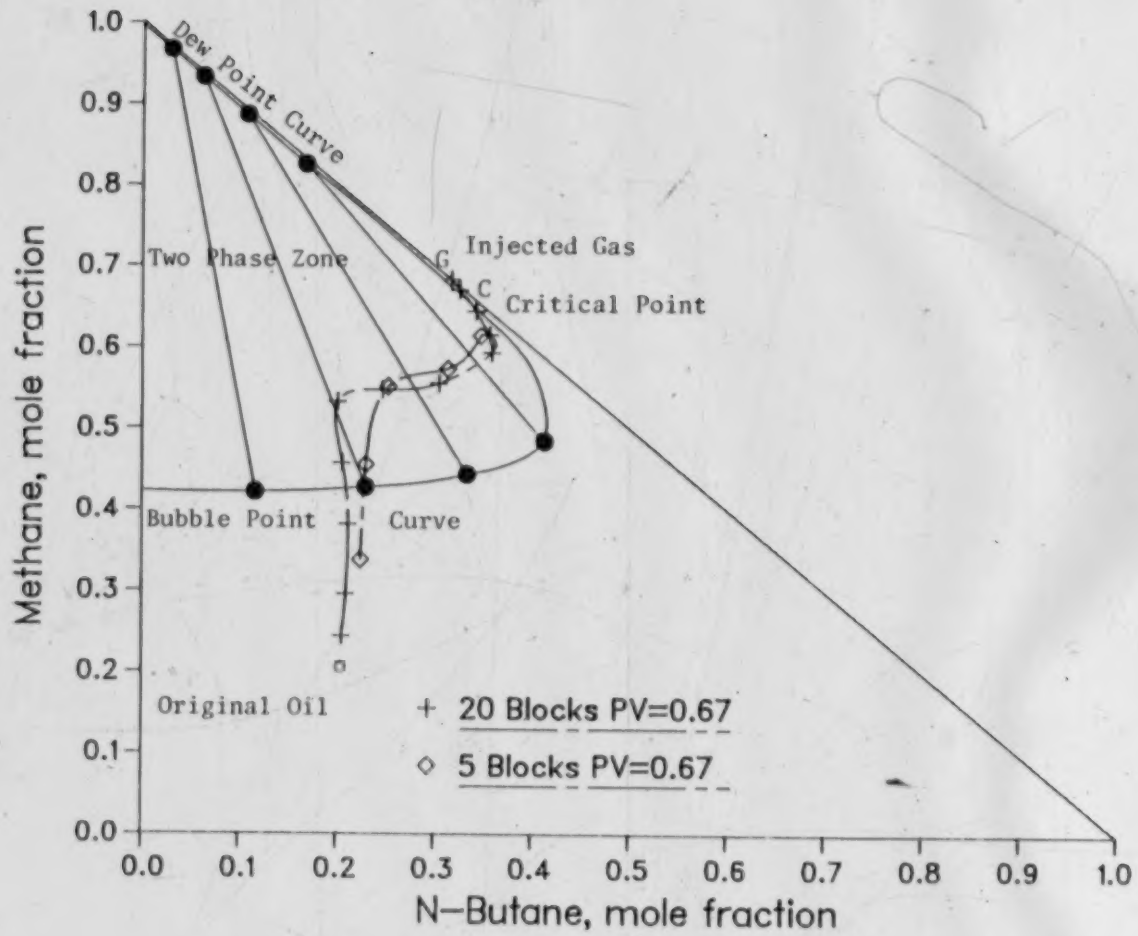

Figure 7.27 Effect of grid size on composition path at 0.67 PV for Example Problem 1: condensing gas drive, multicontact miscible displacement

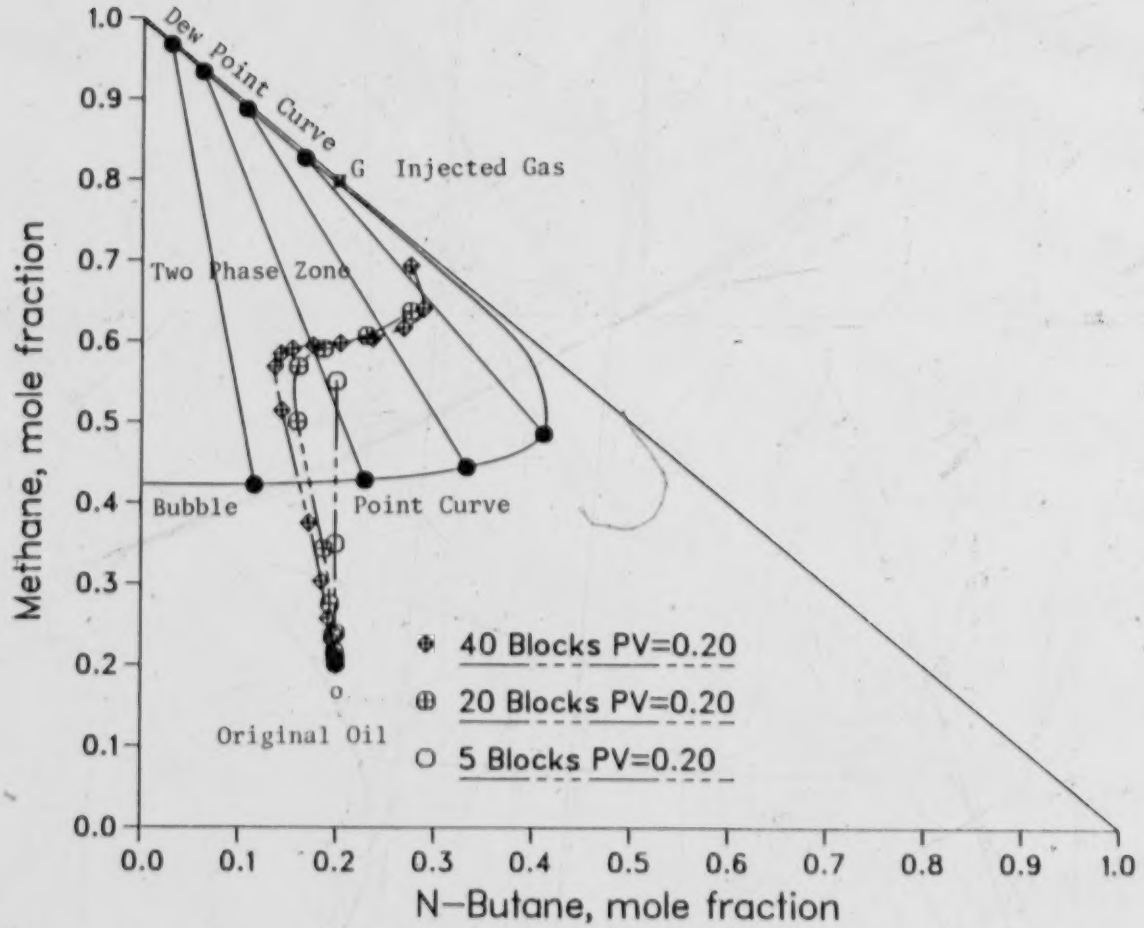

Figure 7.28 Effect of grid size on composition path at 0.20 PV for Example Problem 2: condensing gas drive, immiscible displacement

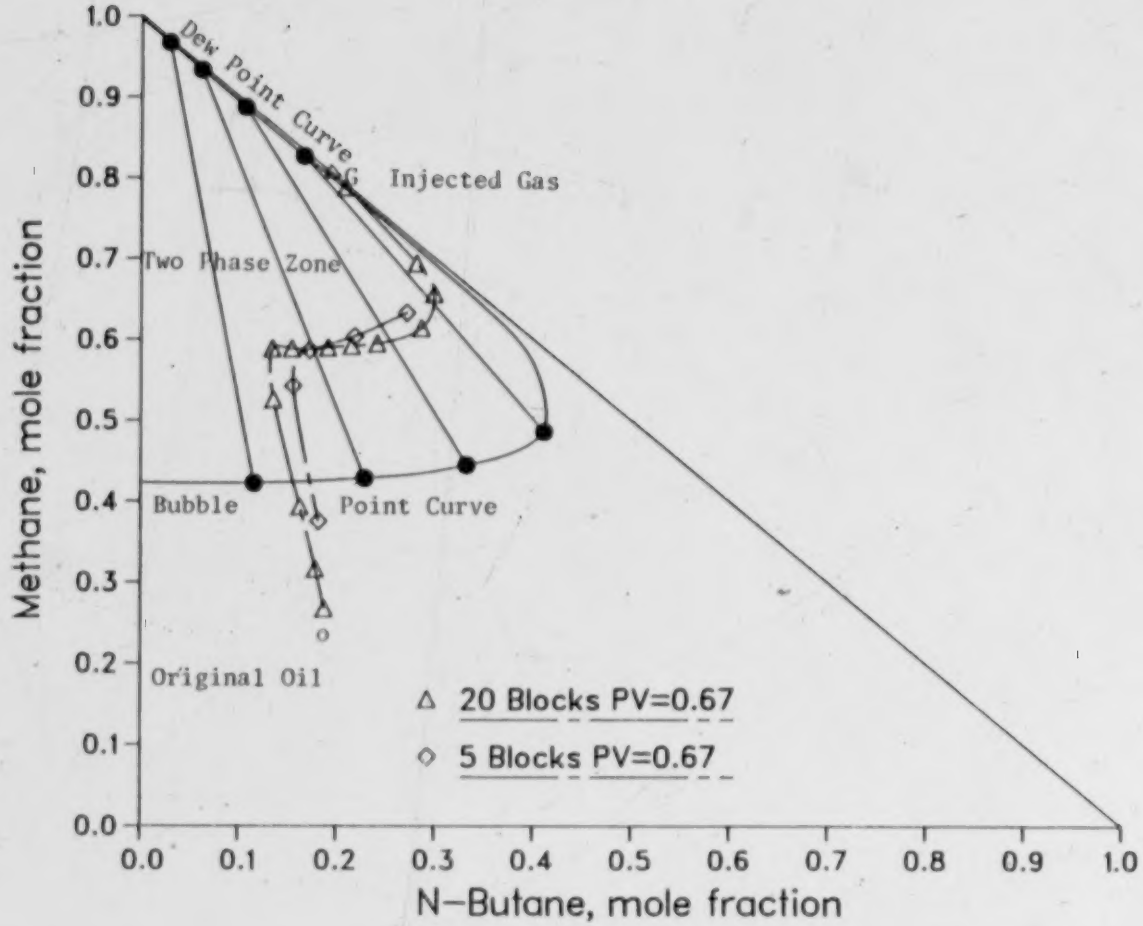

Figure 7.29 Effect of grid size on composition path at 0.67 PV for Example Problem 2: condensing gas drive, immiscible displacement

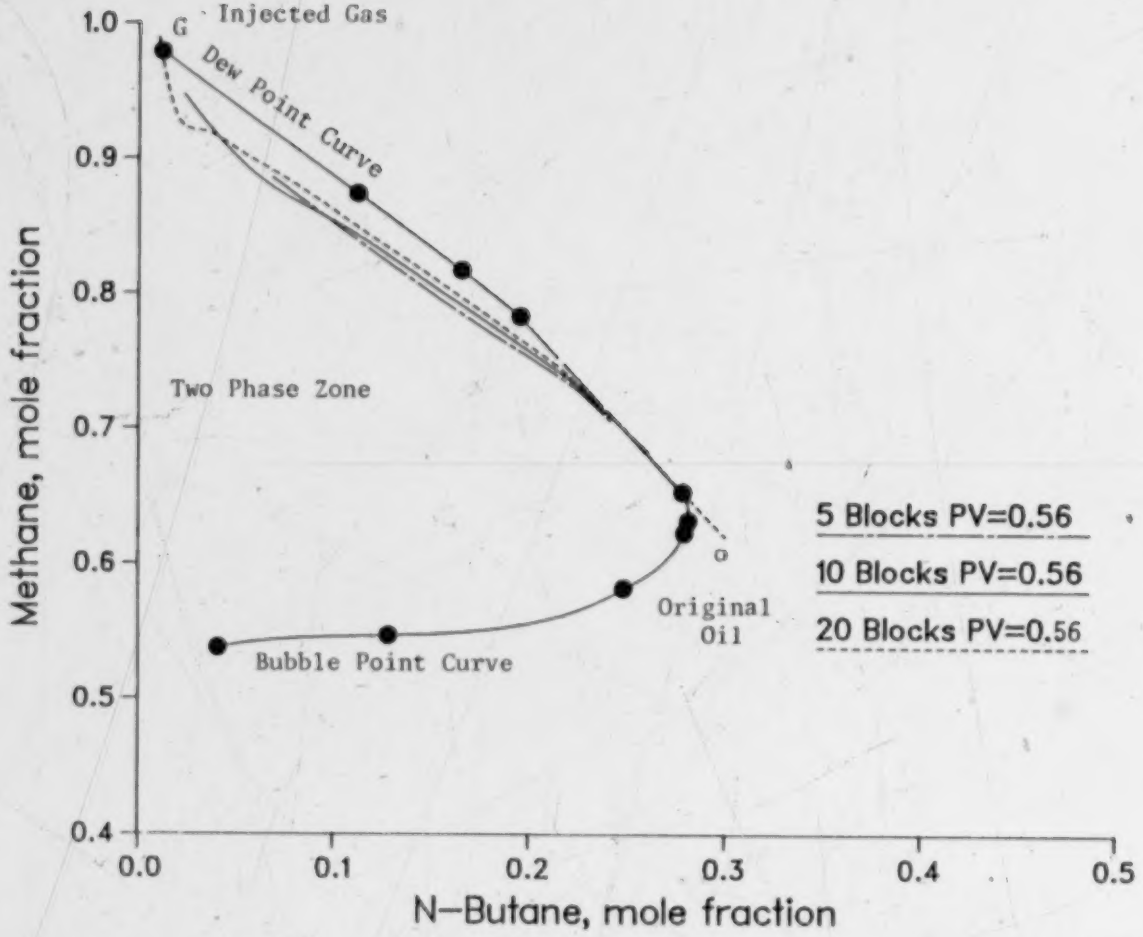

Figure 7.30 Effect of grid size on composition path at 0.56 PV for Example Problem 3: high pressure gas drive, immiscible displacement

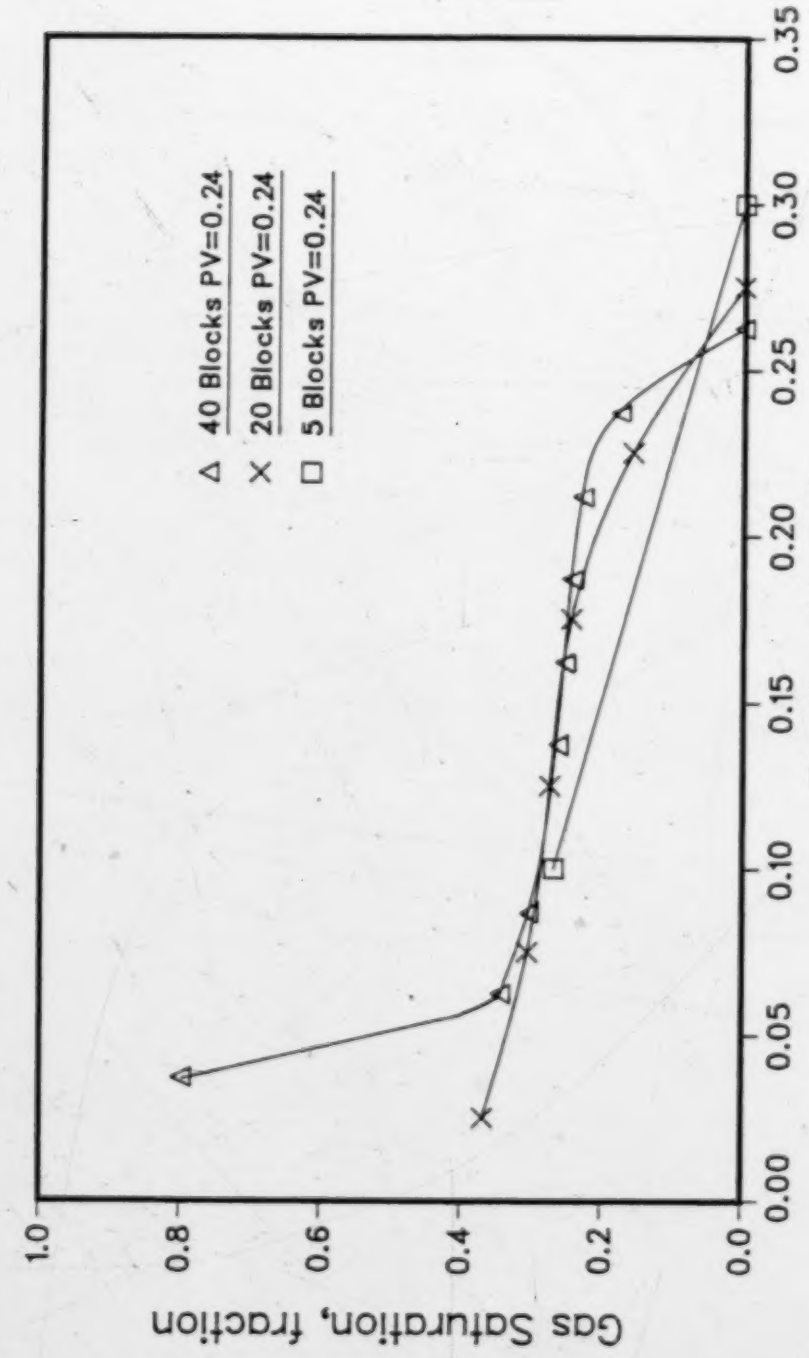

Figure 7.31 Effect of grid size on gas saturation profile at 0.24 PV for Example Problem 1: condensing gas drive, multicontact miscible displacement

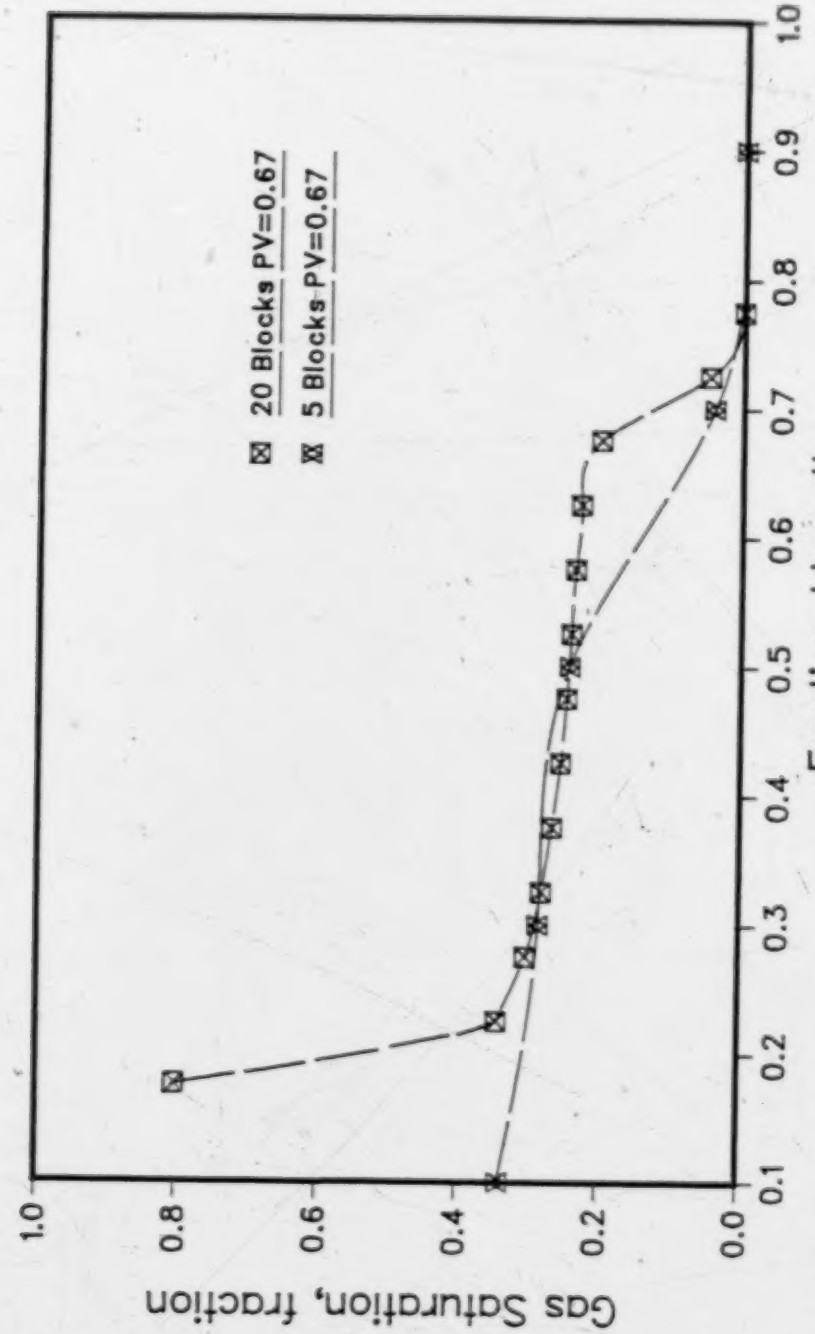

Figure 7.32 Effect of grid size on gas saturation profile at 0.67 PV for Example Problem 1: condensing gas drive, multicontact miscible displacement

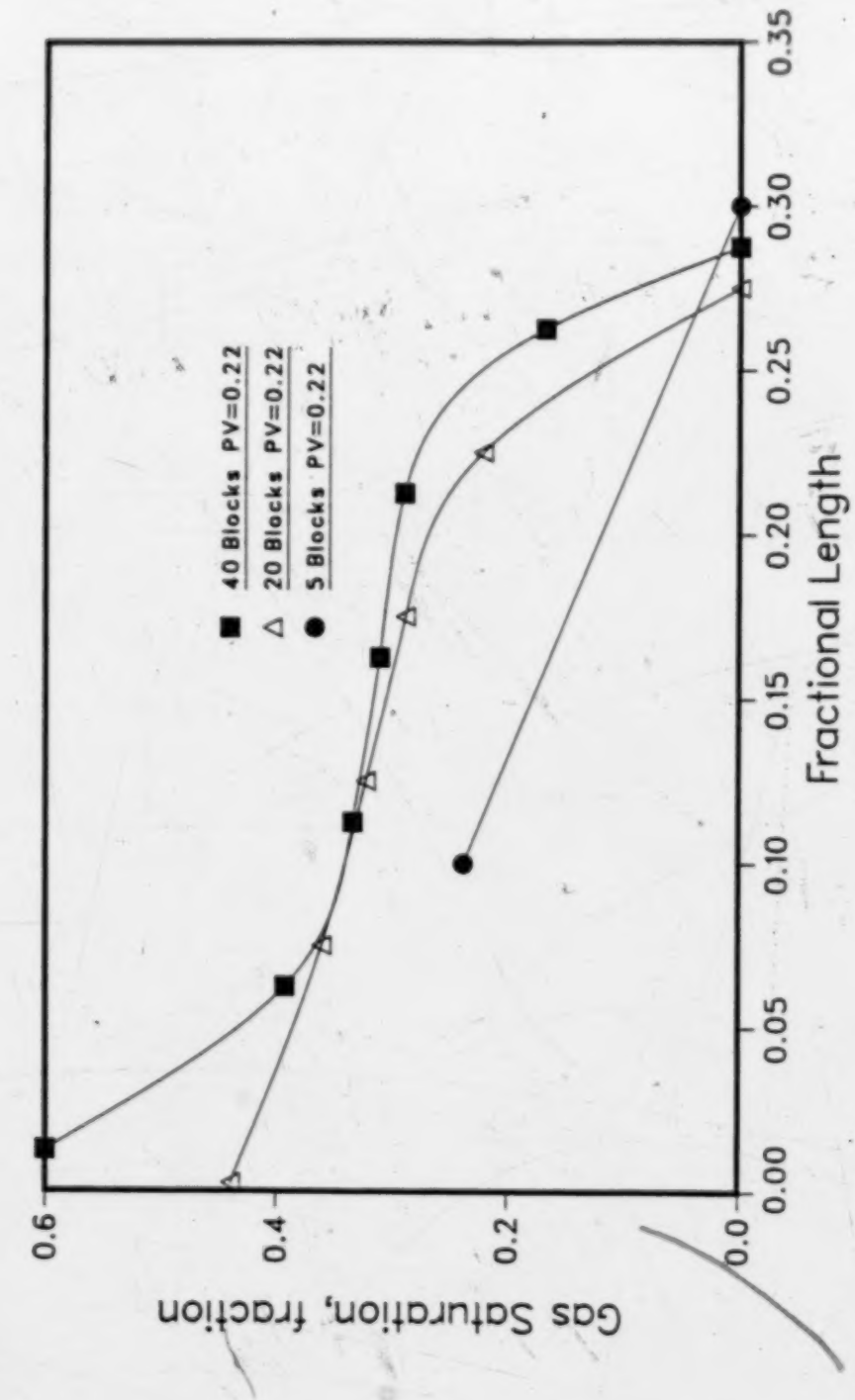

Figure 7.33 Effect of grid size on gas saturation profile at 0.22 PV for Example Problem 2: condensing gas drive, immiscible displacement

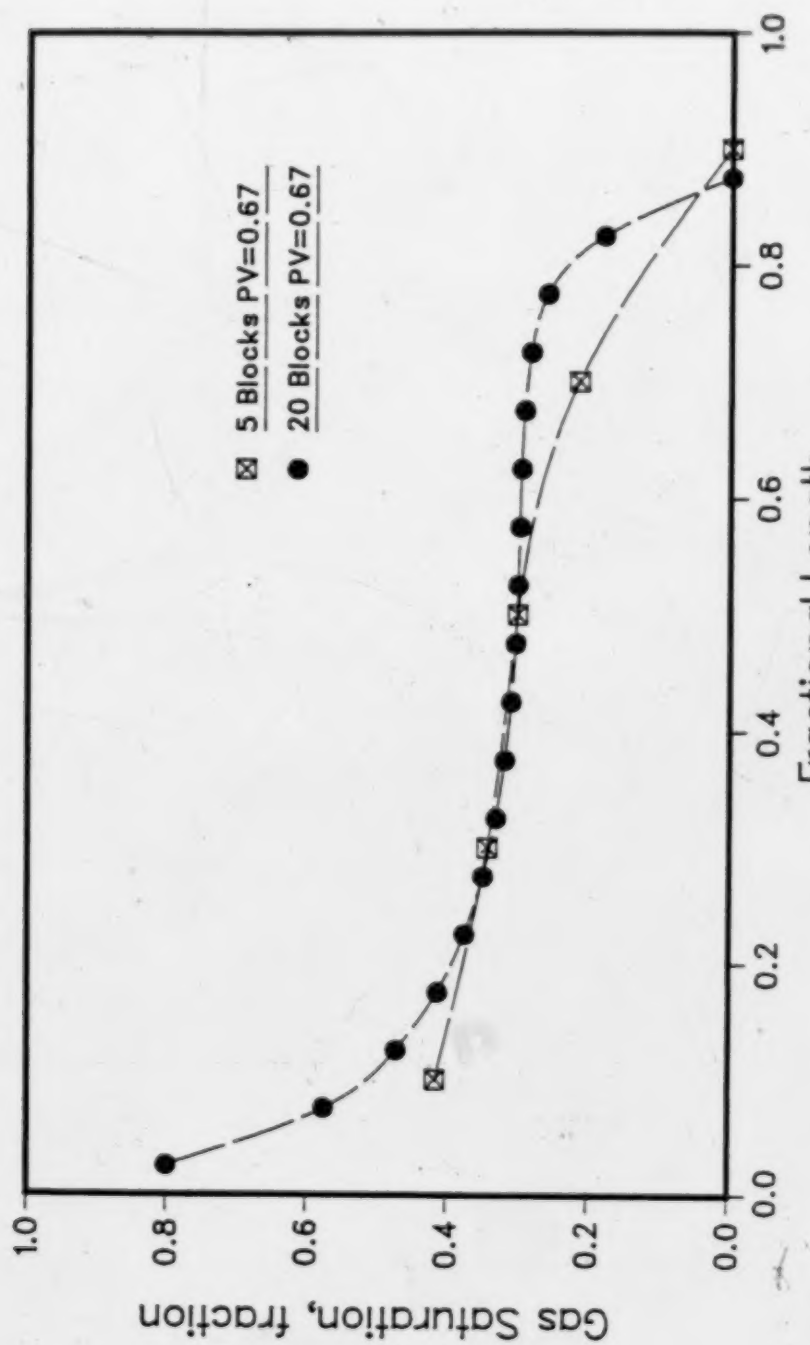

Figure 7.34 Effect of grid size on gas saturation profile at 0.67 PV for Example Problem 2: condensing gas drive, immiscible displacement

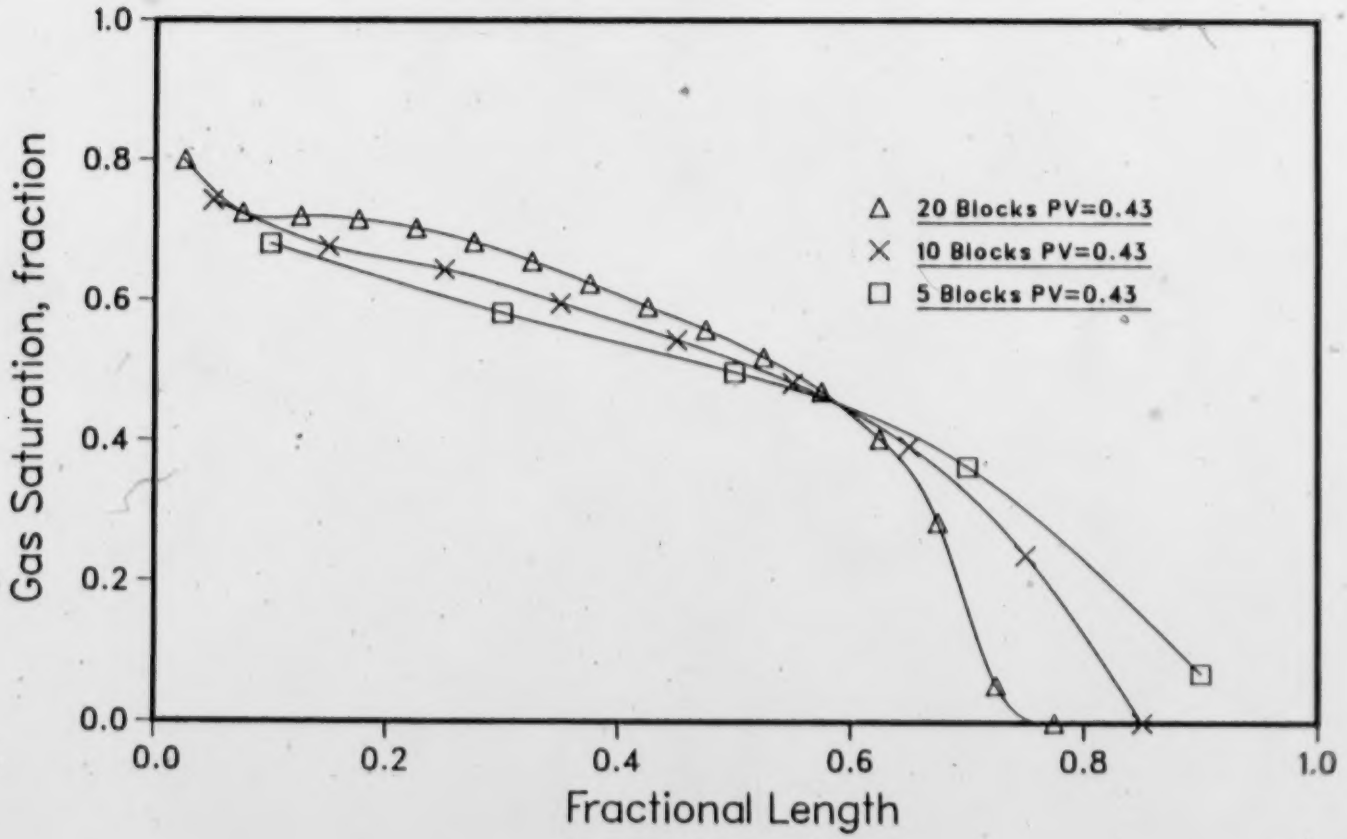

Figure 7.35 Effect of grid size on gas saturation profile at 0.43 PV for Example Problem 3: high pressure gas drive, immiscible displacement

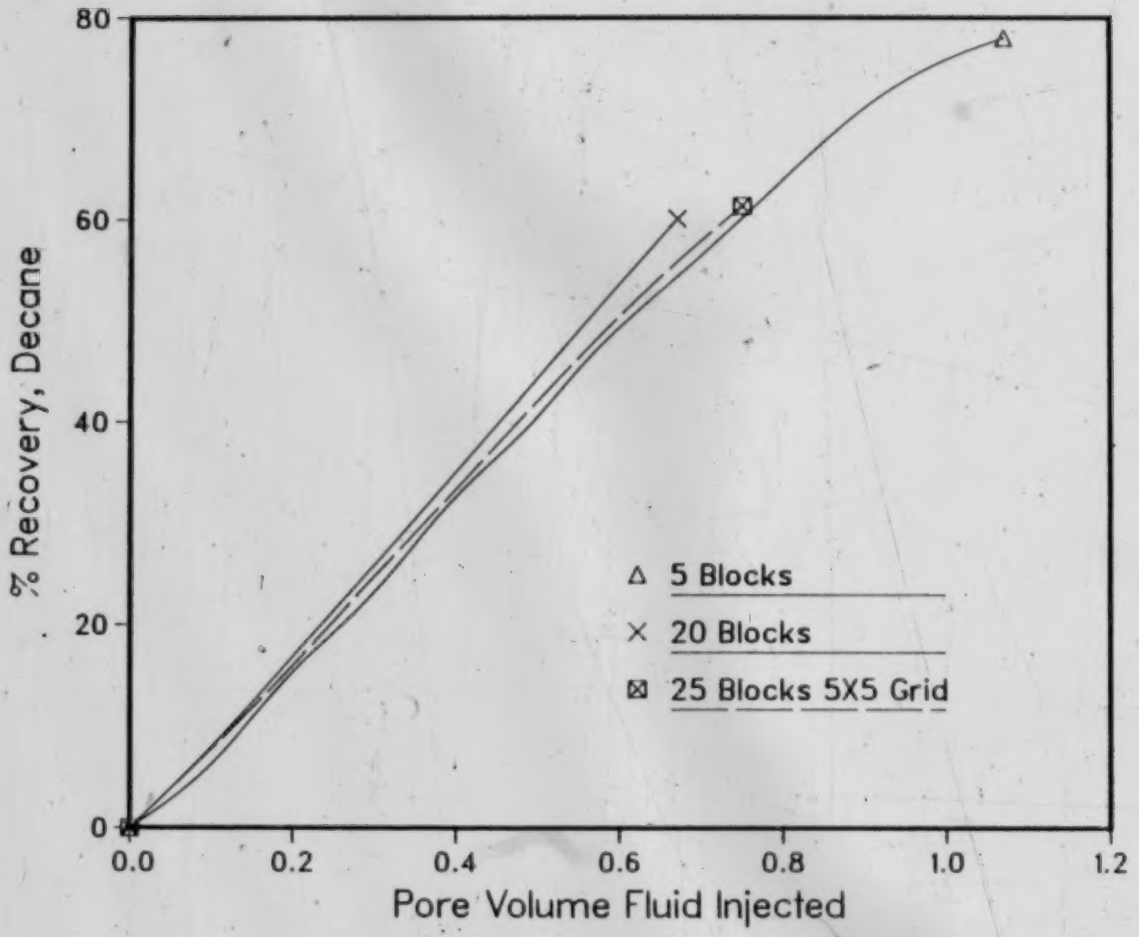

Figure 7.36 Effect of grid size on recovery of decane and comparison with two-dimensional reservoir for Example Problem 1

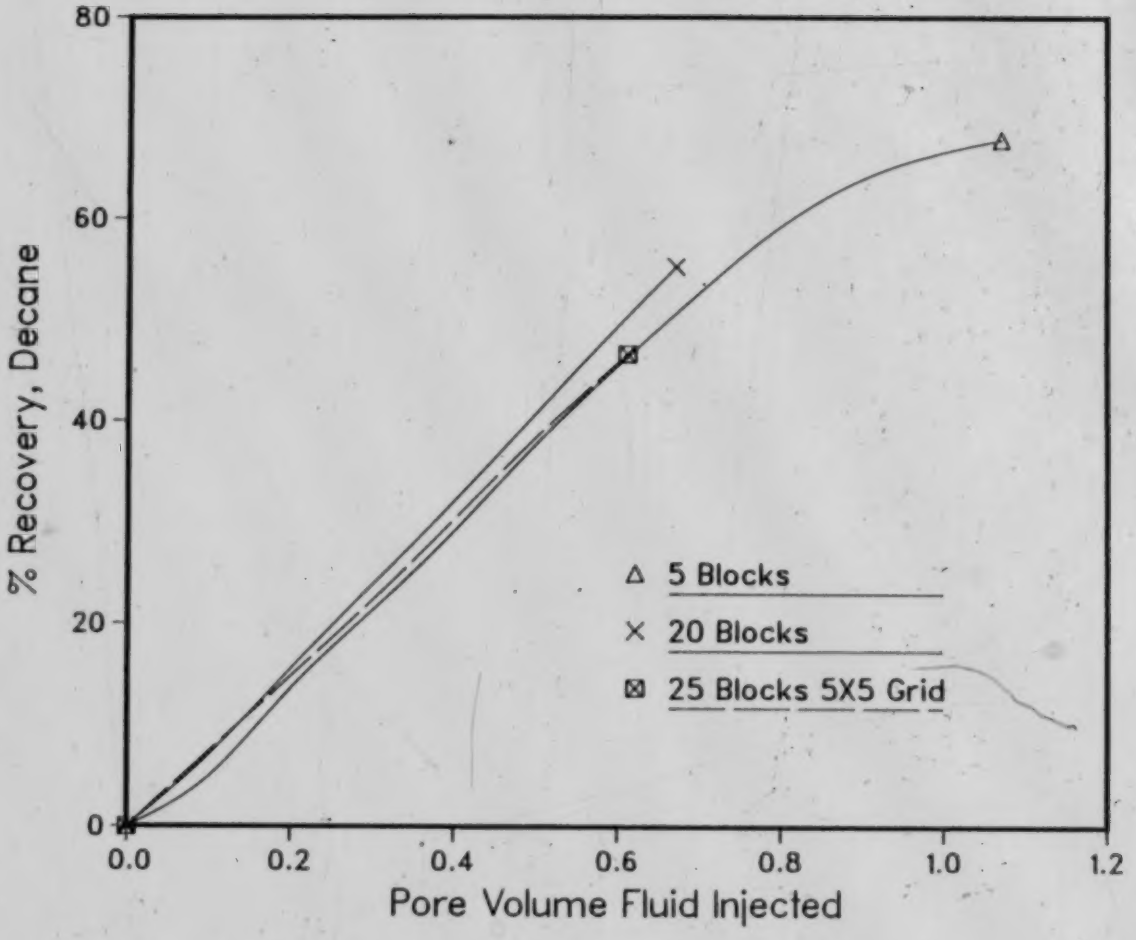

Figure 7.37 Effect of grid size on recovery of decane and comparison with two-dimensional reservoir for Example Problem 2

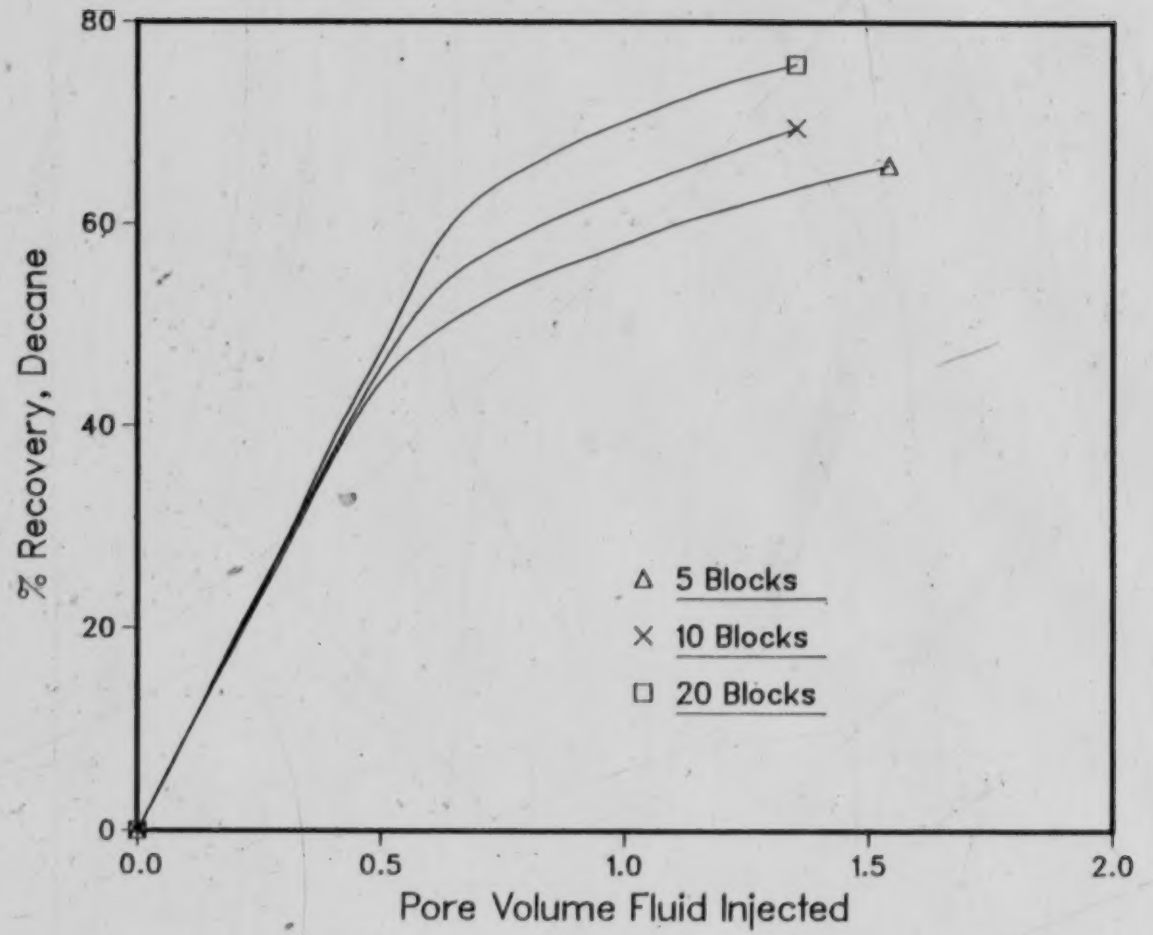

Figure 7.38 Effect of grid size on recovery of decane for Example Problem 3

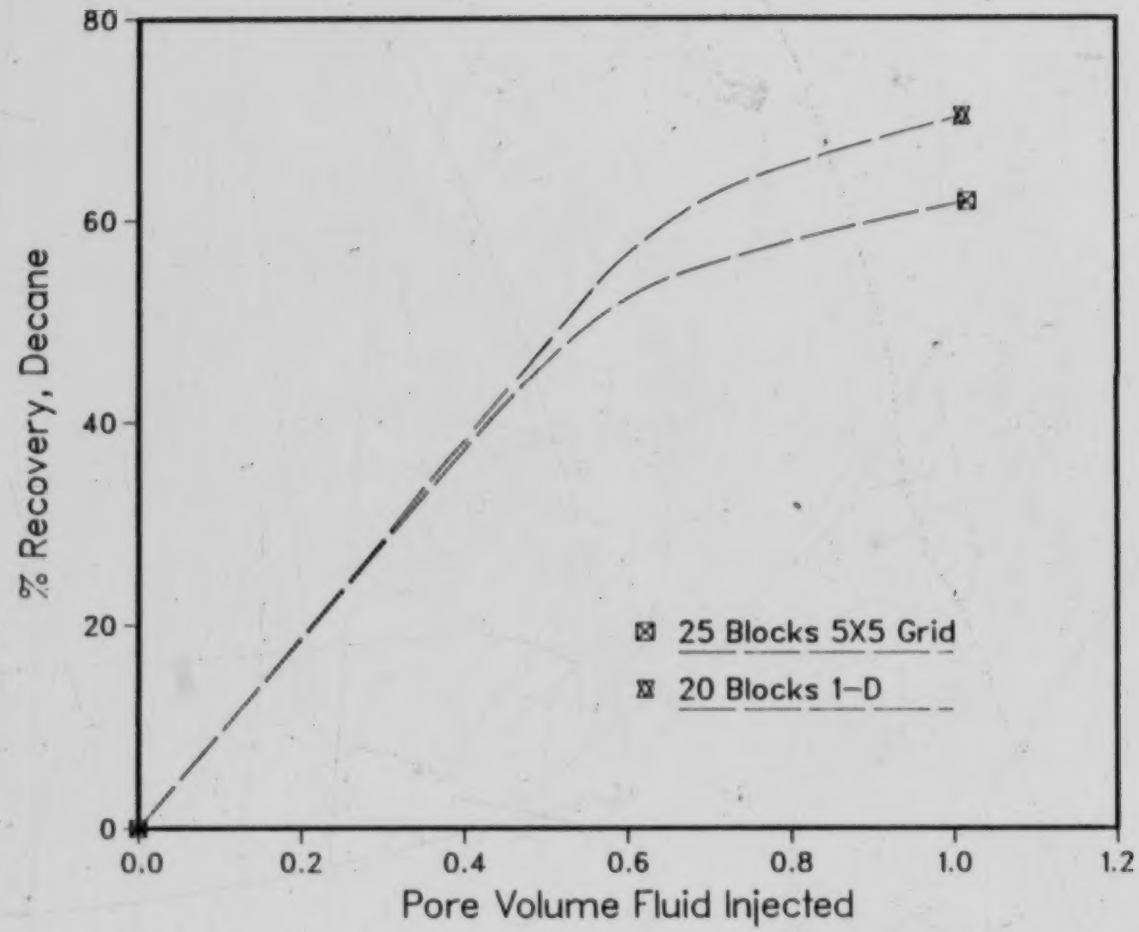

Figure 7.39 Comparison of decane recovery between one- and two-dimensional reservoirs for Example Problem 3

condensing gas drive, Figures 7.31 to 7.34, shows good agreement in the two-phase zone where the number of grid blocks is greater than 20; at high values of pore volumes injected (0.67 PV) the two-phase zone agrees very well for 5 and 20 grid blocks (Figure 7.34). These figures show more dispersion close to the injection point than at the front, especially for the miscible example (Figures 7.31, 7.32).

Figure 7.35 shows that for the vaporization example problem, dispersion is more pronounced before and at the front than in the zone close to the injection point.

Figure 7.36 and Figure 7.37 show that the recovery curves of decane for the condensing gas examples are affected by numerical dispersion to a lesser extent than the recovery curves for the high pressure gas drive (Figure 7.38).

In Figures 7.36 to 7.37 one can observe the effect of the type of grid: one-dimensional (linear) in comparison to the two-dimensional (areal) grid for the examples tested, on the recovery of decane. For a 5×5 grid, the recovery is close to the values of recovery for 5 grid blocks in linear reservoirs for both the immiscible and miscible examples. Figure 7.39 presents a comparison of decane recovery of the high pressure gas drive examples for two-dimensional and one-dimensional runs, both with the same reservoir volume. For the 1-D test, the dimensions of the reservoir were length 48.76m (160 ft), width 30.48m (100 ft) and thickness 15.24m (50 ft).

As can be observed, the run for two dimensions gives a lower recovery than the one-dimensional test, showing that more numerical dispersion was present for 2-D than for 1-D runs. The three example problems compared showed similar behaviour.

Two-Dimensional Reservoir

In order to study the grid size sensitivity in a two-dimensional areal reservoir, a 8×8 grid was selected. Using the data of Example Problem 6, two runs were made with time steps of 1 and 1.5 days. The cpu times for these runs were 44.5 and 62.5 seconds, respectively, for two time steps of simulation. Such large cpu times make the runs prohibitively expensive.

VII.6 Validation of Simulator Results

Numerical reservoir model results have been compared with analytical solutions for simplified cases, experimental data, field data, and with results obtained on models validated previously.

1. Simulator results compared with those for previous simulators

The results obtained using the present model were compared with those reported by Coats[10] and Thele[54] for a fully implict formulation.

Figure 7.40 shows excellent agreement of the overall composition profile in the reservoir at a 0.56 PV for Example Problem 1, or the multicontact miscible displacement, passing through the critical point.

Figure 7.41 shows that the overall composition profiles in the reservoir at 0.56 PV are in good agreement for Example Problem 2 for condensing gas, immiscible displacement. It also shows some differences at the leading edge of the two-phase zone and in the monophasic oil zone due to the numerical dispersion control used in this example by Thele[54].

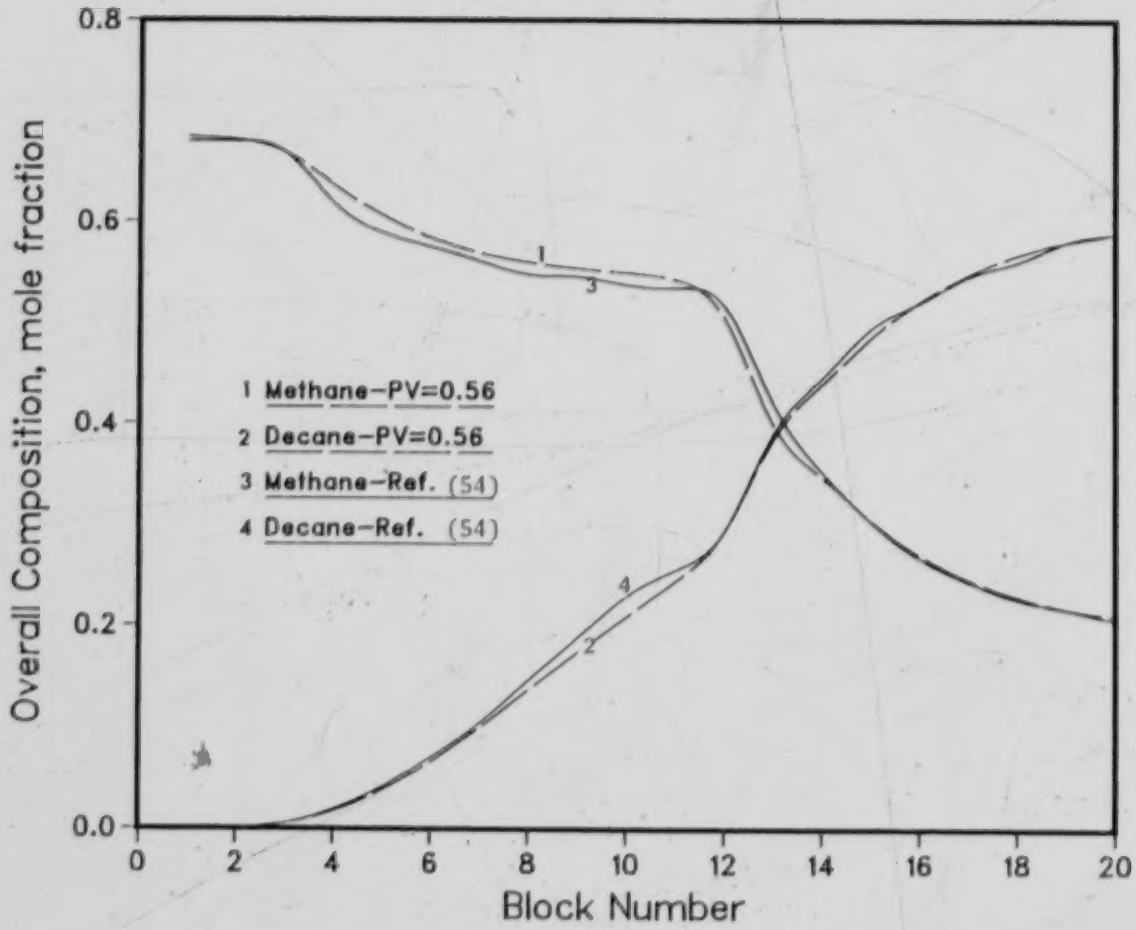

Figure 7.40 .Overall composition comparison for Example Problem 1: condensing gas drive, multicontact miscible displacement at 0.56 PV with Ref (54)

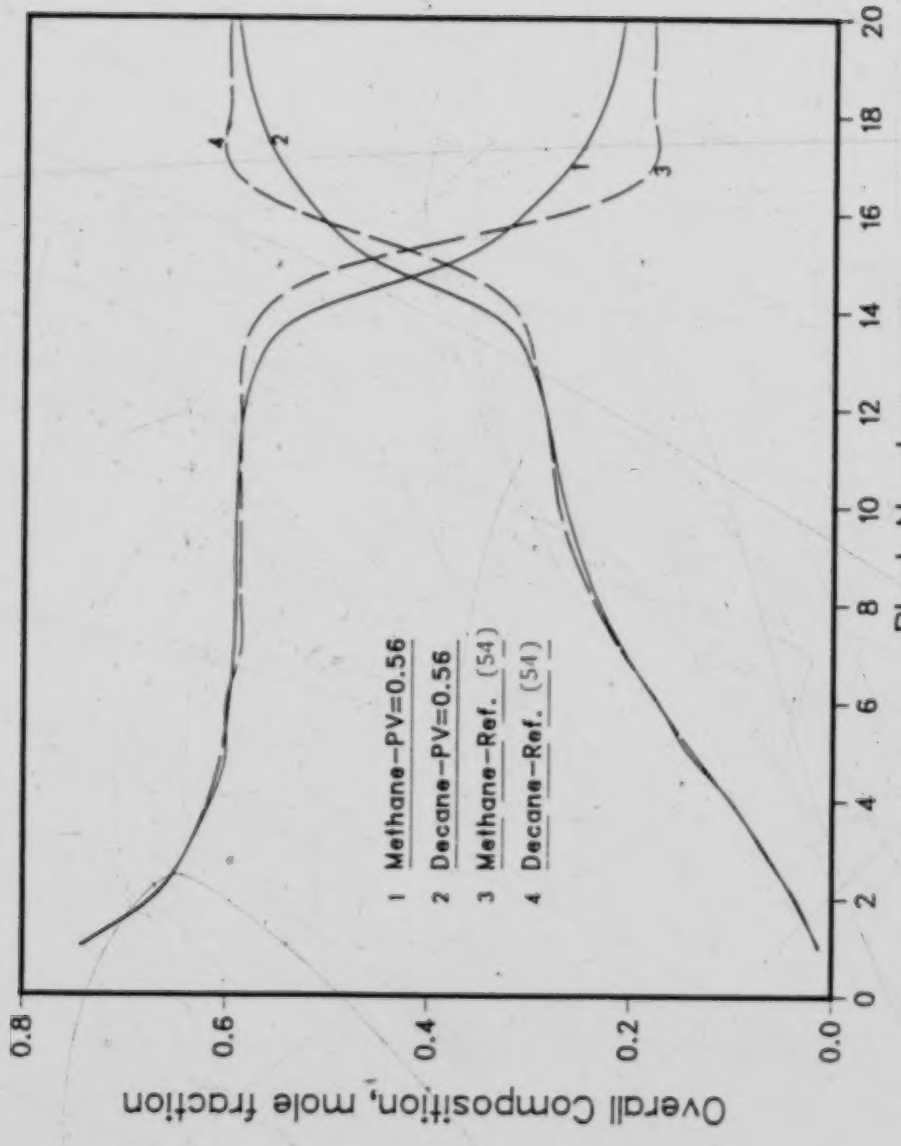

Figure 7.41 Overall composition comparison for Example Problem 2: condensing gas drive, immiscible displacement, at 0.56 PV with Ref (54)

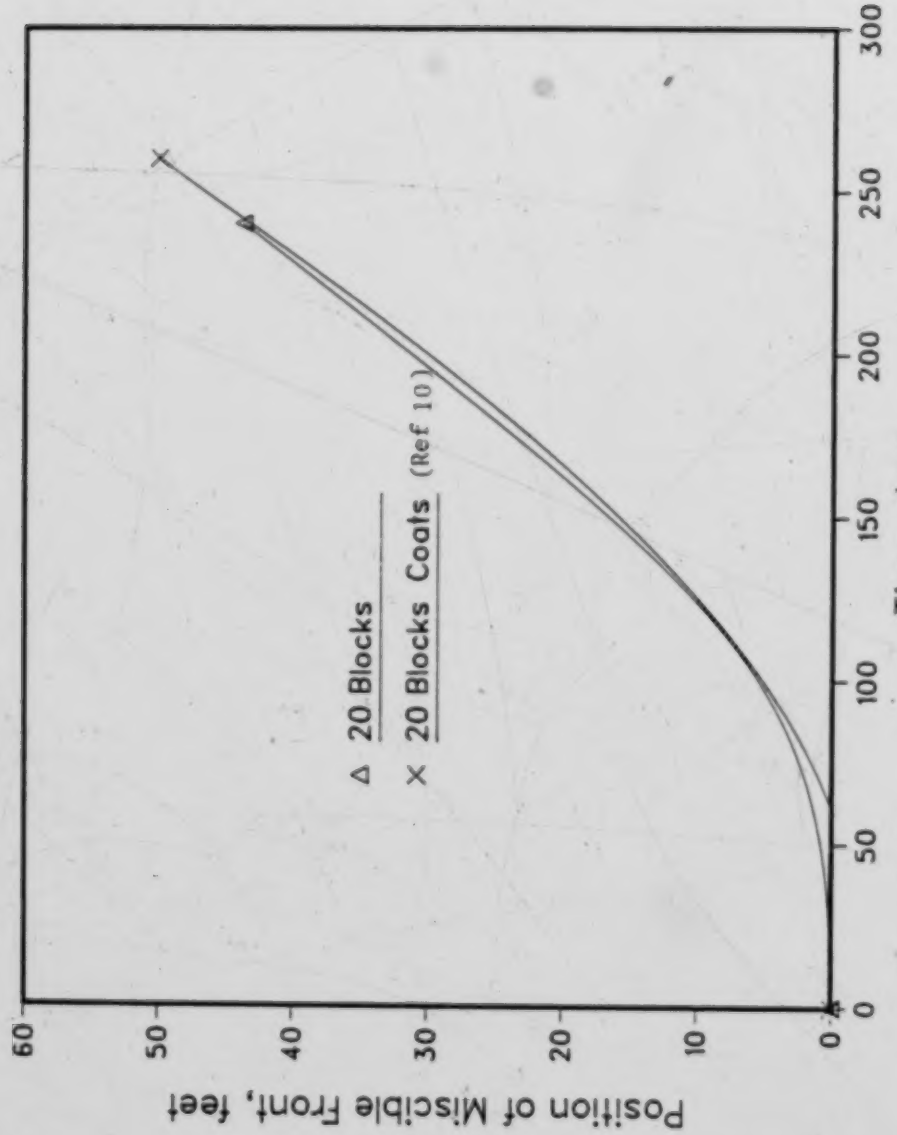

Figure 7.42 Velocity of miscible front for Example Problem 1

Figure 7.42 demonstrates that the miscible front velocity of Example 1 is in very good agreement with the results reported by Coats[10].

2. Simulator results compared with experimental data

In order to test the validity of the results of the present model, a comparison with experimental data was made. The data chosen was reported by Van Quy et al.[57], and Table VII.7 and Figure 7.43 show the physical and relative permeability data, respectively. The process consists of a gas displacing oil in thermodynamic equilibrium. The hydrocarbon system consists of methane, n-butane and decane at 71.1°C (160°F).

The Peng-Robinson (P-R) equation of state was used to calculate the phase equilibrium, with a methane-decane interaction coefficient of 0.042. The Lorenz-Bray-Clark[28] correlation was used to calculate the gas and oil viscosities.

The average pressure of the experiment was 18.96 10^6 Pa (2750 psia), while with the P-R equation of state the average pressure was found to be 18.9 10^6 (2754.6 psia).

The process can be visualized on a ternary diagram: an oil displaced by its equilibrium gas are both located on the phase equilibrium curve and on the same tie line. The composition path lies entirely in the two-phase zone and it is the tie line that passes through the oil and gas compositions noted above.

Figures 7.44 and 7.45 show the close agreement between the experimental data and results computed by the present simulator.

TABLE VII.6

BASIC RESERVOIR DATA USED TO COMPARE WITH EXPERIMENTAL DATA[57]

Length, m (ft.)	2.0 (6.56)
Porosity, fraction	0.3417
Permeability, m^2 (darcy)	3.89 (3.94)
Temperature, °C (°F)	71.1 (160)
Pressure, initial and producing Pa (psi)	$18.99\ 10^6$ (2754.6)
Injection rate at 71.1°C and 2754.6 psia m/s	$1.05\ 10^{-2}$
Oil composition, mole fraction	
Methane	0.579
N-Butane	0.253
Decane	0.168
Gas composition, mole fraction	
Methane	0.874
N-Butane	0.113
Decane	0.015
Productivity index, m^3 Pa·s/Pa·s	$4.78\ 10^{-14}$
Total time s(days)	86400 (1)

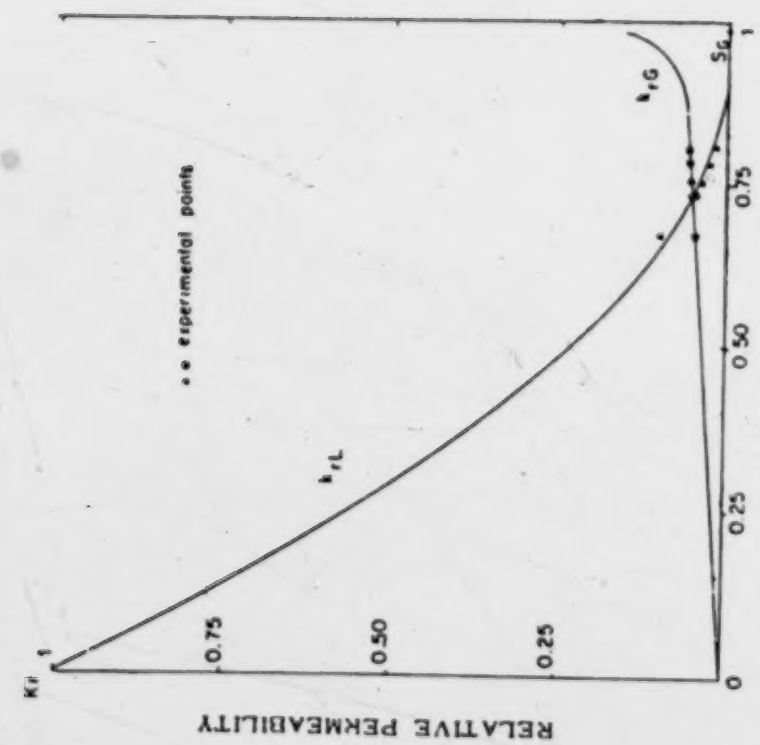

Figure 7.43 Relative permeability reported for Van Quy[57] et al.

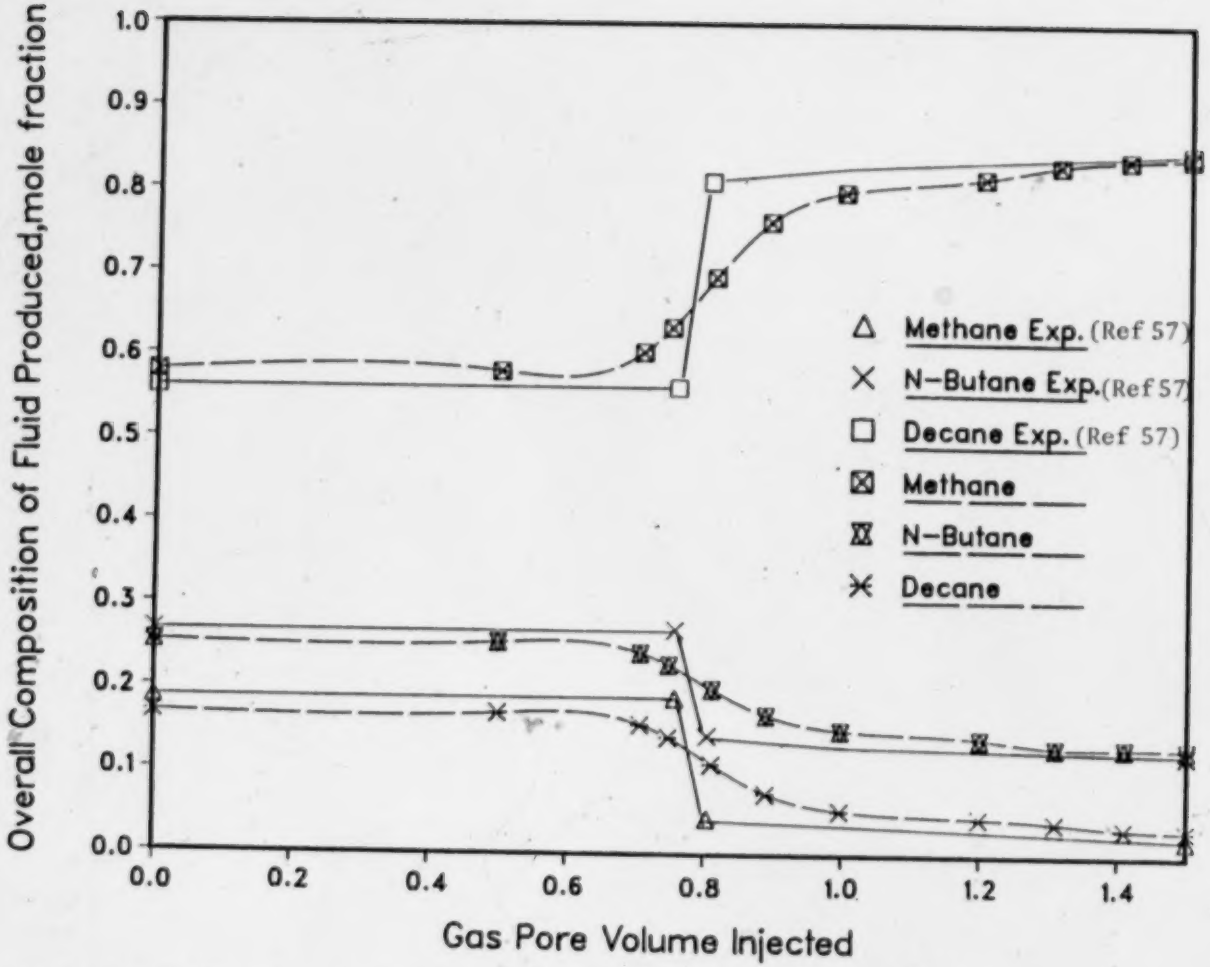

Figure 7.44 Simulator results compared with experimental data.[57] Overall composition of fluid produced vs. gas pore volume injected.

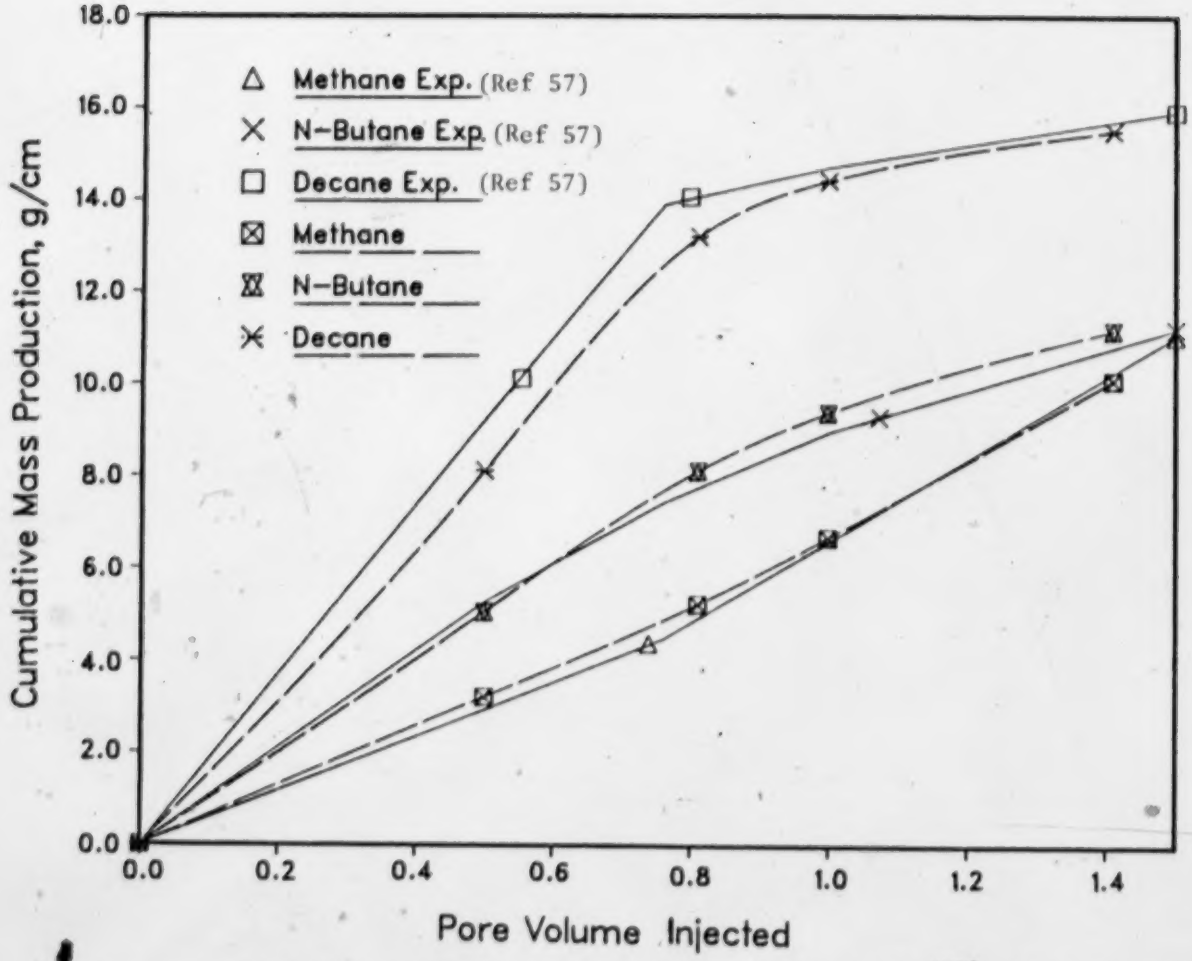

Figure 7.45 Simulator results compared with experimental data.[57] Cumulative mass produced per unit of area vs. pore volume injected.

Figure 7.44 shows that the overall experimental composition at the outlet of the model changes drastically after breakthrough, while the results computed with 10 grid blocks present a more gradual change, due to the coarse grid used. Note that the overall composition computed by the present model at the producing well is the same as the composition of the corresponding grid block. Also the outlet composition reached after 1.5 PV injected is the equilibrium composition corresponding to a residual oil saturation of 0.1.

Figure 7.45 presents the cumulative mass production of each component per unit of area with pore volume of injected gas. Closer agreement was found for methane and n-butane than for decane, showing that a more efficient displacement occurred in the real process or experiment.

VII.7 Efficiency of the Model

The computing time mentioned here corresponds to AMDAHL 5860 cpu (m sec), using a FORTRAN G compiler. Table VII.6 shows the computational time for all example problems studied. Example Problem 1 (MCM) required 36.75 m sec per time step per block per component, and an average of 6 iterations per time step. The same example for a two-dimensional reservoir, Example Problem 4, required 51 m sec per time step per block per component, and an average of 6.5 iterations per time step. The difference in time is explained by the increased number of grid blocks (form 20 to 25 grid blocks) or simultaneous equations solved, and due to the increased matrix band width. For

TABLE VII.7

COMPARISON OF COMPUTATIONAL TIME (m sec) USING

AMDAHL 5860 (FORTRAN G)

Example Problem	Grid Blocks	cpu/Time step/ Block/Component (ms)	cpu/Time step Block/Component/ Iteration (ms)	Iteration Number
MCM				
	10	25.45	3.654	6-7
1	20	36.75	6.12	6-0
4	5×5	51.0	7.69	6-7
IM				
	10	15.69	3.92	4-5
2	20	25.69	5.7	4-5
5	5 5	38.6	7.1	5-6
IM				
	10	35.93	3.38	10-11
3	20	41.10	5.11	8
6	5 5	49.4	6.79	7

Example Problems 2 and 5, the same behaviour in time difference is observed.

For immiscible displacement (Example Problems 2 and 5), the cpu time and the number of iterations were smaller than those for miscible displacement (Example Problems 1 and 4) (Table VII.6), as was expected.

For immiscible displacement Example Problem 2, Thele et al.[54] report an average of 7.98 iterations per time step for the fully implicit formulation. The present model required 4.5 iterations per time step.

Example Problems 3 and 6 show higher cpu time per time step (Table VII.6) than the other examples due to the increased number of iterations. These values were expected as the maximum change in saturation per time step was allowed to be greater than 20%. But, as shown in Table VII.6, the cpu time per time step per block per component per iteration is in the same range as for the other examples.

The computational efficiency of the present model is comparable to that reported by Thele et al.[54]. The efficiency decreased as the number of grid blocks and matrix band width increased.

CHAPTER VIII

NUMERICAL AND MECHANISTIC PROBLEMS ENCOUNTERED IN THE DEVELOPMENT OF THE MODEL

The following discussion presents the sequential problems encountered in the development of the compositional model as well as their solutions. The problems to be discussed arise, first, because an equation of state is used for the phase equilibria calculation, and secondly because the condition of equality of fugacity is coupled with the flow equations in a porous medium to form the fully implicit model.

Two types of problems were encountered. First, separation of hydrocarbon phases was problematic when a second hydrocarbon-phase appeared in a grid block, and second, convergence was difficult in a multiple contact miscible process in a region near the critical point.

These two problems were solved by estimating good initial values for iterations: pressure, composition and distribution of the hydrocarbon phases for each grid block by successive substitution iterations. With these estimates in place convergence was accomplished at every time step for the examples tested.

A discussion of the sequential problems mentioned above is presented next.

1. Initially, the phase appearance routine did not include an external flash calculation, as described in Chapter V. It only consisted of detecting the appearance of a second hydrocarbon phase when the saturation pressure was greater than the grid block pressure.

In the model, when the flow equations are solved simultaneously with the fugacity constraints, a flash calculation is performed automatically.[10] Then, the model should separate the appearance of a second hydrocarbon phase, from initial estimates of composition and distribution of the phases. The initial estimates of composition were obtained from the results of the saturation pressure calculation, and the saturation of the new hydrocarbon phase was set to 0.001, decreasing the saturation of the other hydrocarbon phase by the same amount.

This procedure worked only when the saturation pressure of the grid block in question was close to the block pressure, as the initial estimate of the iteration parameters (composition and distribution of the hydrocarbon phases) were good estimates of the solution of the phases. In other words, it was not necessary to perform an external flash calculation to find the compositions and distribution of the phases in that grid block.

The need for an external flash calculation was not obvious at first, as the very first example tested consisted of an oil displaced by a gas in equilibrium, which implies that the compositions of oil and gas were constant (equilibrium K-values constant) through the displacement.

After 0.61 pore volumes were injected (PV), the model failed to converge. When a second hydrocarbon gas phase appeared, and its saturation S_g was smaller than 0.001, the grid block was considered one phase and convergence was attained for this time step. In the next time step, the same block displayed a higher saturation pressure than the block pressure, as the grid block was not initiated

as a two-phase grid block, and then the gas phase was forced to go into solution, increasing the saturation pressure. Then, given initial iteration values of composition from the previous saturation pressure the second hydrocarbon phase could not be separated and the model failed to converge.

At this stage the problem was solved by not ignoring even a very small hydrocarbon phase. But when the second example was tested: oil displaced by a gas (immiscible displacement), the model was not able to converge, because the equilibrium K-values were not constant anymore, and better initial estimates were needed.

Therefore, the implementation of the external flash routine was necessary: among many trials, the only successful one was when the estimate of the composition of the phases (y_i, x_i) and saturations (S_g, S_o) were the correct separation of the total composition of the grid block during an iteration, i.e., when the new estimates satisfied the material balance condition of the grid block and, therefore, no disturbance was introduced in the next iteration.

2. When the third example: multiple contact miscible displacement, was tested, the model ran only when a grid block approached the critical point, as there was no convergence in the residuals of several other blocks. It was as if, when the model converged for one block, other blocks were disturbed and lost their equilibrium.

The problem was pinpointed in the automatic flash calculation. It failed to converge close to the critical point causing imbalance (no equilibrium) among several blocks.

It has been demonstrated that Newton type methods when applied

to phase equilibria calculations with an equation of state can converge close to a critical point and phase boundaries.[17] Baker and Luks [7] pointed out that better initial estimates are necessary in order to get convergence. They suggested, in their method of getting better initial estimates, starting with a few successive substitution iterations (SSI) and then switching to Newtonian iterations.

Following these ideas, successive substitution iterations (SSI) were implemented, in order to get better initial estimates of the parameters (composition and distribution of the phases) for the imbalance blocks, to start the next Newtonian iteration. The criterion of $|f_i^L/f_i^V - 1| > 0.01$ was used to detect such imbalanced grid blocks.

This method can be understood as an extrapolation method of equilibrium K-values, applied to the imbalanced grid blocks, as the initial K-values used in these SSI are calculated from the results of the last Newtonian (outer) iteration. The same level of thermodynamic equilibrium is attained for each grid block before a new iteration is started, which helps the model to converge to a region near to or at the critical point. Even though this method requires more computing time per iteration, it reduces the total Newtonian iterations per time step and allows convergence to the critical point.

Now, the model is able to separate phases and to converge to a critical point under the test conditions.

CHAPTER IX

CONCLUSIONS AND RECOMMENDATIONS

A fully implicit compositional model incorporating an equation of state was developed to simulate compositional problems. The model was tested with the simulation of a condensing gas drive, an immiscible and multicontact miscible displacement (MCM) and a high pressure gas drive in one- and two-dimensional reservoirs. The following conclusions are derived on the basis of the study:

1. The model developed can simulate multicomponent gas drives, from depletion and cycling of volatile oil and gas condensate reservoirs to multicontact miscible displacement.
2. Newton's method can be used to solve effectively the system of complex nonlinear difference equations of compositional problems. The resulting model is very stable.
3. In the multicontact miscible displacement test, continuous convergence of the hydrocarbon phase compositions and properties toward the critical composition was achieved. Thus, stable convergence was achieved with the model near and at the critical point.
4. The fully implicit model requires from 5 to 8 iterations per time step for the residual convergence criterion of 0.01. But when this criterion is set to 0.1 the number of iterations is reduced to a range of 1 to 4. These numbers of iterations are for a maximum change in hydrocarbon saturation of 20% for the immiscible displacement, and up to 50% for the multicontact miscible displacements. The number of iterations increases when the maximum change of saturation

increases.

5. The number of iterations per time step for the present model is comparable to that reported by Thele et al.[54]. But the execution time (cpu sec.) is larger because of the slower Fortran compiler used, the band solver routine (used) or direct method of solution used, and because the test for the appearance of a hydrocarbon phase is made for every single hydrocarbon phase grid block at each iteration. Furthermore, an increase in the number of grid blocks also reduces the efficiency of the model.

6. Numerical dispersion affects the velocity of the miscible front, and to a minor extent it also influences the recovery curves for the examples studied.

7. Newton's method with numerical derivatives can be used effectively to calculate saturation pressure (dew point, bubble point, critical point) with an equation of state. These calculations depend upon the initial estimate of the K-values

8. The distinction between a miscible or immiscible displacement close to the critical point depends strongly upon the calibration of the equation of state with experimental data.[15] (Example Problem 3 is such a case. It was reported by Van Quy et al.[57] as miscible displacement, while with this model it appeared as an immiscible displacement, using the Peng-Robinson equation of state.)

IX.1 Recommendations

The following recommendations are made for continuing the present study so as to improve and extend the present model:

1. Young's[62] method of hydrocarbon-phase appearance could be implemented, i.e. test only single hydrocarbon phase grid blocks if they are beside a two-phase grid block, in order to reduce cpu time.

2. Modify the computer code in order to use a vector processor. The changes could be incorporated without major difficulties. Furthermore, matrix operations are already built into the model.

3. An improved method of solution could be implemented in order to make the model run faster.

4. A semi-implicit option for transmissibility could be programmed.

5. Extensions of the model to vertical cross-section and radial systems could be developed. Extension to three dimensions could be implemented also.

6. Different equation of state could be easily implemented, since numerical derivatives are used in the program.

7. Different methods for the initial estimate of K-values could be implemented to improve separation of phases close to the phase envelope of complex hydrocarbon systems.

8. The option of solubility of hydrocarbons and CO_2 in water for this type of formulation could be included. It will increase the number of unknowns per grid block in n_c, increasing the machine time.

BIBLIOGRAPHY

[1] Abou-Kassem, J.H. "Investigation of Grid Orientation in a Two-Dimensional, Compositional, Three-Phase Steam Model," Ph.D. Thesis, Department of Chemical and Petroleum Engineering, University of Calgary, Alberta, April (1981).

[2] Abou-Kassem, J.H., and Farouq Ali, S.M. "Appraisal of Steamflood Models," paper SPE 13947 presented at the SPE 1985 California Regional Meeting, Bakersfield, Ca., March 27-29, 1985.

[3] Alonso, M., Morineau, Y., Simandoux, P., Bradshaw, A.D. and Bennion, D.W. "A Laboratory Investigation of the Enriched Gas Displacement Process in Vertical Models," J. Can. Pet. Tech. (Jan.-Mar., 1973) 47-58.

[4] Attra, H.D.: "Nonequilibrium Gas Displacement Calculations," Soc. Pet. Eng. J. (Sept. 1961) 130-136.

[5] Au, A.D.K., Behie, A., Rubin, B., and Vinsome, K. "Techniques for Fully Implicit Reservoir Simulation," paper presented at the 55th Annual Fall Technical Conference and Exhibition of the Society of Petroleum Engineers of AIME, Dallas, Texas, September 21-24 (1980).

[6] Aziz, K., and Settari, A. "Petroleum Reservoir Simulation," Applied Science Publishers Ltd., London, pp. 75-77, 156-169, 187, 330-337, and 395-401 (1979).

[7] Baker, L.E. and Luks, K.D. "Critical Point and Saturation Pressure Calculations for Multipoint Systems," Soc. Pet. Eng. J. (Feb. 1980) 15-24.

[8] Carr, N.L., Kobayashi, R. and Burrows, D.B. "Viscosity of Hydrocarbon Gases Under Pressure," Trans., Aime (1954) 201, 264-272.

[9] Chien, M.C.H., Lee, S.T. and Chen, W.H. "A New Fully Implicit Compositional Simulator," paper SPE 13385 presented at the SPE 1985 Reservoir Simulation Symposium, Dallas, Tex., Feb. 10-13, 1985.

[10] Coats, K.H.: "An Equation of State Compositional Model," Soc. Pet. Eng. J. (Oct. 1980) 363-376.

[11] Coats, K.H. "A Highly Implicit Steamflood Model," Soc. Pet. Eng. J., Vol. 18, No. 5, pp. 369-383, October (1978).

[12] Corteville, J., Van Quy, N. and Simandoux, P. "A Numerical and Experimental Study of Miscible or Immiscible Fluid Flow in Porous Media with Interphase Mass Transfer," paper SPE 3481 presented at SPE-AIME 46th Annual Fall Meeting, New Orleans, Oct. 3-6, 1971.

[13] Culham, W.E., Farouq Ali, S.M., and Stahl, C.D. "Experimental Flow with Interphase Mass Transfer in One and Two Dimensions," Soc. Pet. Eng. J. (Sept. 1969) 323-337.

[14] Dumore, J.M., Hagoort, J., and Risseeuw, A.S. "An Analytical Model for One-Dimensional Three-Component Condensing and Vaporizing Gas Drives," paper SPE 10069 presented at the SPE 56th Annual Fall Meeting, San Antonio, Oct. 5-7, 1981.

[15] Firoozabadi, A. and Aziz, K. "Analysis and Correlation of Nitrogen and Lean Gas Miscibility Pressure," paper SPE 13669 presented at the SPE 1985 California Regional Meeting, Bakersfield, Ca. March 27-29, 1985.

[16] Fussell, L.T. and Fussell, D.D. "An Iterative Technique for Compositional Reservoir Models," Soc. Pet. Eng. J. (Aug. 1979) 211-220.

[17] Fussell, D.D. and Yanosik, J.L. "An Iterative Sequence for Phase Equilibrium Calculations Incorporating the Redlich-Kwong Equation of State," SPE J. (June 1978) 173-182.

[18] Gonzalez, M., Eakin, B.E. and Lee, A.L. "Monograph on API Research Project 65 Viscosity of Natural Gases," American Petroleum Institute, New York (1970).

[19] Grabowski, J.W., Vinsome, P.K., Lin, R.C., Behie, A. and Rubin, B. "A Fully Implicit General Purpose Finite-Difference Thermal Model for In-Situ Combustion and Steam," paper presented at the 54th Annual Fall Technical Conference and Exhibition of the Society of Petroleum Engineers of AIME, Las Vegas, Nevada, September 23-26 (1979).

[20] Hoffmann, A.E., Crump, J.S. and Hocott, C.R. "Equilibrium Constants for a Gas - Condensate System," Trans., AIME (1953) 198, 1-10.

[21] Hough, E.W. and Warren, H.G. "Correlation of Interfacial Tension of Hydrocarbons," Soc. Pet. Eng. J. (Dec. 1966) 345-349.

[22] Hubbert, M.K. "Darcy's Law and the Field Equations of the Flow of Underground Fluids," Trans., AIME (1956) 207, 222-239.

[23] Hutchinson, C.A. and Braun, P.H. "Phase Relations of Miscible Displacement in Oil Recovery," A.I.Ch.E.J. (March 1961) 64-72.

[24] Jacoby, R.H. and Berry, V.J. "A Method for Predicting Depletion Performance of a Reservoir Producing Volatile Crude Oil," Trans., AIME (1957) 210, 27-33.

[25] Jossi, J.A., Stiel, L.I. and Thodos, G. "The Viscosity of Pure Substances in the Dense and Liquid Phases," A.I.Ch.E.J. (March 1962) 8, 59-63.

[26] Kazemi, H., Vestal, C.R. and Shank, G.D. "An Efficient Multicomponent Numerical Simulator," Soc. Pet. Eng. J. (Oct. 1978) 355-368.

[27] Kniazeff, V.J. and Naville, S.A. "Two-Phase Flow of Volatile Hydrocarbons," Soc. Pet. Eng. J. (March 1965) 37-44.

[28] Lohrenz, J., Bray, B.G. and Clark, C.R. "Calculating Viscosities of Reservoir Fluids From Their Compositions," Soc. Pet. Eng. J. (Oct. 1964), 1171-1176.

[29] Mansoori, J. "Discussion of Compositional Modeling with an Equation of State," Soc. Pet. Eng. J. (April 1982) 202-203.

[30] McFarlane, R.C., Mueller, T.D. and Miller, F.G.: "Unsteady-State Distribution of Fluid Compositions in Two-Phase Oil Reservoirs Undergoing Gas Injection," Soc. Pet. Eng. J. (March 1967) 61-74.

[31] Metcalfe, R.S., Fussel, D.D. and Shelton, J.L. "A Multicell Equilibrium Separation Model for the Study of Multiple Contact Miscibility in Rich-Gas Drives," paper SPE 3995 presented at SPE-AIME 47th Annual Fall Meeting, San Antonio, Tex., Oct. 8-11, 1972.

[32] Nghiem, L.X. "A New Approach to Quasi-Newton Methods with Application to Composition of Modeling," paper SPE 12242 presented at the Reservoir Simulation Symposium, San Francisco, Ca., November 15-18, 1983.

[33] Nghiem, L.X., Fong, D.K. and Aziz, K. "Compositional Modeling with and Equation of State," Soc. Pet. Eng. J. (Dec. 1981) 688-698.

[34] Nghiem, L.X. "Author's Reply to Discussion of Compositional Modeling with an Equation of State," Soc. Pet. Eng. J. (April 1982) 204.

[35] Nghiem, L.X., Aziz, K. and Li, Y.K. "A Robust Iterative Method for Flash Calculations Using the Soave-Redlich-Kwong or the Peng-Robinson Equation of State," Soc. Pet. Eng. J. (June 1983), 521-530.

[36] Nolen, J.S. "Numerical Simulation of Compositional Phenomena in Petroleum Reservoirs," paper SPE 4274 presented at the SPE Third Symposium on Numerical Simulation of Reservoir Performance, Houston, Jan. 11-12, 1973.

[37] Peacemen, D.W. "Fundamentals of Numerical Reservoir Simulation," Elsevier Scientific Publishing Co., New York City (1977).

[38] Peacemen, D.W. "Interpretation of Well-Block Pressures in Numerical Reservoir Simulation," SPE J. (June, 1978) 183-194.

[39] Peng, D.Y. and Robinson, D.B. "A New Two-Constant Equation of State," Ind. Eng. Chem. Fund. (Feb. 1976) 15, 59-64.

[40] Perkins, T.K. and Johnson, O.C. "A Review of Diffusion and Dispersion in Porous Media," SPE J. (March 1963) 77-91.

[41] Price, H.S. and Donohue, D.A.T. "Isothermal Displacement Processes with Interphase Mass Transfer," Soc. Pet. Eng. J. (June 1967) 205-220.

[42] Reamer, H.H., Sage, B.H. and Lacey, W.N. "Phase Equilibria in Hydrocarbon Systems: Methane-n-Butane-Decane System," Ind. Eng. Chem. 39:77-82 (1947).

[43] Reamer, H.H., Fiskin, J.M. and Sage, B.H. "Phase Equilibria in Hydrocarbon Systems: Phase Behavior in the Methane-n-Butane-Decane System at 160°F. Ind. Eng. Chem. 41:2871-2815 (1949).

[44] Reamer, H.H., Sage, B.H. and Lacey, W.N. "Phase Equilibria in Hydrocarbon Systems: Volumetric and Phase Behavior of the Methane-n-Butane-Decane System," Ind. Eng. Chem. 43:1436-1444 (1951).

[45] Reid, R.C., Prausnitz, J.M. and Sherwood, T.K. The Properties of Gases and Liquids, Third edition, McGraw-Hill Inc., New York City (1977).

[46] Roebuck, I.F., Ford, W.T., Henderson, G.E. and Douglas, J.Jr. "The Compositional Reservoir Simulator: Case IV - The Two-Dimensional Model," paper SPE 2235 presented at the SPE 43rd Annual Fall Meeting, Houston, Sept. 29-Oct. 2, 1968.

[47] Roebuck, I.F., Henderson, G.E., Douglas, J.Jr. and Ford, W.T. "The Compositional Reservoir Simulator: Case I - The Linear Model," Soc. Pet. Eng. J. (March 1969) 115-130.

[48] Rowe, A.M. and Silberberg, J.H. "Prediction of the Phase Behavior Generated by the Enriched - Gas - Drive Process," SPE J. (June 1965) 150-

[49] Rowe, A.M. The Critical Composition Method - A New Convergence Pressure Method," SPE J. (March 1967) 54-67.

[50] Sage, B.H. and Lacey, W.N. "Monograph on API Research Project 37 Thermodynamic Properties of the Lighter Paraffin Hydrocarbons and Nitrogen," American Petroleum Institute, New York (1950).

[51] Sage, B.H. and Lacey, W.N. "Monograph on API Research Project 37 some Properties of the Lighter Hydrocarbons, Hydrogen Sulfide and Carbon Dioxide," American Petroleum Institute, New York (1955).

[52] Stalkup, F.I. "Miscible Displacement," American Institute of Mining, Metallurgical and Petroleum Engineers Inc., New York (1983).

[53] Stone, H.L. "Estimation of Three-Phase Relative Permeability and Residual Oil Data," J. Can. Pet. Tech. (Oct. 1973) 53-61.

[54] Thele, K.J. and Lake, L.W. "A Comparison of Three Equation of State Compositional Simulators," SPE 12245, paper presented at the Reservoir Simulation Symposium held in San Francisco, Ca., November 15-18, 1983.

[55] Todd, M.R., O'Dell, P.M. and Hirasaki, G.J. "Methods for Increased Accuracy in Numerical Reservoir Simulators," AIME Trans., Vol. 253, pp. 515-530 (1972).

[56] Tsutsumi, G. and Dixon, T.N. "Mathematical Simulation of Two-Phase Flow with Interphase Mass Transfer in Petroleum Reservoirs," paper SPE 4074 presented at the 47th Annual Fall Meeting, San Antonio, Tex., Oct. 8-11, 1972.

[57] Van Quy, N., Simandoux, P. and Corteville, J. "A Numerical Study of Diphasic Multicomponent Flow," Soc. Pet. Eng. J. (April 1972) 171-184.

[58] Wattenbarger, R.A. "Practical Aspects of Compositional Simulation," paper SPE 2800 presented at the 2nd Symposium on Numerical Simulation of Reservoir Performance of the Society of Petroleum Engineers of AIME, Dallas, Tex., Feb. 5-6, 1970.

[59] Watts, J.W. "A Compositional Formulation of the Pressure and Saturation Equations," SPE 12244, paper presented at the Reservoir Simulation Symposium held in San Francisco, Ca., November 15-18, 1983.

[60] Wheatley, M.J. "A Version of Two-Point Upstream Weighting for Use in Implicit Numerical Reservoir Simulators," paper presented at the SPE Fifth Symposium on Reservoir Simulation, Denver, Colorado, February 1-2, (1979).

[61] Welge, H.J., Johnson, E.F., Ewing, S.P.Jr. and Brinkman, F.H. "The Linear Displacement of Oil from Porous Media by Enriched Gas," J. Pet. Tech. (August 1961) 787-796.

[62] Young, L.C. and Stephenson, R.E. "A Generalized Compositional Approach for Reservoir Simulation," paper SPE 10516 presented at the Sixth SPE Symposium on Reservoir Simulation, New Orleans, Feb. 1-3, 1982.

APPENDIX A

DERIVATIVES OF ACCUMULATION AND PRODUCTION/INJECTION TERMS

1. Derivative of Accumulation Term

Recall Equation (V-17)

$$C_i = \frac{V_b}{\Delta t}\,\phi[x_i\bar{\rho}_o S_o + \bar{\rho}_g S_g y_i], \quad i = 1,2,\ldots n_c \qquad (A\text{-}1)$$

and take derivatives with respect to the variables $x_i, y_i, p_g, S_o, S_g, S_w$:

- with respect to oil composition

$$\underline{C}_{ij} = \frac{V_b}{\Delta t}\,\phi\left(\bar{\rho}_o S_o \delta_{ij} + x_i S_o \frac{\partial\bar{\rho}_o}{\partial x_j}\right), \quad \begin{matrix} i = 1,2,\ldots n_c \\ j = 1,2,\ldots n_c \end{matrix} \qquad (A\text{-}2)$$

where δ_{ij} is the Dirac delta function:

$$\delta_{ij} = \begin{cases} 1 & i = j \\ 0 & i \neq j \end{cases} \qquad (A\text{-}3)$$

- with respect to gas composition

$$\underline{C}_{ij} = \frac{V_b}{\Delta t}\,\phi\left(\bar{\rho}_g S_g \delta_{ij} + y_i S_g \frac{\partial\bar{\rho}_g}{\partial y_i}\right), \quad \begin{matrix} i = 1,2,\ldots n_c, \\ j = n_c{+}1,\ldots 2n_c \end{matrix} \qquad (A\text{-}4)$$

- with respect to pressure

$$\underline{C}_{ij} = \frac{V_b}{\Delta t}\,\phi\left(x_i S_o \frac{\partial\rho_o}{\partial p_g} + y_i S_g \frac{\partial\bar{\rho}_g}{\partial p_g}\right) + \frac{V_b}{\Delta t}\,\phi(x_i S_o\bar{\rho}_o + y_i S_g\bar{\rho}_g)\,\frac{1}{\phi}\,\frac{\partial\phi}{\partial p_g}, \quad \begin{matrix} i = 1,2,\ldots n_c \\ j = 2n_c + 1 \end{matrix} \qquad (A\text{-}5)$$

- with respect to oil saturation

$$\underline{C}_{i,2n_c+2} = \frac{V_b\phi}{\Delta t}\left(x_i\bar{\rho}_o + \frac{\partial}{\partial S_o}(y_i S_g \bar{\rho}_g)\right), \quad i = 1,2,\ldots n_c \qquad \text{(A-6)}$$

- with respect to gas saturation

$$\underline{C}_{i,2n_c+3} = \frac{V_b\phi}{\Delta t}\left(y_i\bar{\rho}_g + \frac{\partial}{\partial S_g}(x_i\bar{\rho}_o S_o)\right), \quad i = 1,2,\ldots n_c \qquad \text{(A-7)}$$

- with respect to water saturation

$$\underline{C}_{i,2n_c+4} = \frac{V_b\phi}{\Delta t}\left(y_i\bar{\rho}_g \frac{\partial S_g}{\partial S_w} + x_i\bar{\rho}_o \frac{\partial S_o}{\partial S_w}\right), \quad i = 1,2,\ldots n_c \qquad \text{(A-8)}$$

Recall Equation (V-18)

$$C_i = \frac{V_b}{\Delta t}\phi(S_w\bar{\rho}_w), \quad i = n_c + 1 \qquad \text{(A-9)}$$

and take derivatives with respect to the variables $x_i, y_i, p_g, S_o, S_g, S_w$:

- with respect to oil and gas composition

$$\underline{C}_{ij} = 0, \quad j = 1,2,\ldots n_c,\ldots 2n_c$$
$$i = n_c + 1. \qquad \text{(A-10)}$$

- with respect to pressure

$$\underline{C}_{i,2n_c+1} = \frac{V_b}{\Delta t}\phi\left(S_w\frac{\partial\bar{\rho}_w}{\partial p_g} + \frac{\rho_w S_w}{\phi}\frac{\partial\phi}{\partial p_g}\right),$$
$$i = n_c + 1 \qquad \text{(A-11)}$$

- with respect to oil saturation

$$\underline{C}_{i,2n_c+2} = \frac{V_b\phi}{\Delta t}\left(S_w \frac{\partial \bar{\rho}_w}{\partial S_o} + \frac{S_w \rho_w}{\phi}\frac{\partial \phi}{\partial S_o}\right), \quad i = n_c + 1 \qquad \text{(A-12)}$$

- with respect to gas saturation

$$\underline{C}_{i,2n_c+3} = \frac{V_b\phi}{\Delta t}\left(S_w \frac{\partial \rho_w}{\partial S_g} + \frac{S_w \bar{\rho}_w}{\phi}\frac{\partial \phi}{\partial S_g}\right), \quad i = n_c + 1 \qquad \text{(A-13)}$$

- with respect to water saturation

$$\underline{C}_{i,2n_c+4} = \frac{V_b\phi}{\Delta t}\left(\rho_w + Sw \frac{\partial \rho_w}{\partial S_w} + \frac{\rho_w S_w}{\phi}\frac{\partial \phi}{\partial S_w}\right), \quad i = n_c + 1 \qquad \text{(A-14)}$$

2. Derivatives of Production/Injection Terms

Recall Equation (V-19)

$$Q_i = x_i \bar{\rho}_o q_o + y_i \bar{\rho}_g q_g, \quad i = 1,2,\ldots n_c \qquad \text{(A-15)}$$

and take derivatives with respect to the variables $x_i, y_i, p_g, S_o, S_g, S_w$:

- with respect to oil composition

$$\underline{Q}_{ij} = \bar{\rho}_o q_o \delta_{ij} + x_i\left(q_o \frac{\partial \bar{\rho}_o}{\partial x_j} + \bar{\rho}_o \frac{\partial q_o}{\partial x_j}\right) + y_i\left(\bar{\rho}_g \frac{\partial q_g}{\partial x_j} + q_g \frac{\partial \bar{\rho}_g}{\partial x_j}\right), \quad \begin{matrix} i = 1,2,\ldots n_c \\ j = 1,2,\ldots n_c \end{matrix} \qquad \text{(A-16)}$$

- with respect to gas composition

$$\underline{Q}_{ij} = \bar{\rho}_g q_g \delta_{ij} + y_i \left(q_g \frac{\partial \bar{\rho}_g}{\partial y_j} + \bar{\rho}_g \frac{\partial q_g}{\partial y_j} \right) + x_i \left(\bar{\rho}_o \frac{\partial q_o}{\partial y_j} + q_o \frac{\partial \bar{\rho}_o}{\partial y_j} \right),$$

$$i = 1,2,\ldots n_c$$

$$j = n_c + 1,\ldots 2n_c \qquad \text{(A-17)}$$

- with respect to pressure

$$\underline{Q}_{i,2n_c+1} = x_i \bar{\rho}_o \frac{\partial q_o}{\partial p_g} + y_i \bar{\rho}_g \frac{\partial q_g}{\partial p_g} + x_i q_o \frac{\partial \bar{\rho}_o}{\partial p_g} + y_i q_g \frac{\partial \bar{\rho}_g}{\partial p_g},$$

$$i = 1,2,\ldots n_c \qquad \text{(A-18)}$$

- with respect to oil saturation

$$\underline{Q}_{i,2n_c+2} = x_i \left(\rho_o \frac{\partial q_o}{\partial S_o} + q_o \frac{\partial \bar{\rho}_o}{\partial S_o} \right) + y_i \left(\rho_g \frac{\partial q_g}{\partial S_o} + q_g \frac{\partial \rho_g}{\partial S_o} \right),$$

$$i = 1,2,\ldots n_c \qquad \text{(A-19)}$$

- with respect to gas saturation

$$\underline{Q}_{i,2n_c+3} = x_i \left(\bar{\rho}_o \frac{\partial q_o}{\partial S_g} + q_o \frac{\partial \bar{\rho}_o}{\partial S_g} \right) + y_i \left(\bar{\rho}_g \frac{\partial q_g}{\partial S_g} + q_g \frac{\partial \bar{\rho}_g}{\partial S_g} \right),$$

$$i = 1,2,\ldots n_c \qquad \text{(A-20)}$$

- with respect to water saturation

$$\underline{Q}_{i,2n_c+4} = x_i \left(\bar{\rho}_o \frac{\partial q_o}{\partial S_w} + q_o \frac{\partial \rho_o}{\partial S_w} \right) + y_i \left(\bar{\rho}_g \frac{\partial q_g}{\partial S_w} + q_g \frac{\partial \rho_g}{\partial S_g} \right),$$

$$i = 1,2,\ldots n_c . \qquad \text{(A-21)}$$

Recall Equation (V-20)

$$Q_i = \bar{\rho}_w q_w, \quad i = n_c + 1 \tag{A-22}$$

and take derivatives with respect to the variables $x_i, y_i, p_g, S_o, S_g, S_w$:

- with respect to oil composition

$$\underline{Q}_{ij} = \frac{\partial \bar{\rho}_w}{\partial x_j} q_w + \rho_o \frac{\partial q_w}{\partial x_j}, \quad \begin{matrix} i = n_c + 1, \\ j = 1,2,\ldots n_c. \end{matrix} \tag{A-23}$$

- with respect to gas composition

$$\underline{Q}_{ij} = \frac{\partial \bar{\rho}_w}{\partial y_j} q_w + \rho_w \frac{\partial q_w}{\partial y_j}, \quad \begin{matrix} i = n_c + 1, \\ j = n_c + 1,\ldots 2n_c, \end{matrix} \tag{A-24}$$

- with respect to pressure

$$Q_{i,2n_c+1} = \bar{\rho}_w \frac{\partial q_w}{\partial p_g} + q_w \frac{\partial \bar{\rho}_w}{\partial p_g}, \quad i = n_c + 1 \tag{A-25}$$

- with respect to oil saturation

$$Q_{i,2n_c+2} = \bar{\rho}_w \frac{\partial q_w}{\partial S_o} + q_w \frac{\partial \rho_w}{\partial S_o}, \quad i = n_c + 1 \tag{A-26}$$

- with respect to gas saturation

$$Q_{i,2n_c+3} = \bar{\rho}_w \frac{\partial q_w}{\partial S_g} + q_w \frac{\partial \bar{\rho}_w}{\partial S_g}, \quad i = n_c + 1 \tag{A-27}$$

- with respect to water saturation

$$Q_{i,2n_c+4} = \bar{\rho}_w \frac{\partial q_w}{\partial S_w} + q_w \frac{\partial \bar{\rho}_w^*}{\partial S_w}, \quad i = n_c + 1 \qquad \text{(A-28)}$$

Production Rates

For each of the production flow rates schemes derivatives were taken with respect to all variables:

$$X = \{x_1, \ldots x_{n_c}, y_1, y_2, \ldots y_{n_c}, p_g, S_o, S_g, S_w\}:$$

- For scheme 1-oil flow rate specified

$$\frac{\partial q_\ell}{\partial X_j} + \frac{\partial}{\partial X_j}\left(\frac{\lambda_\ell}{\lambda_o}\right) q_o, \qquad \begin{matrix} j = 1,2,\ldots 2n_c + 1, \\ \ell = o,g,w. \end{matrix} \qquad \text{(A-29)}$$

- For scheme 2-liquid flow rate is specified

$$\frac{\partial q_\ell}{\partial X_j} = \frac{\partial}{\partial X_j}\left(\frac{\lambda_\ell}{\lambda_L}\right) q_L = \frac{\partial}{\partial X_j}\left(\frac{\lambda_\ell}{\lambda_o + \lambda_w}\right) q_L,$$

$$j = 1,2,\ldots 2n_c + 4,$$

$$\ell = o,g,w. \qquad \text{(A-30)}$$

- For scheme 3-total flow rate is specified

$$\frac{\partial q_\ell}{\partial X_j} = \frac{\partial}{\partial X_j}\left(\frac{\lambda_\ell}{\lambda_o + \lambda_w + \lambda_g}\right) q_T,$$

$$j = 1,2,3,\ldots 2n_c + 4$$

$$p = o,g,w. \qquad \text{(A-31)}$$

- For scheme 4 - bottomhole pressure is specified

$$\frac{\partial q_\ell}{\partial X_j} = -PI \left[\frac{\partial \lambda_p}{\partial X_j}(p_g - p^n_{wf}) + \lambda_p \delta_{ij}\right],$$

$$j = 1,2,\ldots n_c + 4, \quad C = 2n_c + 1, \quad \ell = o,g,w. \qquad \text{(A-32)}$$

The mobility terms are considered at time level $n+1$.

Injection Rates

There are no derivatives when the injection flow rates are specified at constant pressure, composition and temperature, i.e. injection is at a constant mass rate.

When the bottomhole pressure is specified, scheme 4 of production flow rate: Equation (A-31) is used.

VITA

NAME: Damarys Lozada-Briceño

PLACE OF BIRTH: Puerto La Cruz, Edo Anzoategui, Venezuela

DATE OF BIRTH: March 28, 1953

POST-SECONDARY EDUCATION: B.Sc. in Petroleum Engineering from La Universidad Central de Venezuela, Caracas, Venezuela (November, 1976)

WORK EXPERIENCE: Petroleum Engineer at Intevep S.A., Los Teques, Edo Miranda, Venezuela since 1977.